Division Multiplexing of 10 Gbit/s Ethernet Signals Synchronized by All-Optical Signal Processing Based on a Time-Lens

Areal, Janaina Laguardia

Publication date:
2013

Document Version
Publisher's PDF, also known as Version of record

Technical University of Denmark

Division Multiplexing of 10 Gbit/s Ethernet Signals Synchronized by All-Optical Signal Processing Based on a Time-Lens

Janaína Laguardia Areal

Ph.D. thesis

February, 2013

DTU Fotonik
Department of Photonics Engineering

Technical University of Denmark

Technical University of Denmark

DTU Fotonik
Department of Photonics Engineering

Technical University of Denmark

Optical Time-Division Multiplexing of 10 Gbit/s Ethernet Signals Synchronized by All-Optical Signal Processing Based on a Time-Lens

Janaína Laguardia Areal

Ph.D. thesis

February, 2013

Optical Time-Division Multiplexing of 10 Gbit/s Ethernet Signals Synchronized by All-Optical Signal Processing Based on a Time-Lens

Author:
Janaína Laguardia Areal

Supervisor(s):
Professor Leif Katsuo Oxenløwe
Professor Anders Thomas Clausen
Professor Michael Stübert Berger

DTU Fotonik
Department of Photonics Engineering
Technical University of Denmark
Building 343
2800 Kgs. Lyngby
DENMARK

Release date: February, 2013

Class: 1 (offentlig)

Edition: 1. udgave

Comments: This thesis is a part of the requirements to achieve a PhD at Technical University of Denmark.

"What we know is a drop, what we don't know is an ocean"

Isaac Newton

"Small minds are concerned with the extraordinary, great minds with the ordinary."

Blaise Pascal

ACKNOWLEDGEMENTS

It is never easy to acknowledge the important people that have been on your side during a PhD. Especially when they are so many and they are special for many different reasons. Hopefully I will not forget anyone.

First of all I would like to thank God, never felt so close to Him, guess you find out about your faith when you really need Him. I did, so, thank you! Second, I would like to thank my Father, for being my idol, my wall. From such a simple man, I have learned how to be grateful for everything. Father, nothing I said would be enough to measure my love and respect for you. Third, my daughter Julia could not make without you my little fighter. You are the one that keeps me moving.

To my Supervisors, Leif, Anders and Michael. Thank you for trusting me, for giving me this big opportunity at DTU. I will always remember you all and how much you fight to keep me up on track. Thank you for all the support and knowledge I have gotten from you.

I would like to thank my special friends and great supporters, Karen and Martin Fredericksen and the little Emilia for being my family during these 3 years. Could not have done it without you all! This thanks is extend to my other friends, that have been always around me, Antonieta and Lars, Antonella Delia, Nirvana Rodrigo, Veronica Valenzuela, Liliana and Gerardo. You all part of my life!

To my Danish family, the Hyldvangs. My dearest Søren, for all your support, love and friendship. To Lisbeth, Jens, Birgitte, Jørgen and for the little ones, Julie and Frederik, thank you all very much for the affection and support during my time with you. Love you all!

To the NOSFERATU Group, Evarist and Hao, thank you for being amazing colleagues. I have learned a lot spending this time with such great researches and amazing minds.

To Ji Hua, Jing, Hans Christian, Michael, Jorge, Darko, Jure, Neil, Antonio. Thank you for your support, friendship, help and caring
Christophe, thank you for your patience and absolutely will to share knowledge. I am very grateful.

ABSTRACT

This Thesis presents 3 years work of an optical circuit that performs both pulse compression and frame synchronization and retiming. Our design aims at directly multiplexing several 10G Ethernet data packets (frames) to a high-speed OTDM link. This scheme is optically transparent and does not require clock recovery, resulting in a potentially very efficient solution.

The scheme uses a time-lens, implemented through a sinusoidally driven optical phase modulation, combined with a linear dispersion element. As time-lenses are also used for pulse compression, we design the circuit also to perform pulse compression, as well. The overall design is: (1) Pulses are converted from NRZ to RZ; (2) pulses are synchronized, retimed and further compressed at the specially designed time-lens; and (3) with adequate optical delays, frames from different input interfaces are added, with a simple optical coupler, completing the OTDM signal generation.

We demonstrate the effectiveness of the design by laboratory experiments and simulations with VPI and MatLab.

RESUMÉ

I denne afhandling præsenteres 3 års arbejde der har fokuseret på et optisk kredsløb, der udfører puls-kompression, ramme synkronisering samt retiming. Vores design skal multiplekse adskillige 10G Ethernet data pakker sammen som derefter kan videresendes på en højhastigheds OTDM forbindelse. Denne løsning er optisk transparent og behøver ikke klokkegendannelses kredsløb, hvilket resulterer i en potentielt meget effektiv løsning.

Det optiske kredsløb er baseret på en tids-linse, som er installeret som en sinus drevet optisk fasemodulation, kombineret med et lineært dispersion element. Idet tids-linser også kan benyttes til puls-kompression, er det er dette også blevet inkluderet som en funktionalitet i det optiske kredsløb. Det samlede design er: (1) pulser konverteres fra NRZ til RZ; (2) pulser synkroniseres, retimes og komprimeres yderligere via den speciel designede tids-linse; og (3) med passende optiske forsinkelses led, kan rammer fra forskellige input interfaces multiplekses sammen via en simpel optisk kobler, hvorved et fuldt OTDM signal kan dannes.

Vi demonstrerer og evaluerer designet ved hjælp af laboratorieforsøg og simuleringer i både VPI og MatLab.

LIST OF PUBLICATIONS

As first Author:

[P-1] Laguardia Areal, Janaina; Hu, Hao; Peucheret, Christophe; Palushani, Evarist; Puttini, Ricardo; Clausen, Anders; Berger, Michael Stübert; Osadchiy, Alexey; Oxenløwe, Leif Katsuo. "Analysis of a time-lens based optical frame synchronizer and retimer for 10G Ethernet aiming at a Tb/s optical router/switch design." In Proc. of 14th Conference on Optical Network Design and Modeling (ONDM 2010), Kyoto, Japan, Jan. 2010.

[P-2] Laguardia Areal, Janaina; Hu, Hao; Palushani, Evarist; Clausen, Anders; Berger, Michael Stübert; Oxenløwe, Leif. "Time-lens based optical packet pulse compression and retiming". In Proc. of SPIE Photonics Europe (SPIE 2010), Brussels, Apr. 2010.

[P-3] Laguardia Areal, Janaina; Hu, Hao; Palushani, Evarist; Oxenløwe, Leif; Clausen, Anders; Berger, Michael Stübert; Jeppesen, Palle. "Time-lens based synchronizer and retimer for 10 Gb/s Ethernet packets with up to ±1MHz frequency offset." In Proc. of 2010 Conference on Lasers and Electro-Optics (CLEO 2010), 2010.

[P-4] Laguardia Areal, Janaina; Hu, Hao; Palushani, Evarist; Ji, Hua; Clausen, Anders; Berger, Michael Stübert; Jeppesen, Palle; Oxenløwe, Leif. "Conversion of asynchronous 10 Gbit/s Ethernet NRZ frame into a synchronous RZ frame and

multiplexing to 170 Gbit/s.” In Proc. of Annual Meeting of the IEEE Photonics Society 2010, Denver, Colorado, USA, 2010.

[P-5] Laguardia Areal, Janaina; Hu, Hao; Palushani, Evarist; Mulvad, Hans Christian; Clausen, Anders; Berger, Michael; Oxenløwe, Leif; Jeppesen, Palle. “Synchronization and NRZ-to-RZ conversion of 10 Gbit/s Ethernet-like data packets and subsequent optical TDM multiplexing to 330 Gbit/s.” In Proc. of 2011 Optical Fiber Communication Conference and Exposition (OFC 2011), Los Angeles, USA, Mar. 2011.

Author Collaboration:

[P-6] Peucheret, Christophe; Oxenløwe, Leif; Mulvad, Hans Christian; Galili, Michael; Jensen, Jesper; Seoane, Jorge; Palushani, Evarist; Hu, Hao; Xu, Jing; Clausen, Anders; Rottwitt, Karsten; Kang, Ning; Laguardia Areal, Janaina; Ji, Hua; Zsigri, Beata; Jeppesen, Palle. "High-speed signal processing using highly nonlinear optical fibres." In Proc. of 8th International Conference on Optical Communications and Networks (ICOCN 2009), invited conference contribution, Beijing, China, 2009.

[P-7] Oxenløwe, Leif; Galili, Michael; Hu, Hao; Ji, Hua; Palushani, Evarist; Laguardia Areal, Janaina; Xu, Jing; Mulvad, Hans Christian; Clausen, Anders; Jeppesen, Palle. "Serial optical communications and ultra-fast optical signal processing of Tbit/s data signals." In Proc. of IEEE International Topical Meeting on Microwave Photonics (MWP 2010), invited conference contribution, Montreal, Quebec, Canada, 2010.

[P-8] Hu, Hao; Laguardia Areal, Janaina; Palushani, Evarist; Oxenløwe, Leif; Clausen, Anders; Berger, Michael; Jeppesen, Palle. "Optical Synchronization of a 10-G Ethernet Packet and Time-Division Multiplexing to a 50-Gb/s Signal Using an Optical Time Lens." IEEE Photonics Technology Letters 22(21) pp. 1583-1585 (DOI: 10.1109/LPT.2010.2073460) 2010.

[P-9] Oxenløwe, Leif Katsuo ; Galili, Michael ; Mulvad, Hans Christian Hansen ; Hu, Hao ; Xu, Jing ; Palushani, Evarist ; Laguardia Areal, Janaina ; Clausen, Anders ; Jeppesen, Palle. "Ultra-high-speed optical signal processing of Tbaud data signals" : [invited]. European Conference and Exhibition on Optical Communication (ECOC) - 36, 2010, Torino, Italy (Invited conference contribution).

[P-10] Hu, Hao; Laguardia Areal, Janaina; Palushani, Evarist; Galili, Michael; Clausen, Anders; Berger, Michael; Oxenløwe, Leif; Jeppesen, Palle. “Synchronization and NRZ-to-RZ format conversion of 10 G Ethernet packet based on a time lens.” In Proc. of 2010 Photonics in Switching (PS 2010), Monterey, CA, USA, 2010.

[P-11] Hu, Hao; Palushani, Evarist; Laguardia Areal, Janaina; Galili, Michael; Clausen, Anders; Berger, Michael; Peucheret, Christophe; Oxenløwe, Leif; Jeppesen, Palle. “Optical frame synchronizer for 10 G Ethernet packets aiming at 1 Tb/s OTDM Ethernet.” In Proc. of 2010 Conference on Optical Fiber Communication (OFC 2010), San Diego, CA, USA, 2010.

[P-12] Oxenløwe, Leif; Galili, Michael; Mulvad, Hans Christian; Hu, Hao; Ji, Hua; Palushani, Evarist; Laguardia Areal, Janaina; Peucheret, Christophe; Clausen, Anders; Seoane, Jorge; Jeppesen, Palle. “Ultra-High-Speed Serial Optical Communications.” In Proc. of 2010 International Symposium, invited conference contribution, Lyngby, Denmark, 2010.

[P-13] Hu, Hao; Laguardia Areal, Janaina; Hans Christian Hansen Mulvad, Michael Galili, Kjeld Dalgaard, Evarist Palushani, Anders Clausen, Michael S. Berger, Palle Jeppesen, and Leif Katsuo Oxenløwe, "Synchronization, retiming and time-division multiplexing of an asynchronous 10 Gigabit NRZ Ethernet packet to terabit Ethernet," Opt. Express 19, B931-B937 (2011)

[P-14] Hu, Hao; Laguardia Areal, Janaina; Mulvad, Hans Christian Hansen; Galili, Michael; Dalgaard, Kjeld; Palushani, Evarist; Clausen, Anders T.; Berger, Michael Stübert; Jeppesen, Palle; and Oxenløwe, Leif Katsuo; "Synchronization, retiming and OTDM of an asynchronous 10 Gigabit Ethernet NRZ packet using a time lens for Terabit Ethernet," in 37th European Conference and Exposition on

Optical Communications, OSA Technical Digest (CD) (Optical Society of America, 2011), paper Tu.3.K.4

[P-15] Oxenløwe, Leif Katsuo; Galili, Michael ; Pu, Minhao; Ji, Hua; Hu, Hao; Yvind, Kresten; Hvam, Jørn Märcher; Mulvad, Hans Christian Hansen; Palushani, E.; Areal, Janaina Laguardia; Clausen, Anders T.; Jeppesen, Palle;. "Ultra-fast optical signal processing in nonlinear silicon waveguides," Group IV Photonics (GFP), 2011 8th IEEE International Conference on , vol., no., pp.335-337, 14-16 Sept. 2011

[P-16] Oxenløwe, Leif Katsuo ; Galili, Michael ; Mulvad, Hans Christian Hansen ; Hu, Hao ; Ji, Hua ; Palushani, Evarist ; Laguardia Areal, Janaina ; Peucheret, Christophe ; Clausen, Anders ; Seoane, Jorge ; Jeppesen, Palle. ” Ultra-High-Speed Serial Optical Communications” part of: Conference Proceedings of International Symposium, 2011, Type: Article in proceedings - Article in proceedings. Presented at: International Symposium, Lyngby

[P-17] Clausen, Anders T.; Mulvad, Hans Christian Hansen; Palushani, Evarist; Galili, Michael; Hu, Hao; Ji, Hua; Xu, Jing; Laguardia Areal, Janaina; Jeppesen, Palle.; Oxenlowe, Leif Katsuo; , "Ultra-high-speed optical signal processing of serial data signals," Transparent Optical Networks (ICTON), 2012 14th International Conference on , vol., no., pp.1-4, 2-5 July 2012 doi: 10.1109/ICTON.2012.6254491

[P-18] Oxenløwe, Leif Katsuo; Galili, Michael; Mulvad, Hans Christian Hansen; Hu, Hao; Laguardia Areal, Janaina; Palushani, Evarist, Ji, Hua; Clausen, Anders T.; Jeppesen, Pale. “Nonlinear Optical Signal Processing for Tbit/s Ethernet Applications,” International Journal of Optics, vol. 2012, Article ID 573843, 14 pages, 2012. doi:10.1155/2012/573843

Books Chapter:

[P-19] Transcending the limitations
Laguardia Areal, Janaina
part of: Beyond optical horizons, today and tomorrow with photonics
(ISBN: 87-92062-34-2), pages: 38 pages: 267, 2009, DTU Fotonik, Kgs. Lyngby.

TABLE OF CONTENT

LIST OF FIGURES

LIST OF TABLES

1 INTRODUCTION

10 Gigabit Ethernet (10GE) has developed rapidly since the first 10-Gigabit Ethernet standard (IEEE 802.3ae) [1] was introduced in 2002. The 10GBase-T standard [2] was released in 2006, and the 40G/100G Ethernet standard [3] was released in 2010.

10G Ethernet is a mature technology today. The costs of 10GE optical modules and ports are decreasing every year, while the number of 10GE port shipments is increasing rapidly. 10G Ethernet is the technology of choice for high availability networks.

For its capability of grown and aggregation, the 10 Gigabit technology is likely to be present in the design of high speed optically transparent switches/routers with Tbit/s interfaces that will aggregate traffic from several lower bit rate links [4].

1.1 This PhD Project

As part of a new national research project, Non-linear optical switching for extremely high data rate communications (NOSFERATU), two Ph.D. positions and one post-doc position at DTU Fotonik, were made available. NOSFERATU was funded by the Danish research council for technology and production sciences (Forskningsrådet for Teknologi og Produktion), and aimed at

developing the world's first optical communication system capable of handling 1 Terabit per second (Tbit/s) serial data transmission.

Since the Ethernet is the predominant technology in today's network and the line rate and transmission range of Ethernet Networks steadily increased over last few years, the project propose an optical Ethernet upgrade from 10 GE to future 100 GE lines and, further on, to serial 1 TE.

Besides local area networks (LAN) applications, Ethernet is considered a promising low-cost solution for optical high-speed Metropolitan Area Networks (MAN) and Wide Area Networks (WAN). Ethernet technology has potential to build end-to-end Ethernet optical networks.

This PhD project was focused on how the future optical telecommunication systems can exploit serial bit rates of more than 1 Tbit/s. It has taken-off from the existing Ethernet protocols with inspiration in e.g. frame format, medium access control (MAC) rules and amount of bits per frame. However, due to some speed constraints on the physical layer, some of the functionalities which are available at lower bit rates may not be accessible at 1 Tbit/s. Thus the network planning would have to modify and suggest other solutions based on e.g. the expected development of ultra-fast optical switches based on various technological platforms and already existing high-speed components.

In particular, aiming at a Tbit/s optical Ethernet link design, it has been investigated how to utilise the optical time division multiplexing (OTDM) scheme for optical Ethernet solutions leading to 1 TE, starting from standard 10 GE equipment and increasing the bit rate through a multiplexing (MUX) structure with synchronisation of incoming Ethernet packets to a local MUX clock.

1.2 Motivation for High-Speed Optical Transmission

Data traffic in communication networks has increased over the last few years by an annual rate of up to 100 percent and is expected to increase 20-50 times within the next five years [4]. At the same time, transport technology is more than ever leading into packet-based designs such as Ethernet [6, 7, 8]. This trend is accompanied by adding the ability to transport Ethernet over different transport technologies (carrier-grade features) so it can be deployed on Wide Area Networks (WANs) [4].

Researchers have estimated that quadrupling the serial line rate has resulted in 40% of cost reduction per bit transmitted, even by reduction of terminal equipment and related power consumption [9]. Therefore, it is clear that there is significant potential for cost savings when using higher serial line rates. Currently, electronic signal processing limits the serial line rate to about 120 Gbit/s [10]. Higher rates, however, have been obtained for various schemes, which are based on optical signal processing, which is well suited for serial data signals, since a single ultra-fast optical switch can process data streams and packets optically.

The need for power reductions is also getting more and more evident: the Internet today emits more than 2% of the global man made CO2 emission [11]. Reduction of this rate can be achieved by increasing the line bit rate, both with a single channel perspective and with a spectral efficiency perspective using advanced modulation formats and latest advances in coherent receiver technology [12].

Transmission in Tbit/s data rates on a single wavelength channel was demonstrated in 2000 [13], using a 640 Gbaud polarization-multiplexing (pol-MUX) and simple on-off-key (OOK). Recently it

has become apparent that Tbit/s bit rates for Ethernet applications will be needed very soon [14] and that the overall necessary capacity per fiber will reach several tens of Tbit/s [15]. One of the most promising techniques used to obtain Tbit/s is Optical Time-Division Multiplexing (OTDM), where very narrow optical pulses originated from different optical communications links/channels are optically multiplexed forming an ultra-high line rate communication link in a single fiber, polarization and wavelength [16]. Some of the advantages of using simple OOK purely serial format OTDM, when compared to other multiplexing techniques, such as Dense Wavelength Division Multiplexing (DWDM), include [9] :

- equipment design with low component count with simple line cards;
- well-established techniques for all-optical signal regeneration.

As 10 Gbit/s Ethernet (10GE) transmissions become more widespread, the need for multiplexing 10GbE data frames for more efficient high-capacity data transmission in future transport networks appears. OTDM systems are potential technologies for establishment of such high-capacity links, as the characteristics listed above combined together can lead to considerable reduction in power consumption and equipment cost.

1.3 Thesis Goals

This thesis aims at designing and demonstrating back-to-back operation of a simple OOK OTDM scheme, multiplexing 10 Gbit/s Ethernet input channels into a single channel, polarization and wavelength, such as illustrated in Figure 1-1. The OTDM-based multiplexing system is proposed as a high-speed bus to carry 10GE

frames in OTDM time slots [9, 10, 16]. 10GE links transmit frames asynchronously with NRZ line code. Also, 10GE standards [17] require that a signal speed variation to nominal must be tolerated, i.e. there can be a frequency offset between input signal and multiplexer clocks. These features have direct implications in the design of optically transparent OTDM multiplexer, as OTDM is a bit-interleaved synchronous system based on RZ [9, 10, 16].

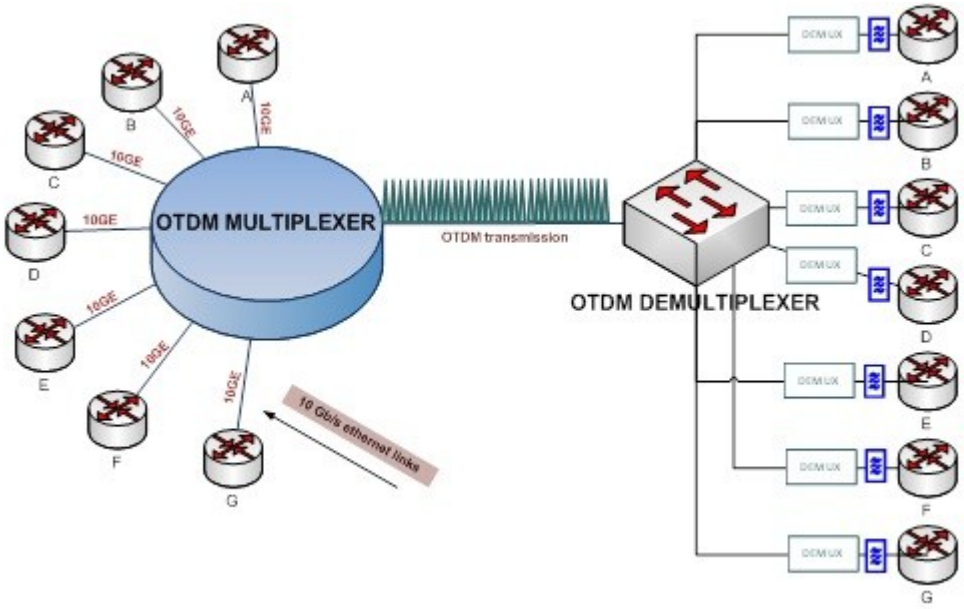

Figure 1-1: OTDM system multiplexing 10GE input frames

We can briefly summarize the functions that must be performed in a 10GE optical signal, in order to prepare it for being multiplexed to a channel of a higher speed OTDM link:

- NRZ-RZ format conversion. 10GE uses NRZ coding. This NRZ signal must be format converted to RZ in order to be multiplexed into an OTDM channel. The pulsewidth of the RZ must be appropriate for Tbit/s operation.
- Retiming of the input 10GE line signal to the system local clock. The 10GE line signal may be time-misaligned with local

clock, as frames are asynchronously transmitted. Retiming is the process of compensate the (initial) time misalignment between the line signal (input signal) and the system local clock.

- Synchronization of the 10GE line signal bit rate (referred to as its fundamental frequency f) to the local clock frequency (f_L), which is the base rate frequency of the OTDM signal. Frequency offset ($\Delta f = f - f_L$) may arise in 10GE from the bit repetition rate deviation (e.g., ±100 ppm in 10GBASE-R PHY tolerance) [17] from the nominal standardized bit rate. Synchronization is the process of adjusting the line signal bit rate to the local clock bit rate, eliminating this frequency offset.

In our proposed OTDM system, these functions are performed by an optical signal processing device. This device is called Format-conversion, Retiming, and Synchronization unit, or simply FRS-unit. The FRS-unit design is based on the time-lens effect [18]. A time-lens is a concept that arises from the time-space duality in optical processing that refers to the analogy between the paraxial diffraction of light beams through space and the dispersion of narrowband pulses through dielectric media in time [19, 20, 21]. Practical time-lenses within fiber optics are usually realized by an optical phase modulator (PM) driven with an electrical sinusoidal signal, combined with a dispersive element, such as dispersive fiber like a single mode fiber (SMF) or dispersion compensated fiber (DCF) [18, 19, 24, 25].

After being optically processed by the FRS-unit, the 10GE input signal is converted to RZ coding, retimed and synchronized to the OTDM multiplexer local clock. There is no need to perform clock recover of the input channels of the multiplexer, as the optical signal is synchronized and retimed directly to the multiplexer local clock. This local clock is used to drive all circuits.

The multiplexer design is completed with passive optical components. The RZ pulses must be sufficient narrow to be multiplexed to OTDM [26]. A highly non-linear fiber (HNLF) is used to provide pulse compression in order to convert the pulse train into sufficiently narrow RZ pulses, which are subsequently multiplexed to the OTMD channel in a passive fiber delay and polarization maintaining multiplexer (MUX). Finally, the OTDM signal is demultiplexed by a nonlinear optical loop mirror (NOLM) demultiplexer (DEMUX) [16]. All components, i.e. FRS-unit, pulse compression unit, passive fiber delay multiplexer and NOLM demultiplexer are described and analyzed in this thesis both with numerical simulation and laboratory experiments.

The remaining of this thesis is organized as follows. Chapter 2 presents a brief overview about 10 Gbit/s Ethernet standards, highlighting characteristics of the common physical layer definitions. Chapter 3 discusses the time-lens-based FRS-unit, which is used to perform NRZ-RZ format conversion and retiming. The analysis in this chapter do not consider the frequency offset effect, i.e. the evaluation is done for the case where $\Delta f = f - f_L = 0$. Numerical simulation and laboratory experiments are reported as to validate the operational conditions of the proposed FRS-unit device. In Chapter 4, we extend the analysis of the FRS-unit in the presence of frequency offset, i.e. $\Delta f \neq 0$. We report the numerical simulations and laboratory experiments that were used to validate the synchronization of asynchronous 10GE-like frames to the system local clock, using the FRS-unit. In Chapter 5, we describe the remaining modules of the OTDM multiplexing system, which includes the MUX and DEMUX components. Back-to-back (error-free) operation is demonstrated through laboratory experiment, reporting the design and operation of a 330 Gbit/s OTDM multiplexing and demultiplexing system that performs add and drop operations on a 10GE-like channel. A FRS-unit is used to synchronize the 10G Ethernet asynchronous data frame to the OTDM MUX local master clock. Finally, in Chapter 6 we present our conclusions and future works.

1.4 Original Contributions

The following original contributions to the field of optical signal processing and optical fiber communication have been made in the course of this research work:

- Design, analytical evaluation, and experimentation (numerical simulation and laboratory experiments) of practical time-lenses for performing retiming of 10 Gbit/s RZ signals (Sections 3.2 and 3.5) [27].
- Design, analytical evaluation, and experimentation (numerical simulation and laboratory experiments) of the time-lens-based FRS-unit, aiming at optically processing 10GE-like frames in preparation for OTDM multiplexing. (Sections 3.3, 3.4, 3.5, and Chapter 4) [28, 29].
- Design and demonstration (laboratory experiment) of (error-free) back-to-back operation of OTDM systems that aggregates 10 GE input channels into a single high-capacity data transmission OTDM link, using the FRS-unit device for synchronization of 10 GE-like frames to the local master clock of the OTDM multiplexer (Chapter 5) [30, 31].

2 BRIEF INTRODUCTION TO 10G ETHERNET

The evolution of the Ethernet in the 70's [4, 32] not only brought a new phase in the networking speed but also spread rapidly throughout the networking world. The greatest advantages of the Ethernet are its low cost, scalability and ease to deploy and maintain [4].

The Ethernet technology has grown beyond its limited boundaries of LAN's to encompass the long distance Point-to-point links in Metropolitan Area Networks (MAN). The current generation of Ethernet standards encompasses channel speeds up to 100Gbps [34] and requires a network designed by considering bandwidth consumption and incorporate network control and management into the high capacity Metropolitan Area Network [35].

In this Chapter we present a brief review of 10 Gigabit Ethernet standards, which are used as base input/output channels for our OTDM design and experiments. In special, we highlight the asynchronous nature of 10GE and common requirements related to signal processing, including synchronization and retiming of 10GE frames.

2.1 10 Gigabit Ethernet Frame Format

The key requirement in the development of the 10 Gigabit Ethernet Frame Format [37] standards was the use of the standard Ethernet Medium Access Control (MAC) frame format, specified in IEEE 802.3 standards [36]. The main reason for this relates to seamless integration of the 10GE devices with existing Ethernet plants. More specifically, there is no need for fragmentation/reassembling and address translation, implying faster switching. The most common MAC frame format is depicted in Figure 2-1 and contains the following fields:

- **Preamble (7 bytes):** This field is an alternating pattern of ones and zeros that are used to signaling the start of an incoming frame and provides physical signaling used to retiming the frame-reception portions of receiving physical layers with the incoming bit stream. In older Ethernet standards these signaling were also used to collision detection in shared medium physical layer implementations.
- **Start-of-Frame Delimiter – SFD (1 byte):** This field is an alternating pattern of ones and zeros, ending with two consecutive 1-bits, indicating to physical layers that the next bit is the first bit of the MAC portion of the frame.
- **Destination Address – DA (6 bytes):** This field identifies which station(s) should receive the frame.
- **Source Addresses – SA (6 bytes):** This field identifies the sending station.
- **Length/Type (2 bytes):** This field indicates either the number of data bytes (payload) that are contained in the data field of the frame, or the frame type ID, if the frame is assembled using an optional format.
- **Data:** This field is a sequence of n bytes ($46 \leq n \leq 1{,}500$) of user data (frame payload).
- **Frame Checking Sequence – FCS (4 bytes):** This field contains a 32-bit cyclic redundancy check (CRC) value computed from all previous fields except from Preamble and

SFD. The encoding function is defined by the following generating polynomial in Eq. 2.1:

$$G(x) = x^{32} + x^{26} + x^{23} + x^{22} + x^{16} + x^{12} + x^{11} + x^{10} + x^8 + x^7 + x^5 + x^4 + x^2 + x + 1 \quad (2.1)$$

7	1	6	6	2	46 ≤ n ≤ 1,500	4
Preamble	**SFD**	**DA**	**AS**	**Length Type**	**Data unit + pad**	**FCS**

Source: Adapted from [17]

Figure 2-1: Ethernet Frame Format

One important feature of Ethernet frames regards to its variable and bounded frame size [1, 3, 17]. This is due to the variable-sized *Data* field, which has standardized minimum (i.e. 46 bytes) and maximum (i.e. 1,500 bytes) size. As a consequence, Ethernet MAC frames have minimum size of 64 bytes and maximum size of 1,518 bytes, not considering the *Preamble* and *SFD* fields, which are used by the physical layer. Since the full-duplex operation is used, the link distance does not affect the MAC frame size. The minimum MAC frame size will be made equal to 64 octets as specified in previous Ethernet standards. Carrier extension is not needed, as there is no CSMA/CD (Carrier Sense Multiple Access with Collision Detection) [17].

2.2 10 Gigabit Ethernet

The IEEE 802.3ae or simply 10 Gigabit Ethernet (10GE), allows high-speed communication at rates of 10 Gbit/s. 10GE is a full-duplex im-

plementation which can use optical fiber as a transmission medium to provide point-to-point connectivity in LAN, MAN, and WAN topologies. It maintains compatibility with previous Ethernet standards (i.e. 10Mbps, 100Mbps, and 1,000Mbps Ethernet) and allows them to be scaled to the 10 Gbit/s pattern. One major benefit of optical 10GE links is the length of a physical link, which can reach up to 40 km [17]. The network architecture of 10GE is shown in Figure 2-2.

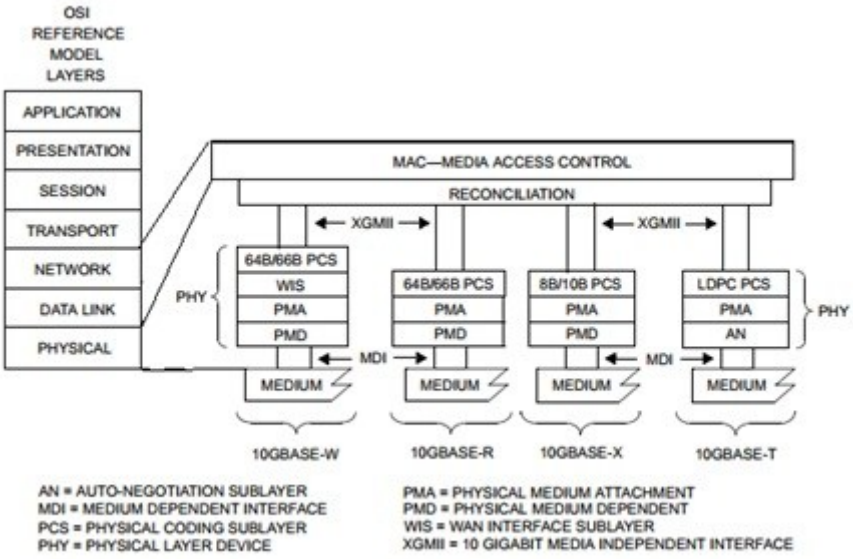

Source: adapted from [17], pp. 2

Figure 2-2: Architecture of 10GE

2.2.1 Types of 10 G Ethernet Physical (10GE PHY)

These are the most used 10GE PHY nowadays:

- **10GBASE-W (WAN):** defines WAN encoding for 10GbE, it encodes the frames so that they are compatible with *Synchronous Optical Network* (SONET) STS-192c data rates and *Synchronous Digital Hierarchy* (SDH) VC-4-64 transmission standards allowing for 10 Gbit/s transmission across a WAN.

It does this by wrapping the 64B/66B payload [17] into a SONET frame, making the effective rate 9.95 Gbit/s.

- **10GBASE-R (LAN):** is the serial encoded *Physical Coding Sublayer* (PCS) that allows for Ethernet framing at a rate of approximately 10.3 Gbit/s, i.e. a MAC rate of 10.0 Gbit/s is obtained by using a 10.0 * 66/64= 10.3125 Gbit/s equivalent line coding rate in order to compensate for the 64B/66B encoding scheme.
- **10GBASE-X (LAN)**: uses similar coding methods as 10GBASE-R but is only used in the definition of 10GBASE-LX4 [17]. This is mainly because LX4 operates on both single and multimode fibers, giving it a unique set of specifications as defined in its PMD.
- **10GBASE-T (Copper / LAN):** provide 10 Gbit/s connections over unshielded or shielded twisted pair cables, over distances up to 100 meters.

2.2.2 10GE 64B/66B PCS (Physical Coding Sublayer)

In data networking and transmission, 64B/66B is a line code that transforms 64-bit data to 66-bit line code to provide enough state changes to facilitate clock recovery and time-alignment (i.e. retiming) of the data stream at the receiver [38].
The PCS [40] uses a transmission code to improve the transmission characteristics of information to be transferred across the link and to support transmission of control and data characters.

The encoding also preserves the likelihood of detecting any single or multiple bit errors that may occur during transmission and reception of information. In addition, the synchronization headers of the code enable the receiver to achieve block alignment on the incoming PHY bit stream. The 64B/66B transmission code specified for use in 10GE standards has a high transition density and is a run-length-limited code [38].

2.2.3 10GE PMA (Physical Medium Attachment)

The PMA [41] provides a medium-independent means for the PCS to support the use of a range of physical media and performs the following functions for 10GBASE-R and 10GBASE-W [17], which are the standards we are using in this thesis:

- Mapping of transmit and receive data streams between the PCS and PMA via the PMA service interface.
- Serialization and deserialization of bits for transmission and reception on the underlying serial Physical Medium Dependent (PMD) sublayer.
- Clock recovery from the received data stream.
- Mapping of transmit and receive bits between the PMA and PMD via the PMD service interface.
- Optionally provides data loopback at the PMA service interface.

2.2.4 10GE PMD (Physical Medium Dependent)

The Physical Medium Dependent (PMD) [42] sublayer consists of a transceiver for the physical medium and performs the transmission and reception of base band (NRZ) serial bit streams on the underlying medium.

Optical transceivers, called Physical Media Dependent (PMD), are defined for single-mode fibers, which can be used in LAN and WAN networks. With this setting, arose two new kinds of physical layer (PHY): LAN PHY and WAN PHY. The first is used to transmit Ethernet frames in a local network, while the second enables the transport on existing infrastructures like SONET or SDH (Synchronous Digital Hierarchy) [17]. This is the most relevant physical sublayer to the work presented in this thesis, as it defines the line coding format of optical pulses.

The interface with the physical medium is accomplished by a standard called 10Gigabit Attachment Unit Interface (XAUI), offering seven different types of connections: 10GBASE-LX4, 10GBASE-SR, 10GBASE-LR, 10GBASE-ER, 10GBASESW, 10GBASE-LW and 10GBASE-EW, which differ in the type of physical layer applied (LAN PHY or WAN PHY) and the model used fiber (SMF or MMF).

2.2.5 Asynchronous Nature of 10 GE

The 10GE Optical links transmit frames asynchronously with Non-Return-to-Zero (NRZ) line code [41, 43] and nominal frequency (bit rate) *f*. The latter varies up to ± 20 ppm of the nominal transmission rate, i.e. up to ± 200 kHz frequency offset according to the 10GBASE-W PHY (WAN PHY) standard, and up to ±100 ppm, i.e. up to ± 1 MHz frequency offset according to the 10GBASE-R PHY (LAN PHY) [17]. This thesis addresses these features since they have direct implications on multiplexing 10GbE data into OTDM, as OTDM is a bit-interleaved synchronous system based on Return-to-Zero (RZ) narrow pulses. These particularities are addressed in Chapters 4 and 5 of this thesis.

3
10GBIT/S NRZ-RZ FORMAT CONVERSION AND RETIMING

This Chapter presents the proposed FRS-unit for performing the NRZ-RZ format conversion and retiming functions. Thus, in this Chapter, there is no frequency offset between incoming signal and the local clock ($\Delta f = 0$). Format conversion is based on an intensity modulator implemented by a Mach-Zehnder Modulator (MZM) driven by an electrical sinusoidal RF signal with the frequency of the OTDM local clock fundamental frequency (f_L) [12]. Retiming is based on a time-lens device [25, 27], which the concept relies on the mathematical equivalence between spatial diffraction and temporal dispersion, the so called space-time duality. A lens held at fixed distance from an object produces a magnified visible image. The lens imparts a quadratic phase shift to the spatial frequency components of the optical waves; in conjunction with the free space propagation (object to lens, lens to eye), this generates a magnified image. Owing to the mathematical equivalence between paraxial diffraction and temporal dispersion, an optical waveform can be temporally imaged by a three-step process of dispersing it in time, subjecting it to a phase shift that is quadratic in time (the time lens itself), and dispersing it again [20].

A time-lens is usually composed by a dispersive element and the use of a phase modulator that is driven by the sinusoidal signal. Sinusoidal signals are easily generated and have no discontinuities in its time derivative, as opposed to periodic parabolic signals, which have time

derivative discontinuities (i.e. for each $t = nT_L$) see Figure 3-5. Indeed, a sinusoidal signal is a good approximation to the ideal parabolic drive, near the maximum (or minimum) of the signal.

In order to process a pulse train, the signal frequency f_L should equal the fundamental frequency of the bit rate (e.g. a pulse train of 10 Gbits/s should have f_L = 10 GHz). This Chapter discusses and analyzes the limitations of this optical processing device, both analytically and by using numerical simulation.

The analysis in this Chapter do not consider the full operation of the FRS unit as the frequency offset between incoming signal and the local clock is zero, (i.e., $\Delta f = 0$). Synchronization and frequency offset compensation are considered in Chapter 4, while the complete design of the OTDM multiplexing system shown in Figure 1-1 is discussed in Chapter 5.

3.1 NRZ-RZ Format Conversion

On-off-key (OOK) NRZ and RZ are intensity modulation formats [12]. NRZ-RZ format conversion in this proposal is obtained by a pulse carver that is used to turn an optical NRZ format into its RZ equivalent. A pulse carver can conveniently be implemented as a sinusoidally driven Mach-Zehnder Modulator (MZM). MZM enables the possibility of independently modulating intensity and phase of the optical field reference. A possible drawback is the polarization dependence of the device, which requires some control of the State of Polarization (SOP) of the incoming signal.

In this design, the MZM is used as an intensity modulator which is driven by sinusoidal signal, biased at $Vpp/2$, oscillating at the OTDM local clock frequency f_L, which corresponds to the bit rate of the input NRZ signal. This results in RZ optical pulses with full-width at half-

maximum of 50% (duty cycle of 50%)[12, 44], as shown in Figure 3-1.

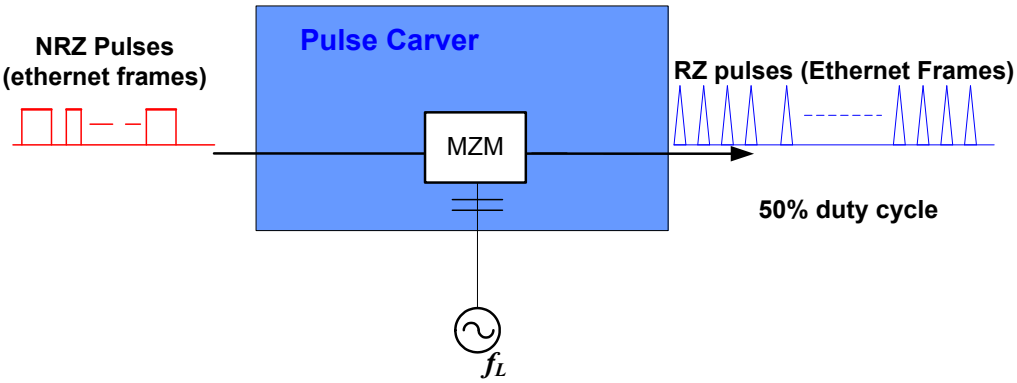

Figure 3-1: Pulse carver (MZM)

Note that, in order for this scheme to be effective, the sinusoidal drive signal must be reasonably time-aligned to the center of the NRZ input pulse. Let Δt represent the time misalignment between NRZ input pulse and the local clock signal and Δt is formally defined as the time difference between the time position of the center of the input pulse and the time position of the maximum of the local clock. As $T_L = T$ ($\Delta f = 0$), all the incoming pulses will have the same Δt in this particular case. Figure 3-2 illustrates different input pulses with distinct values for Δt. For $|\Delta t| > \Delta t_{op}$, the output RZ-converted pulse becomes distroced. Therefore, we can establish an operational range for the circuit based on the condition expressed in Eq. 3.1, where $\Delta t_{op\ (\text{pulse carver})}$ denotes the operational range of the pulse carver. A similar operational conditional is established for the time-lens retiming circuit (see Sections 3.2). These conditions are experimentally evaluated in this thesis.

$$| \Delta t | < \Delta t_{op\ (\text{pulse carver})} \qquad (3.1)$$

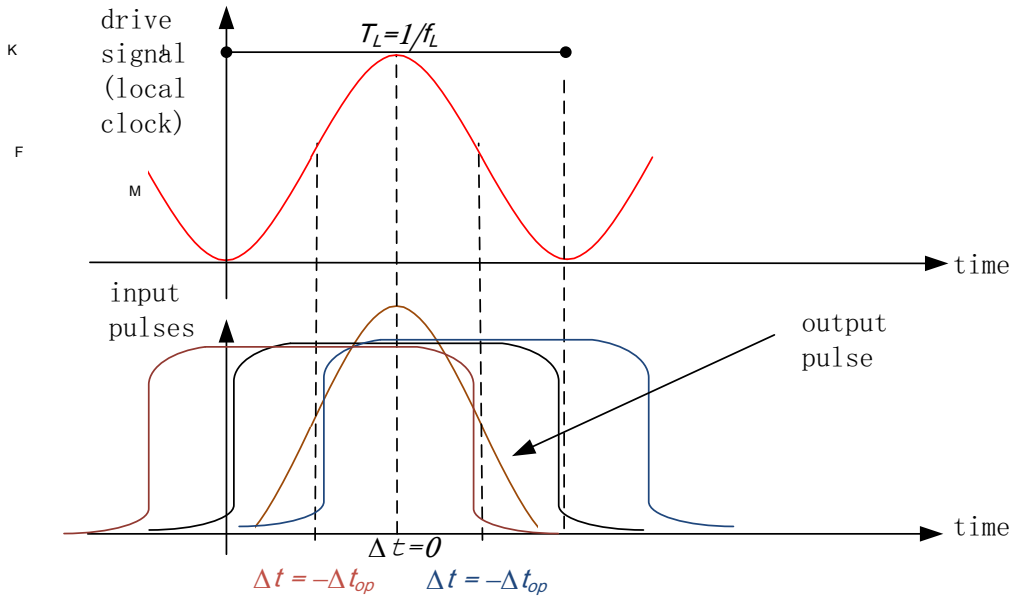

Figure 3-2: Time-misalignment of NRZ input pulses and MZM sinusoidal driving signal

3.2 Retiming of RZ pulses with Time-Lens

An ideal time-lens is realized by quadratic phase modulation combined with dispersion [20, 22, 27]. The reason for using quadratic phase modulation is that this is used to induce a linear chirp in the optical signal, which can be easily compensated with linear optical dispersion. An optical pulse that is subjected to this ideal time-lens, i.e. implemented with perfectly quadratic phase modulation, can be linearly compressed (or expanded) [45] in the time scale, without distortion in the pulse shape.

The interest here is in processing an OOK RZ pulse train, each pulse having a period of $T = 1/f$, where f is the frequency of the bit rate, as shown in Figure 3-3. Therefore, in order to process this pulse train, the signal driving the phase modulator (PM) should be periodic. The periodic parabolic drive is depicted in Figure 3-3.

The ideal time-lens is, then, implemented as a phase modulator (PM) driven by a parabolic periodical signal with frequency f_L – the local clock – followed by a dispersive element, such as a piece of fiber (SMF or DCF) [18, 19, 20, 21, 22, 24, 25]. In this section, we are considering $T_L = T$, or simply, $f = f_L$ ($\Delta f = 0$).

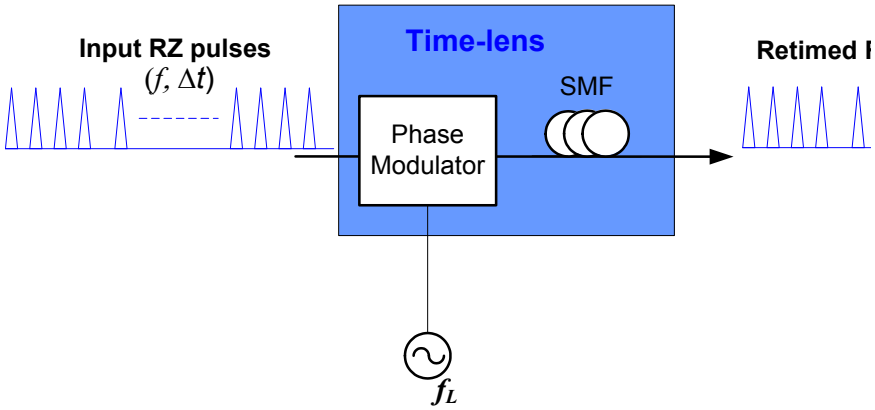

Figure 3-3: Time-lens used for Retiming of RZ input pulses

Previously, optical NRZ-to-RZ conversion has been demonstrated by various approaches including the use of high non-linear fiber (HNLF) [46, 47], semiconductor optical amplifier (SOA) [48], micro-ring resonator [49] and optoelectronic oscillators [50]. However, some of these schemes could introduce serious inter channel cross-talk when applied to a multi-channel system.

Again, let Δt represent the time misalignment between input pulse and the local clock signal. We are using here the same definition for Δt as provided in Section 3.1, i.e. Δt is defined as the time difference between the time position of the center of the input pulse and the time position of the maximum of the local clock. As $T_L = T$ ($\Delta f = 0$), all the incoming pulses will have the same Δt in this particular case. Figure 3-4 illustrates different input pulses with distinct values for Δt.

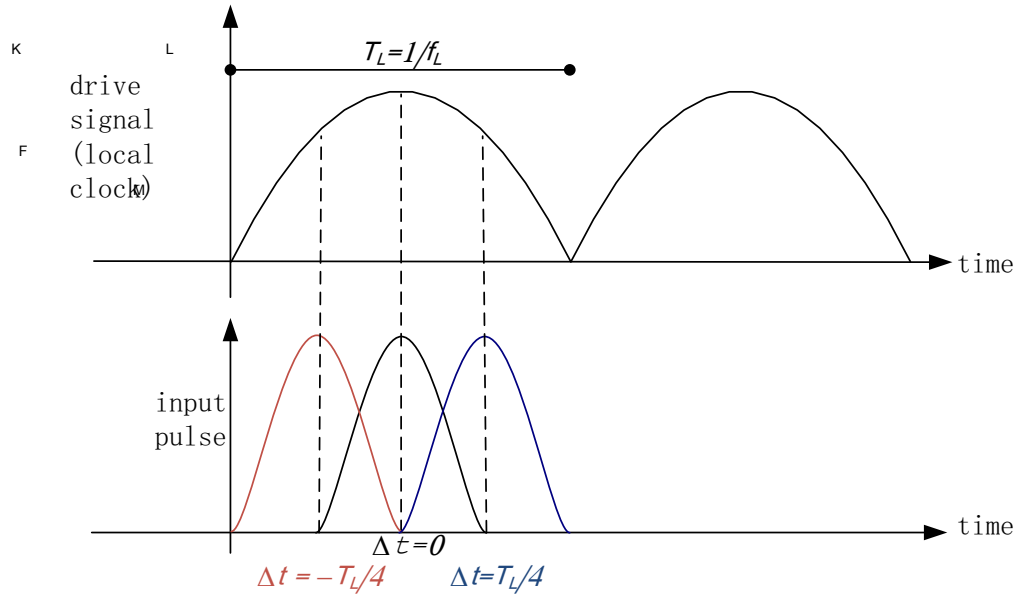

Figure 3-4: Time-misalignment between RZ input pulses and parabolic local clock

Note that the parabolic signal represented in Figure 3-4 has discontinuities in its time derivative near the transitions of the bit period, i.e. where the signal reaches its minimum ($t = nT_L$). Therefore, such type of periodic signals cannot be used for time misalignments

where the input pulse is subjected to a phase modulation driven in the discontinuity range [51]. This extreme case is shown in Figure 3-5.

Therefore, the ideal time-lens circuit can only be used for certain values of Δt. This condition is expressed in Eq. 3.2, where Δt_{op} (time-lens) defines the operational range for the circuit. Note that Eq. 3.1 and 3.2 have similar expressions, although each circuit has a specific value for Δt_{op}.

$$|\Delta t| < \Delta t_{op}\ \text{(time-lens)} \qquad (3.2)$$

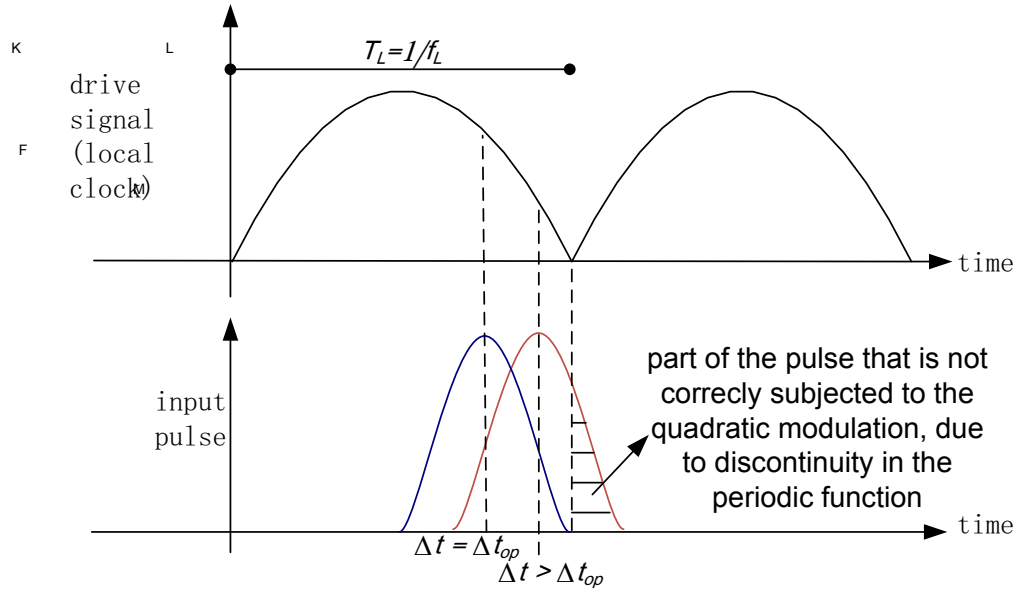

Figure 3-5: Operational range of a time-lens with periodic quadratic phase modulation

The limitation expressed in Eq. 3.2, together with the need for an arbitrary waveform generator in order to get a parabolic signal, en-

courage the use of practical time-lenses where the driving signal is sinusoidal, as this signal can be easily generated using a synthesizer. For a sinusoidal driving signal expressed in Eq. 3.3, the driving signal is approximately quadratic for Δt close enough to the local clock maximum (or minimum). Note that this condition can be expressed in the same way of Eq. 3.2. Let us consider that the incoming signal is phase modulated by a sinusoidal signal of frequency f_L. The voltage signal ($V(t)$) driving the phase modulator is represented in the time domain as Eq. 3.3:

$$\mathrm{V}(t) = \frac{\mathrm{Vpp}}{2}\cos(\omega_L t) \qquad (3.3)$$

where *Vpp* is the peak-to-peak voltage variation and $\omega_L = 2\pi f_L$ is the angular frequency of the sinusoidal drive signal (i.e., the system local clock).

The phase shift induced by the phase modulator is given in Eq. 3.4:

$$\varphi\,(t) = \pi\,\frac{V(t)}{V_\pi} \qquad (3.4)$$

This can be expressed as Eq. 3.5:

$$\varphi\,(t) = \frac{\pi}{2V_\pi}\mathrm{V_{pp}}\cos(\omega_L t) \qquad (3.5)$$

Introducing the notation for the modulation index *M* as defined in

Eq. 3.6:

$$M = \frac{\pi}{2V_\pi} \mathrm{V_{pp}} \tag{3.6}$$

The phase shift induced in PM can be, therefore, expressed as Eq. 3.7:

$$\varphi(t) = M \cos(\omega_L t) \tag{3.7}$$

If the time misalignment Δt is close enough to the maximum of the cosine function, the phase shift can be approximated locally by Eq. 3.8:

$$\varphi(t) \simeq \mathrm{M} \left(1 - \frac{\omega_L^2 \Delta t^2}{2}\right) \tag{3.8}$$

The relative phase shift at time misalignment Δt, when compared to the one at $\Delta t = 0$ (i.e. the pulse is aligned with the maximum of the cosine) becomes (Eq. 3.9):

$$\Delta\varphi(\Delta t) \simeq -M \frac{\omega_L^2 \Delta t^2}{2} \tag{3.9}$$

The corresponding chirp is the variation of the optical frequency of the signal (or variation on wavelength) due to the phase modulation and is given by the time derivative of the phase deviation, as shown

in Eq. 3.10:

$$\delta\omega(t) = -\frac{\partial\varphi}{\partial t} \qquad (3.10)$$

The chirp therefore is expressed as in Eq. 3.11:

$$\delta\omega(\Delta t) = M\omega_L^2\Delta t \qquad (3.11)$$

From Eq. 3.11, it is clear that the chirp is linear, with a chirp rate expressed by $C = M\omega_L^2$.

The chirp (or deviation from a reference optical frequency ω_0) of a pulse depends on the temporal misalignment Δt with respect to the maximum of the sinusoidal phase modulation. If the signal is further propagated in a dispersive medium of dispersion β_2 and the length L, the different frequency components travel at different velocities, and one will obtain a timing misalignment, with respect to a pulse located at $\Delta t = 0$, of (Eq. 3.12):

$$\Delta t_{fiber} = \beta_2 L\delta\omega = \beta_2 LM\omega_L^2\Delta t \qquad (3.12)$$

Therefore, the total time misalignment at the output of the time-lens is expressed in Eq. 3.13.

$$\Delta t_{\text{total}} = \Delta t + \Delta t_{\text{fiber}} = \Delta t\,(1 \pm \beta_2 L M \omega_L^2) \quad (3.13)$$

Retiming is achieved when $\Delta t_{\text{total}} = 0$, hence (Eq. 3.14):

$$1 \pm \beta_2 L M \omega_L^2 = 0 \text{ or } \beta_2 L = \frac{1}{M\omega_L^2} \quad (3.14)$$

From Eq. 3.14, we can find the condition linking the modulation index and the fiber parameters β_2 and L in order to retime the signal to f_L. Note that Eq. 3.14 also expresses the compression ratio for the output pulses due to group velocity dispersion (GVD) [52]. $\beta_2 L$ can be set to a value that is greater than one, leading to pulse compression [24].

Figure 3-6 presents some of the consequences of using a more practical sinusoidal phase modulation, instead of the theoretical quadratic phase modulation. The dark blue line shows the modulating sinusoidal signal ($\Delta\varphi$), with its maximum placed to the center position ($\Delta t = 0$). The green line shows the induced chirp ($\Delta\omega$), which is the time derivative of the phase shift produced by the phase modulation driven by the sinusoidal signal. The red line shows the ideal linear chirp that would result from the quadratic phase modulation ($\Delta\omega_{\text{ideal}}$). The chirp from sinusoidal signal deviates from the linear chirp for all signals except at $\Delta t = 0$. However, there is a time interval where the deviation is so small that, in practice, the sinusoidal and the quadratic modulations can be assumed to have identical effects in the optical pulse. This deviation is shown by the light blue line ($\Delta\omega - \Delta\omega_{\text{ideal}}$).

The conclusions for analyzing Figure 3-6 are that, in the case of the

sinusoidal drive, there will be an operational range Δt_{op}, which can also be expressed as by Eq. 3.1. This Δt_{op} is used to express the values of Δt for which the sinusoidal function is a good approximation for a quadratic function. In this thesis, we derive this operational range with numerical simulations and laboratory experiments, rather than obtaining an analytical expression for this.

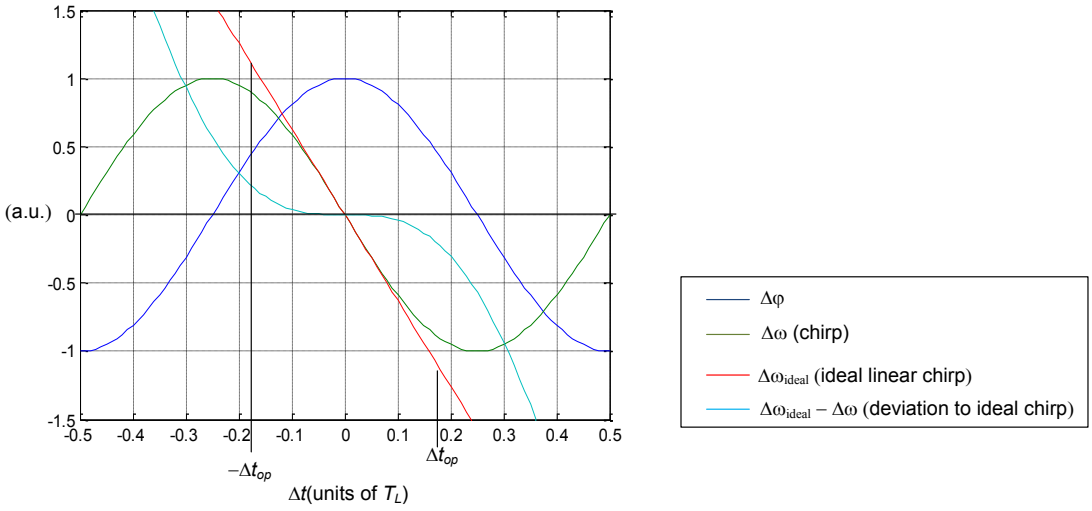

Figure 3-6: Ideal quadratic chip vs. sinusoidal chirp

Figure 3-7 illustrates the cases where $|\Delta t| = \Delta t_{op}$, which correspond to the limits of the operational range for the circuit. For pulse with Δt outside the operational range, we expect to observe the following effects:

- Pulses can become distorted (in shape), as the chirp would not be considered linear for the whole pulse duration.
- Retiming would not work properly, which should be translated in some remaining time-misalignment after the pulse has been processed by the time-lens.

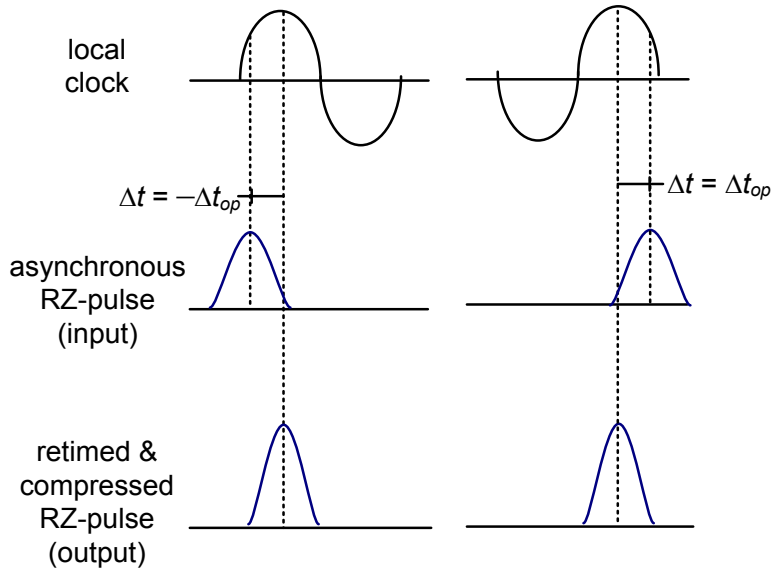

Figure 3-7: Operational range $\Delta t \in (-\Delta t_{op}, \Delta t_{op})$ of a sinusoidally driven time-lens

So, when using the sinusoidal control signal in the PM, we expect to have a practical time-lens that is able to retime input RZ pulses to the local clock (i.e. to the maximum of the sinusoidal signal), and should also produce additional compression of the pulse, which is due to group velocity dispersion of the chirped pulse in the dispersive medium. This is the effect that we use to build our FRS-unit device.

3.3 NRZ-RZ Format Conversion and Retiming with Pulse Carver + Time-lens

Figure 3-8 illustrates the complete FRS-unit, which consists of a Phase Modulator (PM), cascaded with a pulse-carving Mach-Zehnder Modulator (MZM), followed by a piece of fiber as dispersive element.

Both the PM and the MZM are driven by a sinusoidal signal, oscillating at the local clock corresponding to the frequency of the bit rate. Note that bit rate is in bit/s whereas a clock is in Hz. In this configuration, the PM approximates a quadratic phase modulation and is used to introduce linear chirp at the optical signal, while the MZM is used to remove the part of the input waveform subjected to the upper part of the sinusoidal phase modulation. Thus, the MZM acts as a pulse carver, performing NRZ-RZ format conversion. As previously discussed, this design allows for a resulting RZ signal with 50% duty cycle [12, 44]. Finally, the dispersive element (e.g. SMF) provides the temporal focus in the system by eliminating the chirp in the optical signal.

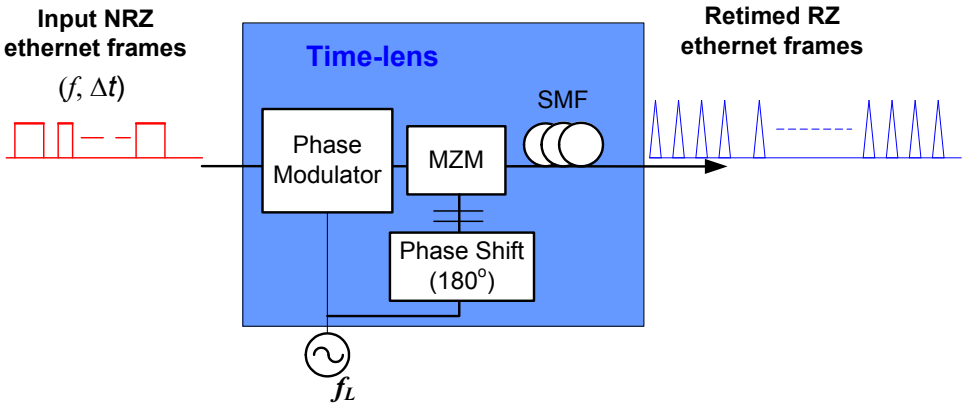

Figure 3-8: FRS-unit based on a pulse carver + time-lens

The circuit in Figure 3-8 is subjected to operational conditions imposed by both the pulse carver (Eq. 3.1) and the time-lens (Eq. 3.2). This can be generalized in as in Eq. 3.15.

$$|\Delta t| < \Delta t_{op} \qquad (3.15)$$

3.4 Analysis of Practical Time-lens for Retiming of Asynchronous Pulses

In order to evaluate the operational range (Δt_{op}) of the pulse carver + time-lens circuit described in the last section, three performance metrics are used: Eye Contrast Ratio (*ECR*), Output Time Misalignment ($\Delta\tau$), and Full Width Half Maximum (*FWHM*), which are presented and discussed in this section.

3.4.1 Eye Contrast Ratio (*ECR*)

The *ECR* is a measure for the vertical opening height of an eye pattern and is defined as the difference between minimum power level representing bits "1" ($P_1 min$) and the maximum power level representing bits "0" ($P_0 max$). This is shown in Eq. 3.16, for power levels expressed in *dBm* and *ECR* in *dB*:

$$ECR\ (dB) = P_1\, min(dBm) - P_0\, max(dBm) \quad (3.16)$$

Figure 3-9 shows the eye contrast ratio, for a typical eye diagram of retimed output RZ signal generated from an input RZ signal using a time-lens as shown in Figure 3-3. This diagram is generated for a time-lens optimized for $f = f_L$ = 10 Gbit/s, as per Eq. 3.14. The incoming signal is a RZ signal with $\Delta t = 0.05 T_L$ and extinction ratio of 20 *dB*.

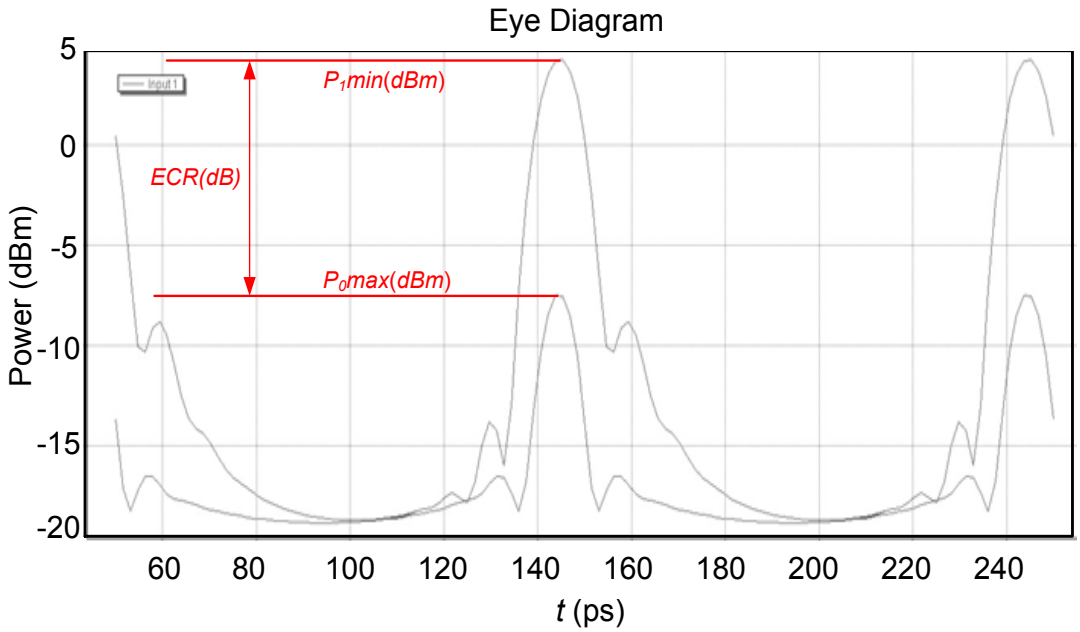

Figure 3-9: Eye Contrast Rate definition ($\Delta t = 0.05T_L$)

In order to evaluate the *ECR* from the eye diagram, the sampling point of the '1' and '0' bit levels must be precisely identified. Based on the definition of *ECR*, the ideal sampling point corresponds to the time where the signal level reaches its maximum, for each '0' pulses, and its minimum, for each '1' pulses. Clearly, if retiming is obtained, these would be the same, as shown in the eye diagram from Figure 3-9.

However, for time misalignments outside the operational range, i.e. when $|\Delta t| < \Delta t_{op}$, the evaluation of *ECR* can be challenging, because of pulse distortions that occurs in the output pulses, due to deviation of the sinusoidal phase modulation in relation to the ideal quadratic phase modulation. Also, the minimum '1' level and the maximum '0' level in the eye diagram can be time-misaligned. These effects can be observed in the eye diagram in Figure 3-10, which shows the *ECR*

calculation for the same time-lens used and RZ input pulses in the example of Figure 3-9, except from the time misalignment parameter that has been set to $\Delta t = 0.25T_L$.

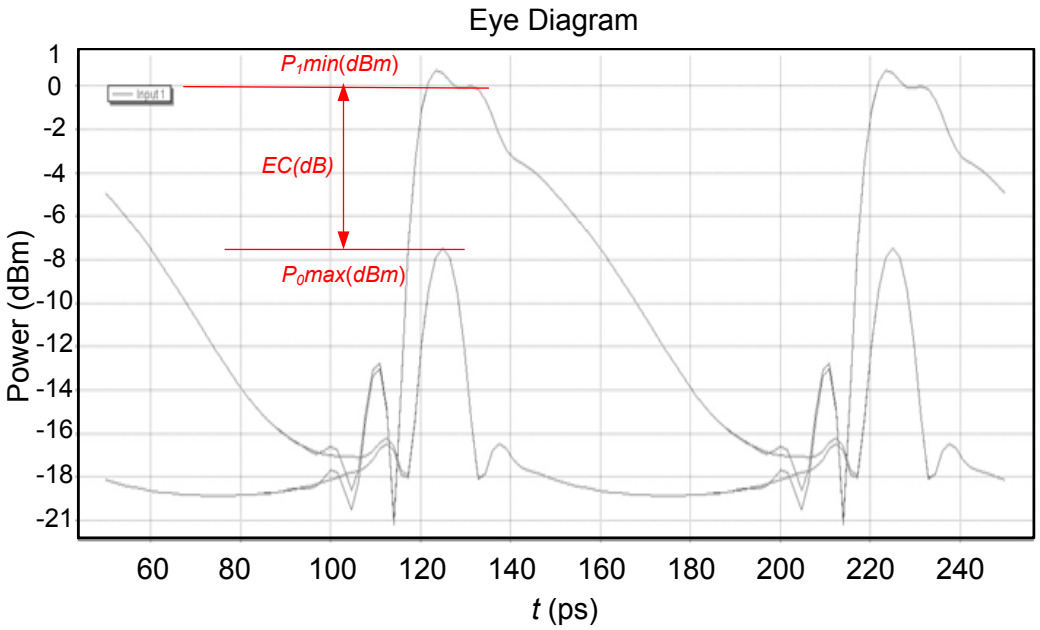

Figure 3-10: Eye Contrast Ratio ($\Delta t = T_L/4$)

3.4.2 Output Time Misalignment ($\Delta\tau$)

The second metric looks for the resulting time misalignment in the output pulse, measured as the time difference of the maximum of the pulse and the maximum of the sinusoidal clock, which represents the focal point of the time-lens. This metric is evaluated from waveform patterns of the output pulses and can be expressed by Eq. 3.17, where $t_{\Delta t=0}$ is the time value where the sinusoidal drive signal reaches its

maximum, and t_{max} is the time value where the output pulse reaches its maximum. In order to calculate $\Delta\tau$ in Eq. 3.17, the waveform of the output pulses representing '1' bits where fit to a Gaussian function in order to estimate its maximum value t_{max}, i.e., the mean parameter in the Gaussian function. The maximum of the sinusoidal signal ($t_{\Delta t=0}$) is deterministically identified.

$$\Delta\tau = t_{\Delta t=0} - t_{max} \qquad (3.17)$$

Figure 3-11 illustrates the output time misalignment ($\Delta\tau$) calculation. The waveforms of the sinusoidal drive signal (i.e., the local clock signal) and the output *RZ* pulses shown in the diagram were obtained from the setup shown in Figure 3-3, for a time-lens optimized for $f = f_L$ = 10 Gbit/s, as per Eq. 3.14. The incoming signal is a RZ signal with $\Delta t = 0.1T_L$.

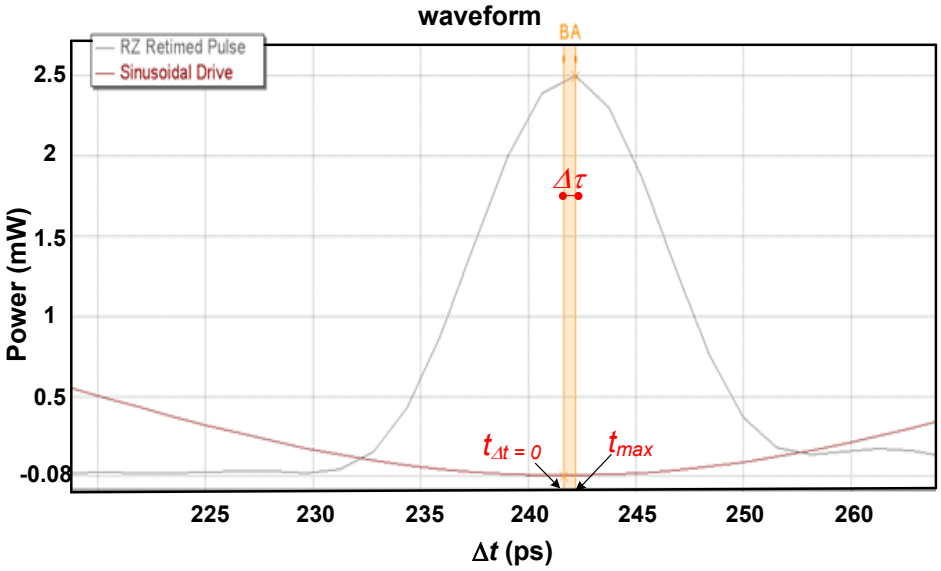

Figure 3-11: $\Delta\tau$ definition: waveforms for (a) output RZ signal, and (b) sinusoidal clock ($\Delta t = 0.1\ T_L$)

3.4.3 Full Width Half Maximum (FWHM)

Full width at half maximum (FWHM) is given by the distance between points on the curve at which the function reaches half its maximum value, as shown in Figure 3-12. FWHM is applied to measure the duration of pulse waveforms, and as a function to determine duty-cycle of RZ pulses.

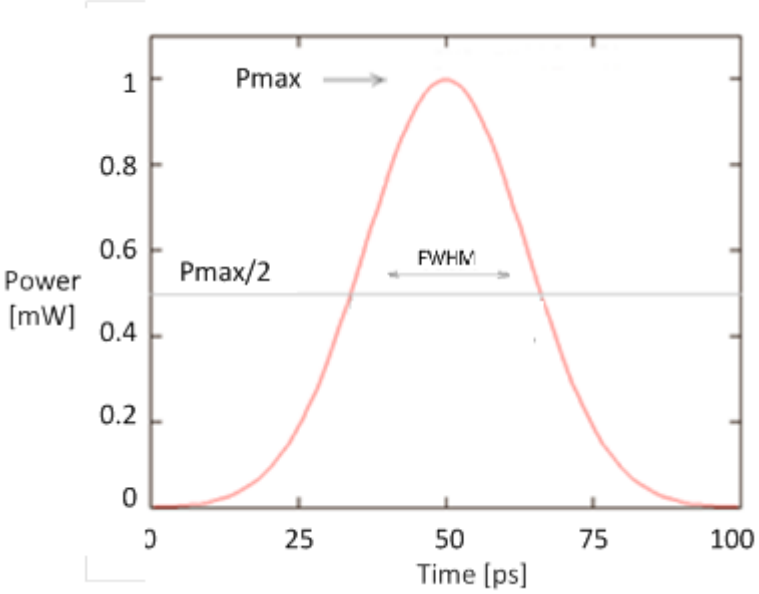

Figure 3-12: FWHM definition

FWHM is evaluated from eye diagram patterns of output pulses, as shown in Figure 3-13, which is obtained for a FRS-unit as shown in Figure 3-8. The time-lens used is optimized for f = fL = 10 Gbit/s, as per Eq. 3.14. The incoming signal is a RZ signal with $\Delta t = 0$. FWHM is defined when eye-diagram for output RZ signal shows it has no time misalignment, $\Delta t = 0$.

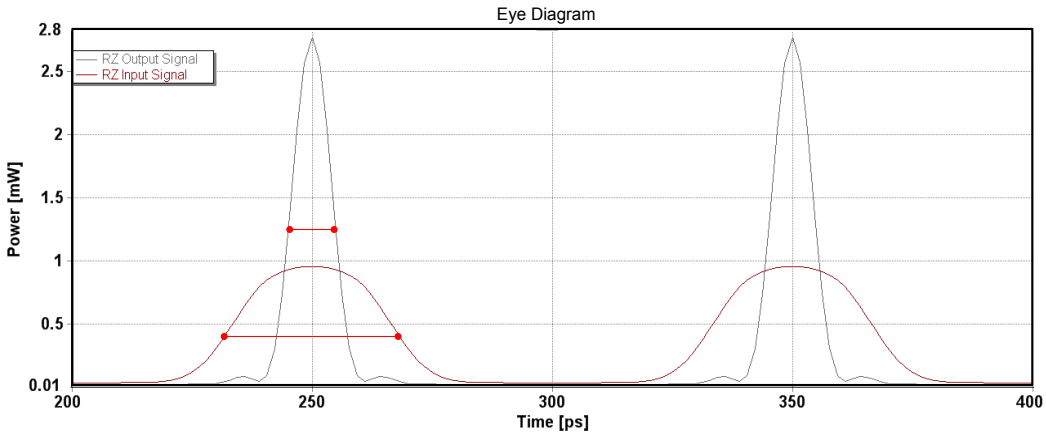

Figure 3-13: FWHM: eye-diagram for output RZ signal ($\Delta t = 0$)

3.4.4 Metrics Evaluation

As shown in Figure 3-6, the induced chirp inside the operational range of the device is approximately linear with Δt, which allows the correct optical processing of the input pulses – the pulses are time position locked to the focal point of the time-lens. However, outside the operational range (i.e., $|\Delta t| > \Delta t_{op}$), the induced chirp is nonlinear. Therefore, the interplay between chirp and dispersion is not optimum, which results in:

- Decreased *ERC*: Pulses that are not subjected to linear chirp are at the output of the FRS unit likely to appear with less peak power (i.e., minimum power for bits '1'), due to the distortions in the pulses, in relation to pulses processed with $|\Delta t| < \Delta t_{op}$. Also, if $T_L/2 > |\Delta t| >> \Delta t_{op}$, it can result in some type of "inter-symbol interference", due to an input pulse being subjected to the sinusoidal phase modulation corresponding to different bit period slots in the local clock. These conditions are detected as a decreasing in the *ECR*.
- Increased $|\Delta\tau|$: Pulses that do not receive enough chirp in the PM and cannot be correctly adjusted to the focal point of the

time-lens. These will be ahead in time ($if\ \Delta t\ > 0$) or delayed ($if\ \Delta t\ < 0$) compared to the local clock reference, i.e. the sinusoidal maximum. This is detected as an increasing in the absolute value of Δt

- Increased *FWHM*: Pulses that do not adjust to the focal point of the system are stretched in time (larger) – compared to pulses that are properly compressed. This is detected as an increasing in the *FWHM* metric.

These properties are evaluated in the next section for:

- RZ input signal
  - Time-lens only
  - No pulse carver, as the setup shown in Figure 3-3
- NRZ input signals
  - Pulse carver
  - Time-lens, as the setup shown in Figure 3-8.

The basic evaluation consists in determining *ECR*, $\Delta\tau$, and *FWHM* as function of Δt ($-T_L/2 < \Delta t < T_L/2$) in order to identify the appropriated operational range (Δt_{op}) of the device by evaluating the deviation of the defined metrics in respect to the reference values established for $\Delta t = 0$ (no time misalignment).

3.5 Analysis of Practical Time-lens: Numerical Simulations

In this Section, the practical time-lens limitations described in the last section are demonstrated by numerical simulations of the schemes presented in Figure 3-3 and Figure 3-8.

Simulations were run with the VPI Transmission Maker Gui Version 8.6 (Build: 284). We have simulated setups for (1) retiming of time-misaligned RZ input pulses (time-lens only, as in Figure 3-3) and (2) NRZ-RZ format conversion and retiming of time-misaligned NRZ input pulses (time-lens + pulse carver, as in Figure 3-8). There is no frequency offset ($\Delta f = 0$) for the simulations described in this Section.

In both cases, the sweep of the time misalignment (Δt) is generated by a controllable phase shift (PS) module, as shown in Figure 3-14, which is used to set the time misalignment of input pulses in relation to the local clock in the simulations

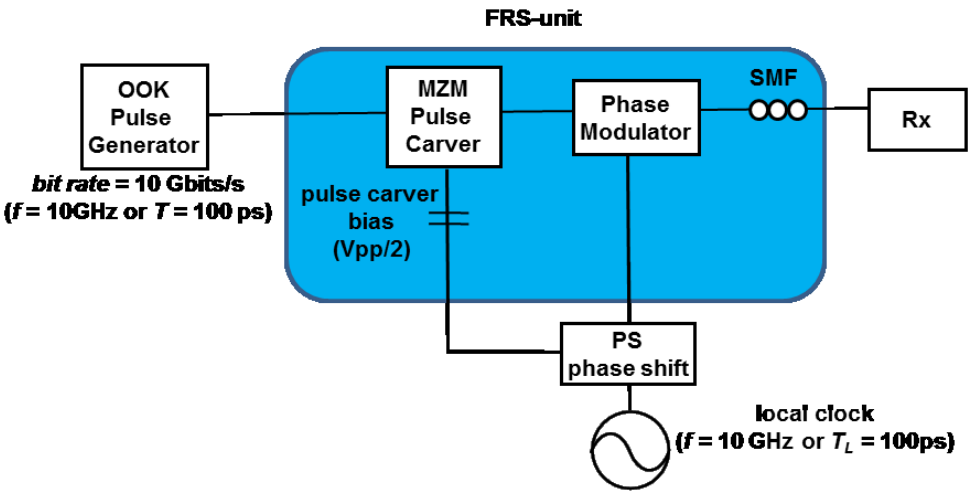

Figure 3-14: Numerical Simulation Setup (NRZ case)

The system parameters for the simulation are as follows:

- OOK
  - Input pulse bit rate: 10Gbit/s (f = *10* GHz and T = 100ps)
  - Input pulse format: *RZ* (33% duty cycle) or NRZ
  - 8.192 bits generated using a Pseudo-Random Binary Sequence (PSBR) with $2^7 - 1$ length.

  - Extinction Ratio = 20 *dB*
- Phase Modulator
  - $M = Vpp / V_{\pi} = 2.7\pi$
- SMF
  - GVD parameter (β_2): -20 ps/m^2
  - Length: 3 km (as designed per Eq. 3.14).
- Local clock
  - f_L = 10 GHz (T_L = 100 ps)

3.5.1 Retiming of RZ Asynchronous Pulses (time-lens only)

Figure 3-15 shows the VPI Transmission Maker setup for the numerical simulations used to characterize the retiming of RZ time-misaligned pulses. Note that, in this case, there is no pulse carver. Very briefly; the simulation set-up consists of the following modules [54]:

- CoderRZ (OOK): Used to produce the RZ signals, where:
  - Each 1 is partially coded as samples with amplitude 1.0, and partially coded with samples with amplitude 0.0.
  - The DutyCycle_RZ (CoderDriver_OOK) and PulseLengthRatio (CoderRZ) defines the width of the 1.0-amplitude part of the bit.
  - Each 0 is coded as samples with amplitude 0.0.
  - No jitter added
- PhotoDetector (PD) – No noise added.
- Signal Analyzer
- Phase Modulator (PM): Phase Deviation of 180.0 × 2.7 deg
- Single Mode Fiber: 3km

- PhotoDetector (PD) – No noise added
- Signal Analyzer
- FuncSineEl: Sinusoidal.
    - Frequency 10e9Hz
    - amplitude of 0.5 a.u.
- PhaseShift
    - used for the pulse delay
- DC
    - Amplitude: 0.5 V

The objective is to derive the operational range Δt_{op} as a function of the performance metrics *ERC*, $\Delta\tau$, and *FWHM*.

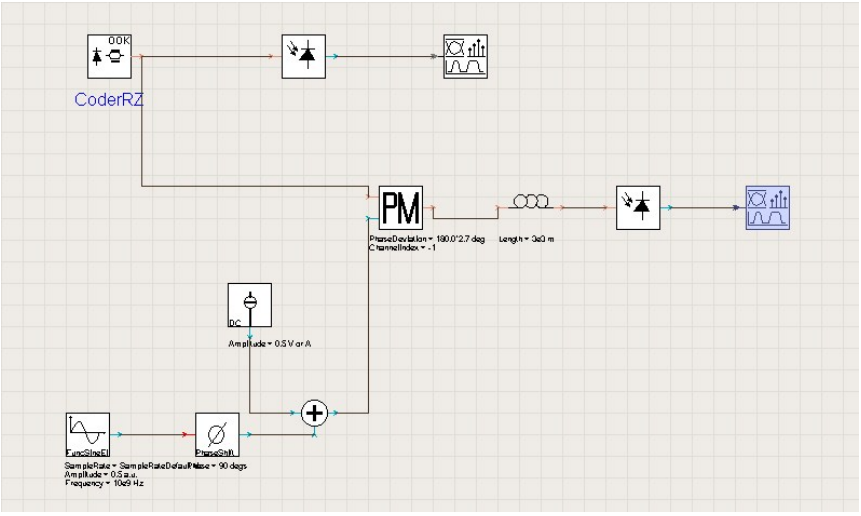

Figure 3-15: Numerical Simulation Setup (VPI Transmission Maker): RZ input pulses

ECR Evaluation

Figure 3-16 shows the *ECR* as a function of the time misalignment, obtained for the setup in Figure 3-15. In order to establish the operational range of the circuit, it is possible to define a *threshold* for the decreasing of *ECR*, as shown in Eq. 3.18:

$$ECR(\Delta t = 0) - ECR(\Delta t_{op}) = threshold \quad (3.18)$$

Three typical values were evaluated for this *threshold*: 1, 2 and 3 *dB*. In Figure 3-16 the *ECR* is determined for the RZ case. The *threshold* and the respective operational range definition are also shown in Figure 3-16.

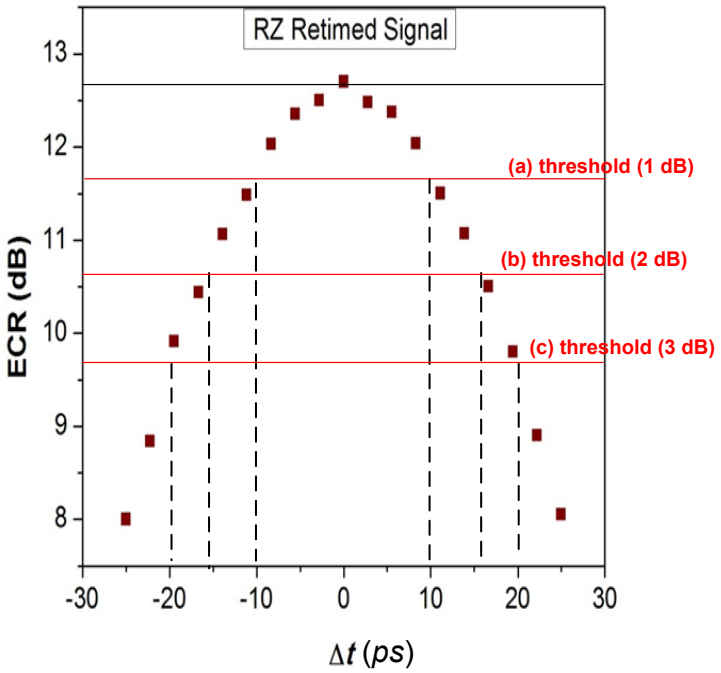

Figure 3-16: ECR versus Δt: operational range of Time-lens (RZ input pulses)

For each *thresholds* value, the operational range obtained from Figure 3-16 is shown inTable 3.1.

Table 3-1: Δt_{op} vs *thresholds* – RZ input pulses

	(a)	(b)	(c)
Threshold	1dB	2dB	3dB
Δt_{op}	10 ps (T_L/10)	16.5ps (T_L/6)	20ps (T_L/5)

Δτ Evaluation

Figure 3-17 shows the $\Delta\tau$ as a function of the time misalignment, obtained for the setup in Figure 3-15. In the operational range of the circuit, $\Delta\tau$ should ideally be zero. Indeed, the line in Figure 3-17 is quite similar to the line representing the deviation to the ideal linear chirp in Figure 3-6. The dotted line in Figure 3-16 represents the time misalignment of the input pulses. Note that it is clear that the time position of the processed pulses are moved significantly. However, there is still some temporal misalignment in the output pulses due to the deviation of the actual amount of chirp induced by the sinusoidal phase modulation, in relation to the required linear chirp.

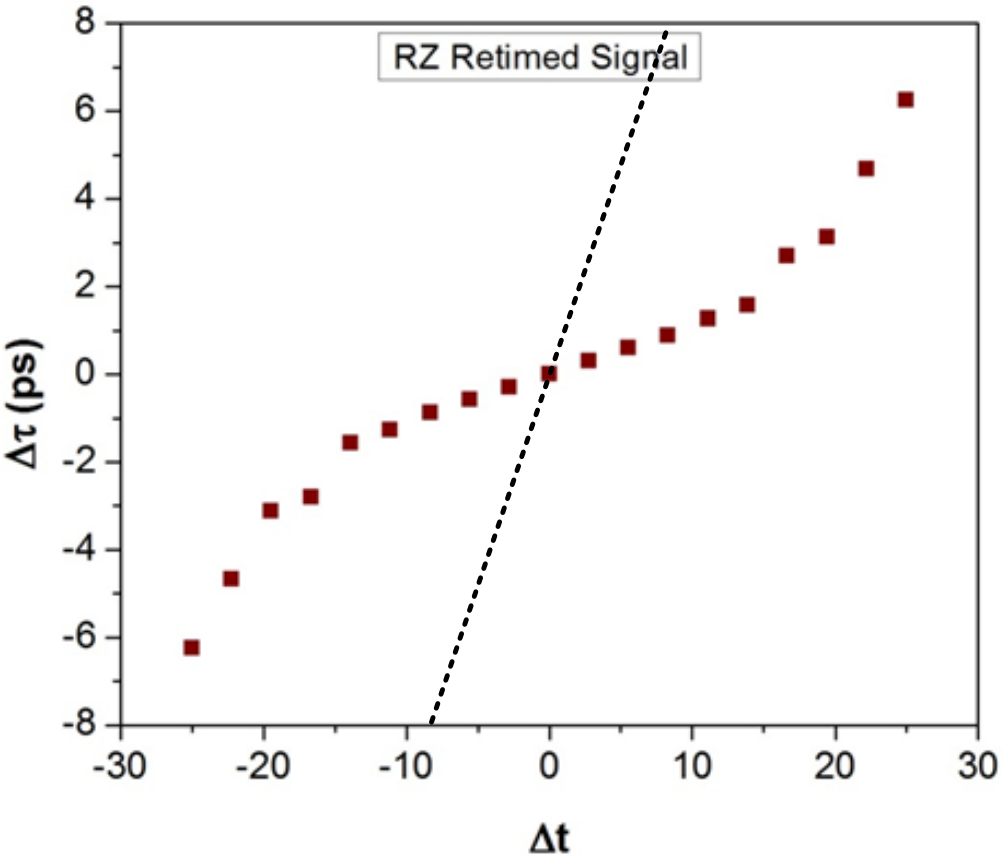

Figure 3-17: $\Delta\tau$ versus Δt : operational range of Time-lens (RZ input pulses)

FWHM Evaluation

Figure 3-18 shows the *FWHM* as a function of the time misalignment, obtained for the setup in Figure 3-15. In the operational range of the circuit, *FWHM* should be constant and equals $FWHM_{output}$ = $FWHM_{input}$ / C = 8.4 ps, where C is given in Eq. 3.11. This theoretical $FWHM_{output}$ is shown in Figure 3-17 as a dotted line. Note that *FWHM* increases as the time misalignment sweeps away from the central posi-

tion (Δt = 0). Again, this effect is due to the deviation of the induced chirp from the ideal linear chirp.

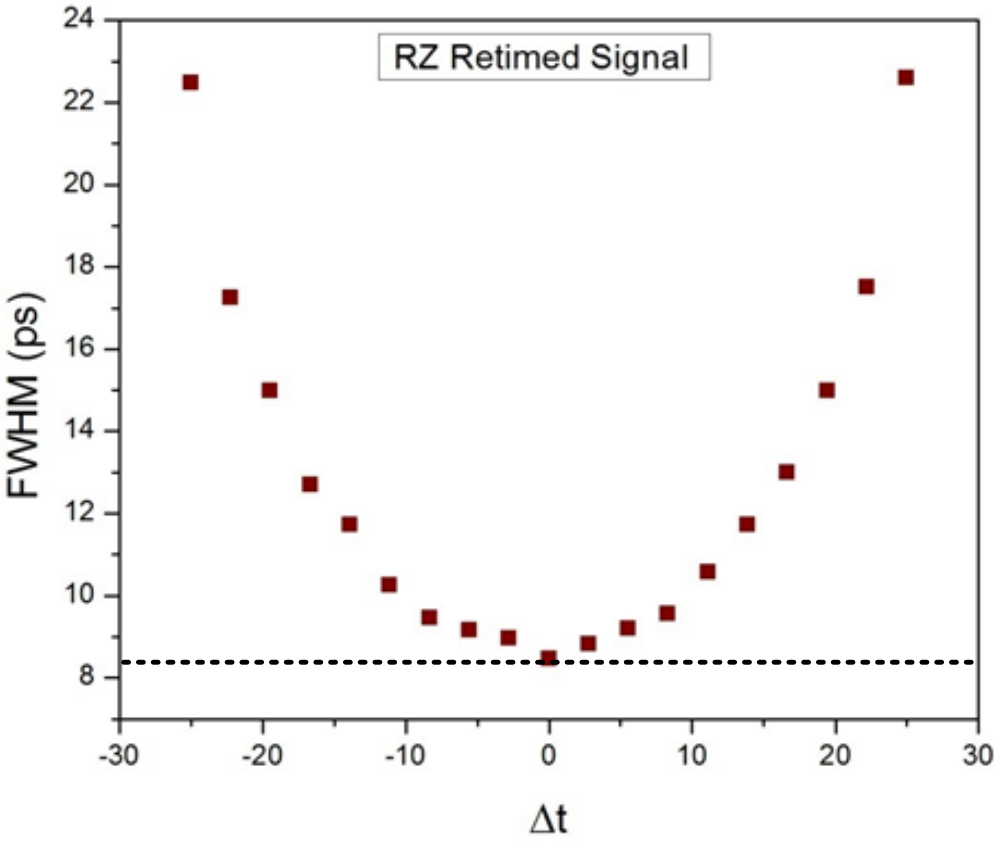

Figure 3-18: *FWHM* versus Δt: operational range of Time-lens (RZ input pulses)

3.5.2

3.5.3 Retiming of NRZ Asynchronous Pulses (pulse carver + time-lens)

Figure 3-19 shows the VPI Transmission Maker setup [54] for numerical simulation used to characterize the retiming of input NRZ time-misaligned pulses. Note that, in this case, there is an additional pulse carver represented by the MZM module in the diagram.

- PRBS: generates many types of data sequence.
    - Generates a sequence of single 1´s and o's at a sample rate of on sample per bit.
- NRZ: Generates NRZ Signals.
    - Each bit is converted into a number of samples equal to SampleRate/BitRate (defined for the whole system)
- RiseTime: used to turn a pulse sequene from thecoders that has a zero rise- and fall times, into a realistic bandwidth-limited signal.
- MZM: Mach-Zehnder Modulator
- PhaseShift
    - used for the pulse delay
- PM: Phase Modulator
    - Phase Deviation of 180.0 × 2.7 deg
- FuncSineEl: Sinusoidal.
    - Frequency 10e9Hz
    - amplitude of 0.5 a.u.
- PhaseShift: used for the pulse delay
- DC
    - Amplitude: 0.5 V
- MZM: Mach-Zehnder Modulator
- Single Mode Fiber: 3km
- Signal Analyzer

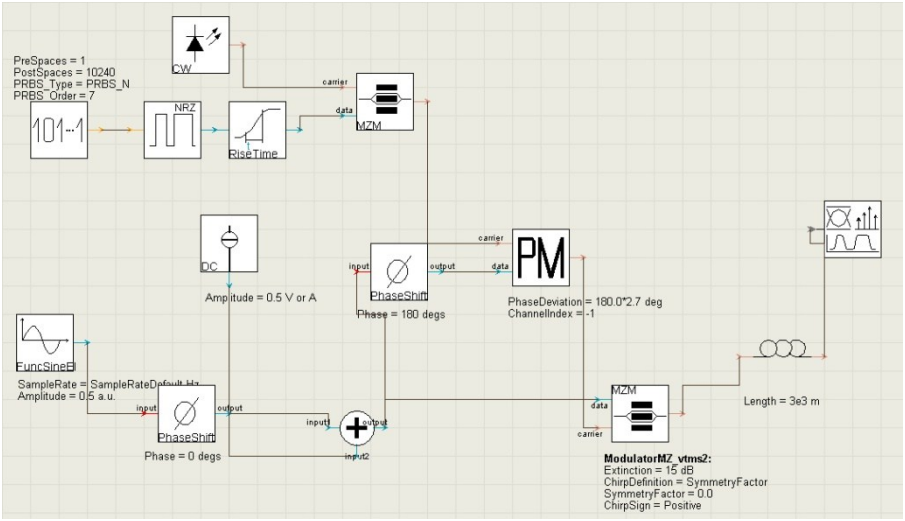

Figure 3-19: Numerical Simulation Setup (VPI Transmission Maker): NRZ input pulses

ECR Evaluation

Figure 3-20 shows the *ECR* as a function of the time misalignment, obtained for the setup in Figure 3-19.

Once again, it is evaluated three typical values for this *threshold*: 1dB, 2 dB and 3 dB. The threshold and the respective operational range definition are also shown in Figure 3-20.

For the evaluated *thresholds*, the operational range is obtained at Figure 3-20 is shown in Table 3.2.

Table 3-2: Δt_{op} vs *thresholds* – NRZ input pulses

	(a)	(b)	(c)
threshold	1dB	2dB	3dB
Δt_{op}	18ps	22ps	25ps (T_L/4)

Note that the operational range is lightly broader for the case of the NRZ case. This is because the pulse carver carves out the RZ pulses in the same time position aligned with the time-lens focus.

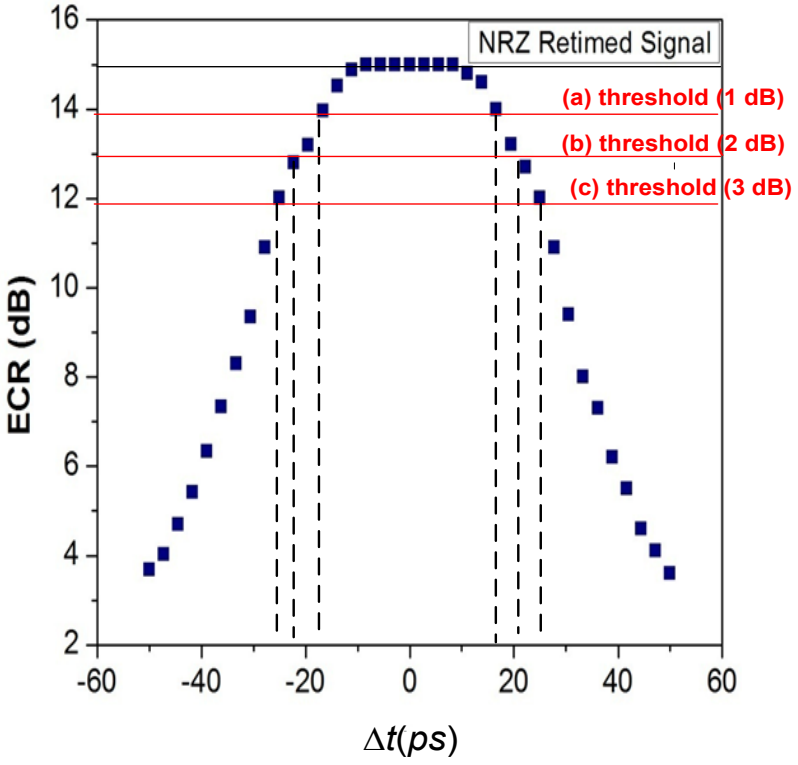

Figure 3-20: ECR versus Δt: operational range of Time-lens (NRZ input pulses)

Δτ Evaluation

Figure 3-21 shows $\Delta\tau$ as a function of the time misalignment, obtained for the setup in Figure 3-19. The dotted line is representing the time misalignment of the input pulses, showing that the processed RZ pulses are actually been moved in time by the time-lens. Once again, we expect that, in the operational range of the circuit, $\Delta\tau$ should be close to zero. Note that there is a deviation in $\Delta\tau$ that is due to the deviation to the expected linear chirp (as a function of Δt). The line in Figure 3-21 is also quite similar to the line representing the deviation to the ideal linear chirp in Figure 3-6. However, this line is carves out the RZ pulses (Figure 3-17) in the same time position aligned with the time-lens focus.

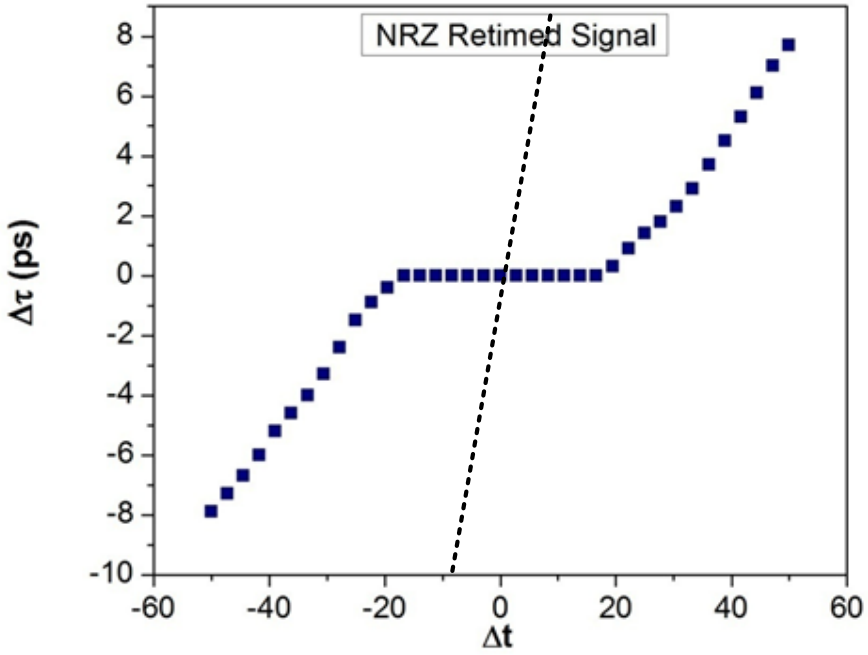

Figure 3-21: Δτ versus Δt: operational range of Time-lens (NRZ input pulses)

FWHM Evaluation

Figure 3-22 shows the *FWHM* as a function of the time misalignment, obtained for the setup in Figure 3-19. In the operational range of the circuit, *FWHM* should be constant and equals $FWHM_{output} = T/2/C =$ 6.4 ps, where C is given by Eq. 3.11. This level is represented by the dotted line in the diagram. Note that *FWHM* increases as the time misalignment sweeps away from the central position ($\Delta t = 0$). This effect is also due to the deviation of the induced chirp in relation to the ideal linear chirp.

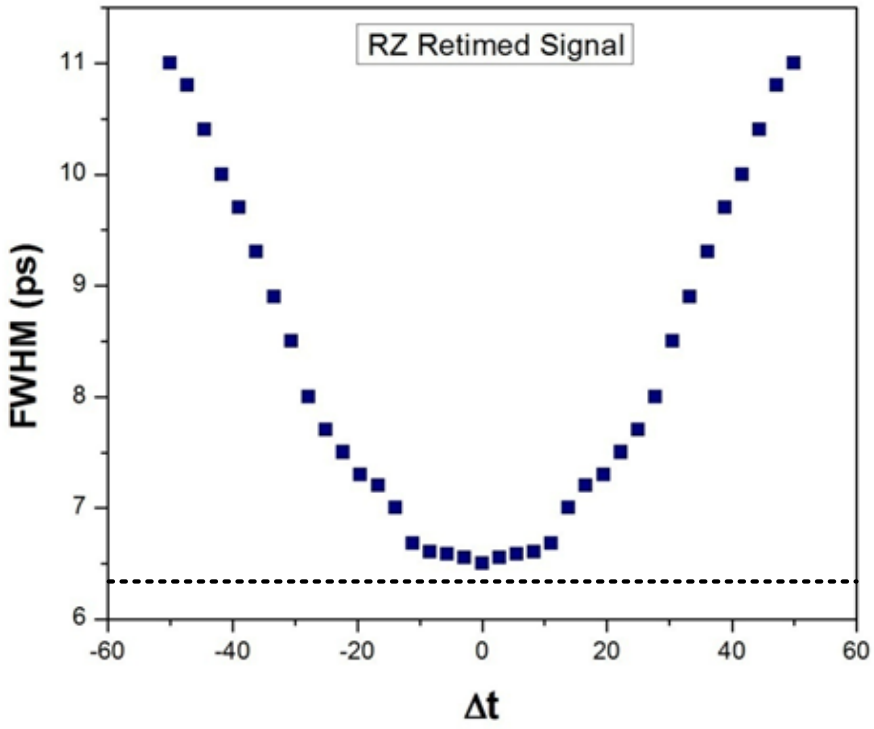

Figure 3-22: FWHM versus Δt: operational range of Time-lens (NRZ input pulses)

3.6 Conclusions

We have defined three metrics for evaluation of the proposed FRS-unit:

Eye Contrast Ratio (ECR), Output Time Misalignment ($\Delta\tau$), and Full Width Half Maximum (*FWHM*), which were evaluated through numerical simulations for two configurations:

- Input RZ pulses (time-lens only), 33% duty cycle:
  - For *ECR* ($\Delta t = 0$) – *ECR* < 3 *dB* (*threshold* = 3dB), an operational range of Δt_{op}= 20ps ($T_L/5$) is established.
  - $|\Delta\tau| < 1$ ps (within the operational range).
  - $FWHM_{output}$ = 8.4ps (within the operational range).

- Input NRZ pulses (time-lens + pulse carver):
  - *For ECR($\Delta t = 0$) – ECR < 3 dB* (*threshold* = 3dB), an operational range of Δt_{op}= 25ps ($T_L/4$) is established.
  - *$|\Delta\tau| < 1$ ps (within the operational range).*
  - $FWHM_{output}$ = 6.4ps (within the operational range).

The operational range is slightly greater for NRZ input pulses. This is due to the pulse carver that is carving out the RZ pulses in the time-lens focus, in NRZ case, while the line signal is present only during 33% of bit period (33% duty cycle were used in the simulations).

In a system level, we conclude that, in order to be fully operational, the time misalignment of the input pulses must be inside the operational range of the designed circuit. Some basic electronic circuits can be used to provide this condition, e.g. an controlled phase shift in the local electrical clock. The phase shift could be controlled by an electronic envelop detector which detects the frame arrival and performs the choice for the correct phase shift. These complementary circuits are electronic, which provides a costly and efficiently design.

4

10GBIT/S NRZ-RZ FORMAT CONVERSION, RETIMING, AND SYNCHRONIZATION

In this Chapter, the FRS-unit for synchronization, retiming and NRZ-RZ format conversion of 10GE-like optical signals [55] is evaluated. Our goal is to analyze the operational conditions of the device for processing asynchronous NRZ-formatted for 10Gbit/s optical signals, in the presence of frequency offset ($\Delta f \neq 0$), i.e. when there is a difference between the local clock frequency (f_L) and the input line signal bit rate (f). Frequency offset is evaluated inside the operational tolerance of the 10GE PHY standards, i.e., ±1 MHz (±100 ppm) for 10GBASE-R and ±200 kHz (±20 ppm) for 10GBASE-W.

4.1 Synchronization with Pulse Carver + Time-lens

Figure 4-1 illustrates the FRS-unit based on a pulse carver + time-lens[31, 69]. The input signal is an asynchronous NRZ frame of size n bits (n < 8 X 1518 = 12144 bits, as per Ethernet MAC standard), bit rate f and initial time misalignment Δt_1 (i.e., time misalignment of the first bit in the frame in relation to the minimum of the local sinusoidal clock). The time-lens consists of a Phase Modulator (PM) and a piece of fiber as dispersive element, interleaved with a pulse-carving Mach-Zehnder Modulator (MZM).

The PM is driven by the local clock sinusoidal signal, oscillating at the nominal bit rate frequency (f_L). In this configuration, the PM approximates a quadratic phase modulation (see Chapter 3) and is used to introduce linear chirp at the optical signal. The MZM is driven by the sinusoidal local clock biased at $V_{pp}/2$, as explained in Section 3.1. In this configuration, the MZM acts as an intensity modulator and removes the part of the input waveform (pulse carving), subjected to the upper part of the sinusoidal phase modulation, performing NRZ-RZ format conversion. Such a design allows for an output RZ signal with 50% duty cycle [12, 44]. Finally, the dispersive element (e.g. SMF) provides the temporal focus in the system by eliminating the chirp in the optical signal [25].

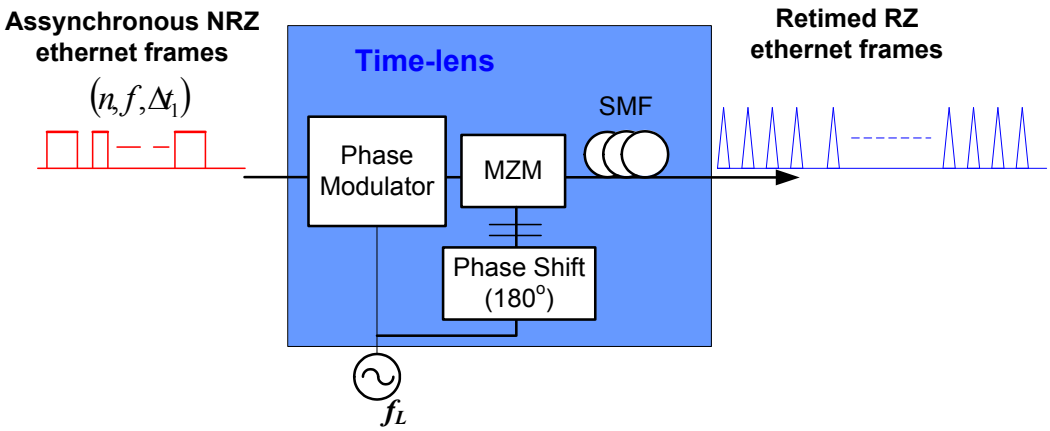

Figure 4-1: FRS-unit based on a time-lens

The detailed explanation of the operational principle is as follows:

- The input signal is an asynchronous frame consisting of serialized NRZ coded data over the fiber, at a line rate expressed by its frequency *f*. The bit period of the input signal is, therefore, T = 1/*f*.

- The local clock is a sinusoidal signal with frequency f_L (nominal rate) and the bit period at the local clock time reference is $T_L = 1/f_L$.
- The frequency offset between clock local frequency and the line rate of the arriving frame is $\Delta f = f - f_L$. Δf is inside the tolerance of 10GE PHY.
- The asynchronous arrival of the input frame implies an initial time misalignment Δt_1 between the local clock and the arriving pulse train.

Recall that the time misalignment Δt is defined as the temporal difference between the center (central position) of the first bit and the maximum of the local clock sinusoidal signal. If there is no frequency offset ($\Delta f = 0$, retiming only), all pulses in the frame will have the same time misalignment $\Delta t = \Delta t_1$. However, if there is frequency offset ($\Delta f \neq 0$), the time misalignment will differ for each pulse in the same frame.

Let Δt_n represent the time misalignment of the center of the n^{th} pulse (bit) in relation to the maximum of the sinusoidal clock at the n^{th} clock cycle. Successive pulses will have the time misalignment (difference between the time position of the center of the input pulse and the maximum of the local sinusoidal clock) varying with the difference between the bit periods of the local clock (T_L) and the arriving signal (T), $\Delta T = T - T_L$. Then, Δt_n can be expressed according to Eq. 4.1 [27].

$$\Delta t_n = \Delta t_1 + (n-1)\Delta T \qquad (4.1)$$

For each input pulse where $|\Delta t_n| < \Delta t_{op}$ (operational range defined in Eq. 3.15), the time misalignment of the output pulse will be adjusted to the central position ($\Delta\tau \sim 0$, Eq. 3.17). This is shown in Figure

4-2 (a) for $f_L < f$ ($\Delta f > 0$). In this case, $T_L > T$, ΔT is negative and the pulse position will travel to the left of the central position at each successive pulse. If $f_L > f$ ($\Delta f < 0$), as shown in Figure 4-2 (b), ΔT is positive, and the pulse position will travel to the right of the central position at each successive pulse.

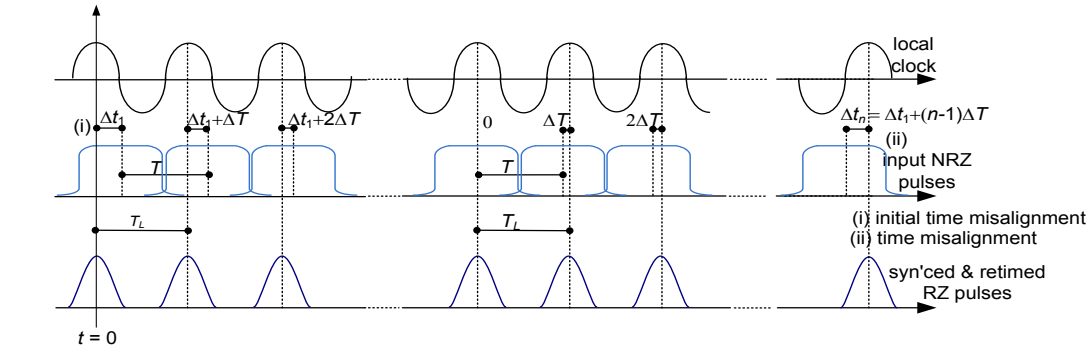

(a) ($\Delta f > 0$)

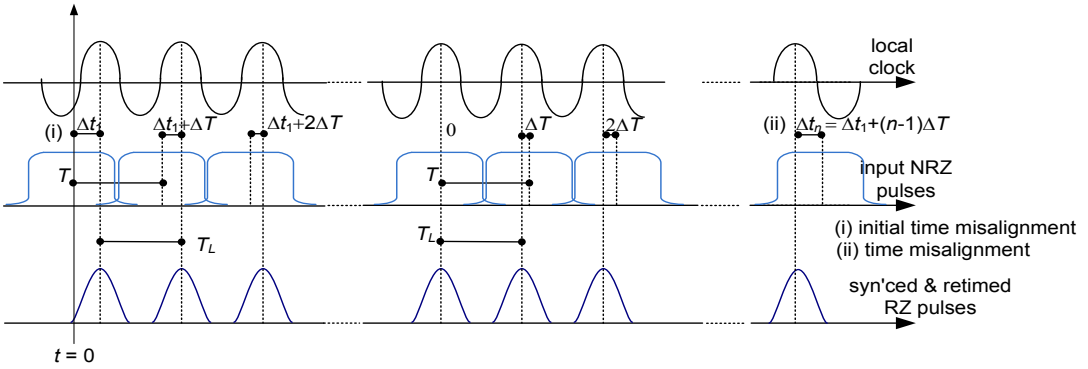

(b) ($\Delta f < 0$)

Figure 4-2: Operational principle of synchronization, retiming and format-conversion unit

As the device operates in a bit-by-bit (pulse-per-pulse) basis, we have the following operational characteristics of the FRS-unit ($|\Delta t_i| < \Delta t_{op}$, for i = 0, 1, … , n):

- **Format Conversion**: NRZ-RZ format conversion is performed through the MZM operation (Section 3.1). Format conversion is enhanced by the pulse compression provided by the time-lens (see FWHM analysis of output pulses in Section 3.5.2).
- **Retiming**: For *each* successive input pulse, the time-misalignment to the local clock signal will be cancelled by the device ($\Delta\tau \sim 0$), i.e., each output pulse is equally retimed to the maximum of the sinusoidal local clock (see $\Delta\tau$ analysis in Section 3.5.2).
- **Synchronization**: For sufficient small frequency differences, the time-misalignment wandering will also be cancelled, as each individual pulse is time-locked to the maximum of the local clock signal, which means that the input pulse train will be synchronized to the local clock frequency. Output pulses will present themselves at a bit rate equal to the local clock frequency. Thus, the device eliminates the frequency offset between the line signal bit rate and the local clock frequency.

Note that, for each pulse where $\Delta\tau \neq 0$, the variation of $\Delta\tau$ presents itself as timing jitter, which should be clearly visible in the eye-diagram of output pulses. Indeed, we expect the peak-to-peak timing jitter to be approximated by the difference between the $\Delta\tau_1$ (time misalignment of the first output pulse) and $\Delta\tau_n$ (time misalignment of the n^{th} output pulse).

4.1.1 Maximum Frame Size

In this Section, the maximum number of bits in the same frame is derived (n_{max}, maximum frame size) [56], in the presence of frequency offset ($\Delta f \neq 0$) that can be processed by the FRS-unit. The operational condition is expressed in Eq. 3.15. Note that in order for this equation

always to hold, we are assuming that the initial time misalignment is $\Delta t_1 = \Delta t_{op}$ and the time misalignment of the last bit is $\Delta t_n = -\Delta t_{op}$, for $\Delta f > 0$, while $\Delta t_1 = -\Delta t_{op}$ and $\Delta t_n = \Delta t_{op}$, for $\Delta f < 0$. This assures that we allow a total time misalignment variation of $2\Delta t_{op}$, where $|\Delta T|$ is the amount of variation contributed by each bit in the same frame. Therefore, the maximum number of bits processed in both cases can be expressed as shown in Eq. 4.2.

$$n_{max} = 2\Delta t_{op}/|\Delta T| + 1 \qquad (4.2)$$

From Eq. 4.2, it is readily derive the maximum number of bits that can be processed by the FRS-unit, using operational range definitions described in Section 3.5.2, under extreme conditions (maximum frequency offset) for the 10G Ethernet 10GBASE-R standard. 10GBASE-R devices transmits data using NRZ at a line rate of 10.3125 Gbit/s (T_L = 97ps) and allows for a frequency offset of up to |1 MHz| ($|\Delta T| \sim 9.4$fs). Results are shown in Table 4-1.

Table 4-1: Max. Number of bits that can be processed by FRS-unit (10GBASE-R)

Δt_{op} (see Section 3.5.2)	n_{max}
$\Delta t_{op} = 9T_L/50$	3711
$\Delta t_{op} = 11T_L/50$	4536
$\Delta t_{op} = T_L/4$	5154

The same way, we can derive the maximum number of bits that can be processed by the FRS-unit, using operational range definitions described in Section 3.5.2, under extreme conditions (maximum frequency offset) for the 10G Ethernet 10GBASE-W standard.

10GBASE-W devices transmit data using NRZ at a line rate of 10.3.125 Gbit/s (T_L = 97ps) and allows for a frequency offset of up to |200 kHz| (|ΔT| ~ 1.88fs). Results are shown in Table 4-2.

Table 4-2: Max. Number of bits that can be processed by FRS-unit (10GBASE-W)

Δt_{op} (see Section 3.5.2)	n_{max}
$\Delta t_{op} = 9T_L/50$	18562
$\Delta t_{op} = 11T_L/50$	22687
$\Delta t_{op} = T_L/4$	25780

From Table 4-1, we can conclude that for $\Delta f = \pm 1$ MHz the FRS-unit is able to process correctly packets with sizes as large as 4 kbits (considering $\Delta t_{op} = 11T_L/50$). This result is encouraging as the simple device can process such long frames.

From Table 4-2, we can conclude that for $\Delta f = \pm 200$ kHz, a full-sized Ethernet frame (12144 bits) can be correctly processed by the FRS-unit.

4.1.2 Ideal Initial Time Misalignment

In this section we aim at deriving the best initial time-misalignment for a given frequency offset (Δf) and frame size (n). The idea here is to maintain the time misalignment for each bit in the frame as closer as possible to the central position where $\Delta t = 0$. This is obtained when Δt_1 and Δt_n are equally distant from the central position or simply $\Delta t_1 = -\Delta t_n$.

Replacing Δt_n as in Eq. 4.1, we have the ideal initial time misalignment expressed in Eq. 4.3:

$$\Delta t_{1(\text{best})} = (1 - n)\Delta T/2 \qquad (4.3)$$

Note that $\Delta t_{1(\text{best})}$ is positive for $\Delta f > 0$ ($f_L < f$) and negative for $\Delta f < 0$ ($f_L > f$).

4.2 Analysis of FRS-unit: Numerical Simulations

In this section we show numerical experiments for evaluating the FRS-unit, in the presence of frequency offset. Once again, all simulations were done with VPI Transmission Maker GUI Version 8.6 (Build: 284). We are using the same setup and VPI scheme of Figure 3-14 for these analyses (we are not repeating the figure here), except from that we make $f \neq f_L$ in order to allow the occurrence of a frequency offset ($\Delta f \neq 0$).

For each case, we are evaluating the synchronization of the output RZ pulses to the local clock, for different frequency offset of $\Delta f = \pm 1$ MHz and $\Delta f = \pm 200$ kHz. This is evaluated for different input frame sizes (i.e., n = 1024; 2048; 4096; 6144; and 12144 bits). In all cases, we have evaluated the operational conditions of the circuit with the following initial time misalignments:

(a) For $\Delta f > 0$:

- $\Delta t_1 = \Delta t_{op}$
- $\Delta t_1 = \Delta t_{1(\text{best})}$ (as shown by Eq. 4.3) and
- $\Delta t_1 = -\Delta t_{op} - (n - 1)\Delta T$ (in this case, we assume that $\Delta t_n = -\Delta t_{op}$ and we obtain Δt_1 using Eq. 4.1).

(b) For $\Delta f < 0$:

- $\Delta t_1 = -\Delta t_{op}$
- $\Delta t_1 = \Delta t_{1(best)}$ (as shown by Eq. 4.3) and
- $\Delta t_1 = \Delta t_{op} - (n - 1)\Delta T$ (in this case, we assume that $\Delta t_n = \Delta t_{op}$ and we obtain Δt_1 using Eq. 4.1).

We are using the following measures:

- Eye diagram visualization: eye diagrams were generated using Matlab.
- Electrical spectrum visualization: measurement of frequency components for the output signal, which should have a clear maximum at f_L. Measurements were made both with Matlab and VPI.
- Peak-to-peak timing jitter: timing jitter was measured with Matlab.

Table 4-3 describes the parameters of the numerical simulation experiments.

Table 4-3: Best Initial Time Misalignment, NRZ

FRS-unit setup		**Format of input signal**		**Δt_{op}**
Pulse Carver + Time-lens		NRZ		$0.25T_L$ (T_L/4)
Δf	N	$\Delta t_1 = \pm\Delta t_{op}$	$\Delta t_1 = \Delta t_{1(best)}$	$\Delta t_1 = \mp\Delta t_{op}-(n-1)\Delta T$
1 MHz	1024	$0.25T_L$ (T_L/4)	$0.0512T_L$	$-0.1476T_L$
	2048	$0.25T_L$ (T_L/4)	$0.1024T_L$	$-0.0452T_L$
	4096	$0.25T_L$ (T_L/4)	$0.2048T_L$	$0.1596T_L$
	6144	out of range ($n > n_{max}$) (Eq. 4.2)		
	12208*	out of range ($n > n_{max}$) (Eq. 4.2)		
200 kHz	1024	$0.25T_L$ (T_L/4)	$0.01024T_L$	$-0.2295T_L$
	2048	$0.25T_L$ (T_L/4)	$0.02048T_L$	$-0.2090T_L$
	4096	$0.25T_L$ (T_L/4)	$0.04096T_L$	$-0.1681T_L$

	6144	$0.25T_L$ ($T_L/4$)	$0.06144T_L$	$-0.1271T_L$
	12208*	$0.25T_L$ ($T_L/4$)	$0.12208T_L$	$-0.0058T_L$
–1 MHz	1024	$-0.25T_L$ ($-T_L/4$)	$-0.0512T_L$	$0.1476T_L$
	2048	$-0.25T_L$ ($-T_L/4$)	$-0.1024T_L$	$0.0452T_L$
	4096	$-0.25T_L$ ($-T_L/4$)	$-0.2048T_L$	$-0.1596T_L$
	6144	out of range ($n > n_{max}$) (Eq. 4.2)		
	12208*	out of range ($n > n_{max}$) (Eq. 4.2)		
–200 kHz	1024	$-0.25T_L$ ($-T_L/4$)	$-0.01024T_L$	$0.2295T_L$
	2048	$-0.25T_L$ ($-T_L/4$)	$-0.02048T_L$	$0.2090T_L$
	4096	$-0.25T_L$ ($-T_L/4$)	$-0.04096T_L$	$0.1681T_L$
	6144	$-0.25T_L$ ($-T_L/4$)	$-0.06144T_L$	$0.1271T_L$
	12208*	$-0.25T_L$ ($-T_L/4$)	$-0.12208T_L$	$0.0058T_L$

* full-sized Ethernet frames

The results of representative simulation experiments are shown in the next pages. We omit some of the tested cases (complete tested cases are represented in Table 4-3), for space limitation reasons.

A. Δf = –200 kHz, 12208 bits (full-sized Ethernet frame)

Setup: NRZ, Pulse Carver + Time-lens

- Input signal: NRZ coding; $2^7 - 1$ PRBS; 12144 bits; bit rate f = 10 Gbps
- Local Clock signal: frequency: 9.9998 GHz (Δf = 200 kHz)
- Initial time misalignments:

  (a) $\Delta t_1 = \Delta t_{op} = 0.25T_L$

  (b) $\Delta t_1 = \Delta t_{1\,(best)} = 0.12208T_L$

  (c) $\Delta t_1 = -\Delta t_{op} - (n-1)\Delta T = -0.0058T_L$

- Measurements:
    - eye diagram (Figure 4-3)
    - electrical spectrum (Figure 4-4)
    - peak-to-peak timing jitter (Figure 4-5)

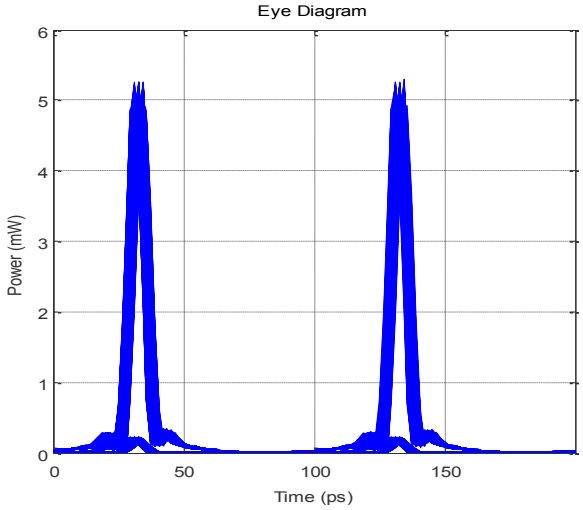

(a) $\Delta t_1 = \Delta t_{op} = 0.25T_L$

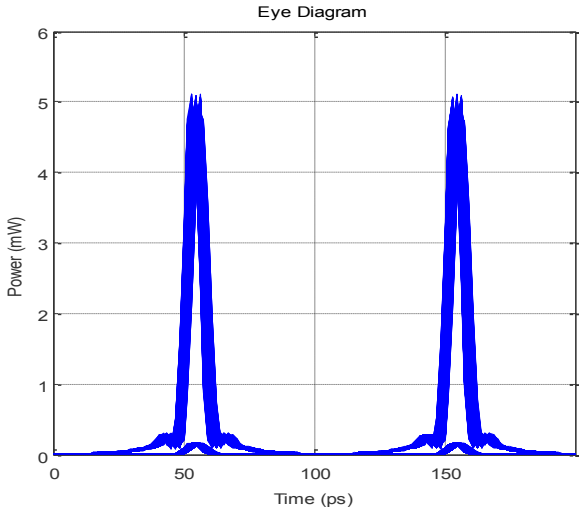

(b) $\Delta t_1 = \Delta t_{1\,(best)} = 0.12208T_L$

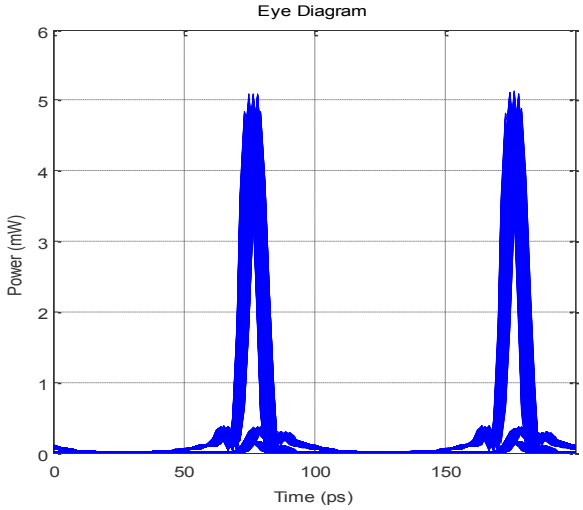

$$\Delta t_1 = -\Delta t_{op} - (n-1)\Delta T = -0.0058 T_L$$

Figure 4-3: Eye diagram (oscilloscope triggered with local clock, f_L = 9.9998 GHz)

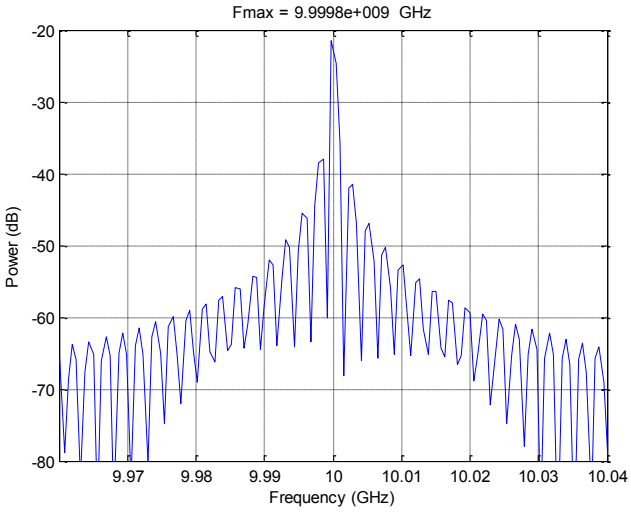

(a) $\Delta t_1 = \Delta t_{\text{op}} = 0.25T_L$

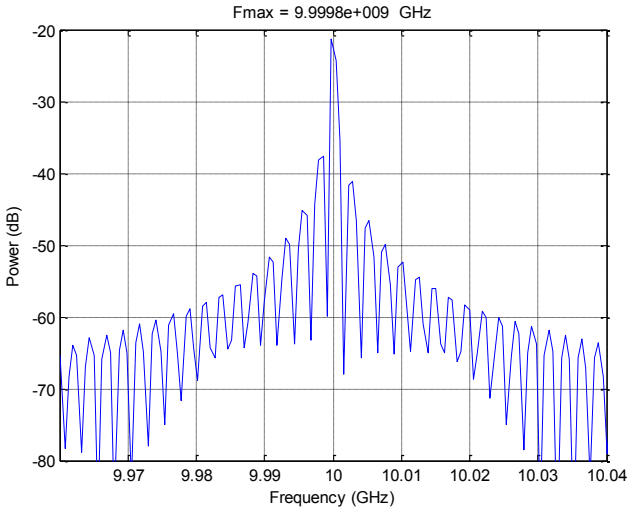

(b) $\Delta t_1 = \Delta t_{1\ (\text{best})} = 0.12208T_L$

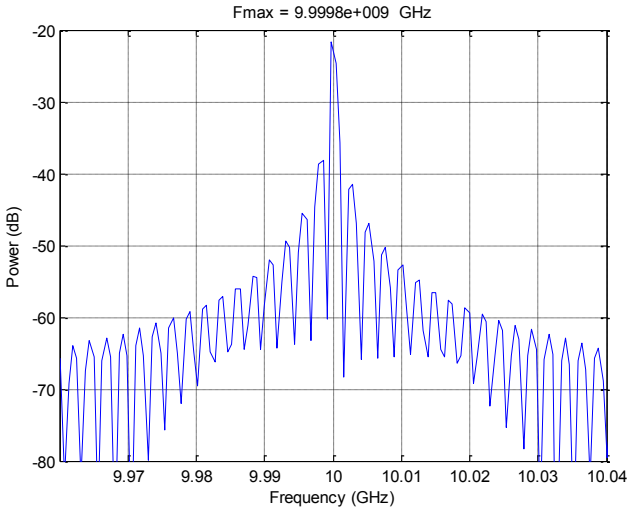

$$\Delta t_1 = -\Delta t_{op} - (n-1)\Delta T = -0.0058 T_L$$

Figure 4-4: *Electrical spectrum*

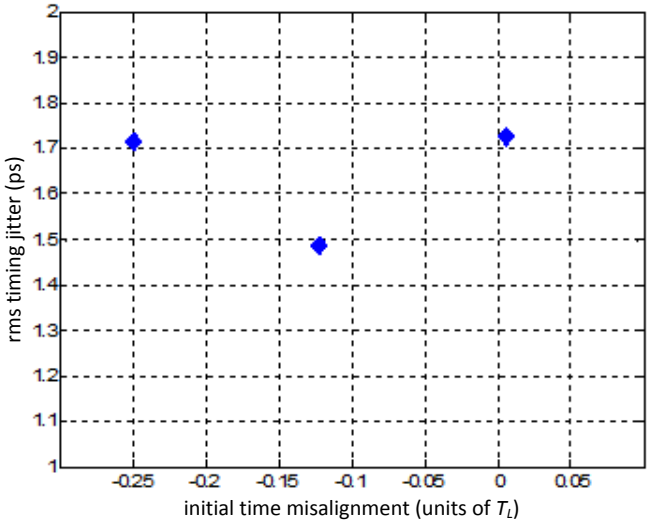

Figure 4-5: Peak-to-peak timing jitter

In Figure 4-3 (a) and (c) the eye diagram refers to the operation of the circuit nearby its operational range. In (a), there are clear asymetrical "bump" at the low level ('0' bits), which appears to the right of the '0'

to ‘1’ transition, i.e. at t = 28ps and t = 128 ps, while in (c) the “bump” appear to the left of the ‘1’ to ‘0’ transitions, i.e. at t = 72 ps and t = 172 ps. This asymmetry is due to the processing of the input pulses with Δt close to (a) Δt_{op} and (c) $-\Delta t_{op}$, respectively. The assymmtry does not appears in Figure 4-3 (b), where the input pulses are processed in the device with Δt close to 0 (central position).

Spectra shown in Figure 4-4 (a)(b)(c) are similar to each other. Proper operation of the synchronization function is demonstrated by the clear peak at the local clock frequency, i.e. 9.9998 GHz.

Figure 4-5 shows that timing jitter is varying from 1.5 ps to 1.7 ps, which also demonstrates the proper operation of the circuit at the rates we demonstrated in this work. Althought it is not acceptable for 1Tbit/s signal, when there is a need to have a more accurated scheme to have acceptable timming jitter.

B. $\Delta f = -1$ MHz, 1024 bits

Setup: NRZ, Pulse Carver + Time-lens

- Input signal: NRZ coding; $2^7 - 1$ PRBS; 1024 bits; bit rate $f = 10$ Gbps
- Local Clock signal: frequency: 10.001 GHz ($\Delta f = -1$ MHz)
- Initial time misalignments:

  (a) $\Delta t_1 = -\Delta t_{op} = -0.25 T_L$

  (b) $\Delta t_1 = \Delta t_{1\,(best)} = -0.0512 T_L$

  (c) $\Delta t_1 = \Delta t_{op} - (n-1)\Delta T = 0.1476 T_L$
- Measurements:
  - eye diagram (Figure 4-6)
  - electrical spectrum (Figure 4-7)
  - peak-to-peak timing jitter (Figure 4-8)

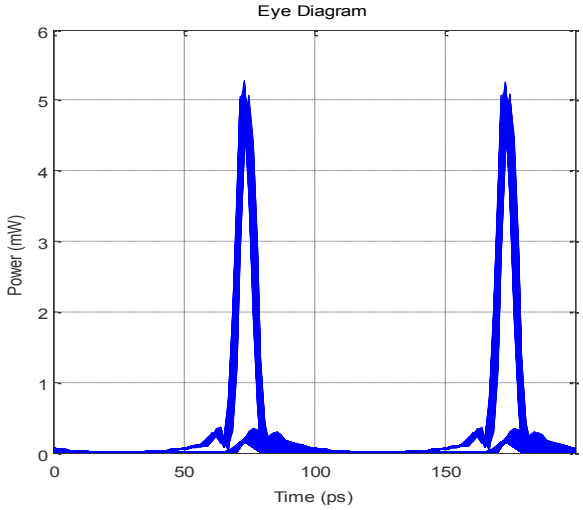

(a) $\Delta t_1 = -\Delta t_{op} = -0.25T_L$

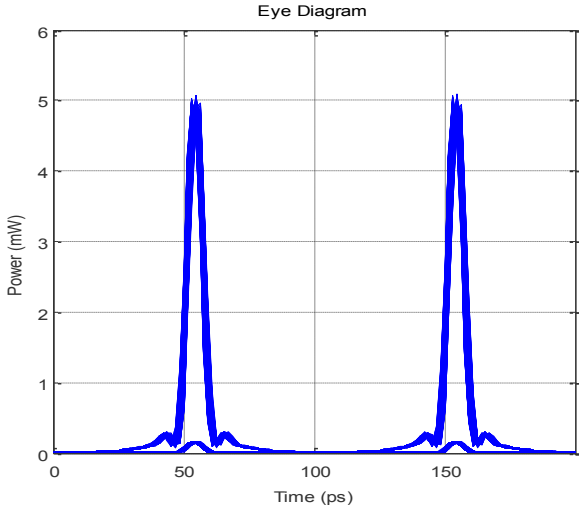

(b) $\Delta t_1 = \Delta t_{1\,(best)} = -0.0512T_L$

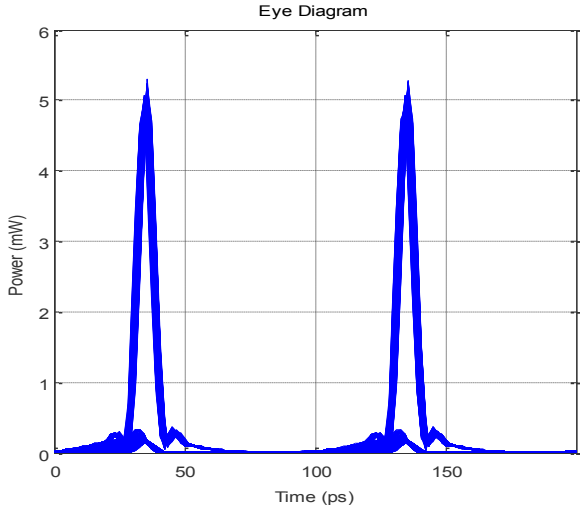

(c) $\Delta t_1 = \Delta t_{op} - (n-1)\Delta T = 0.1476 T_L$

Figure 4-6: Eye diagram (oscilloscope trigged with local clock, f_L = 10.001 GHz)

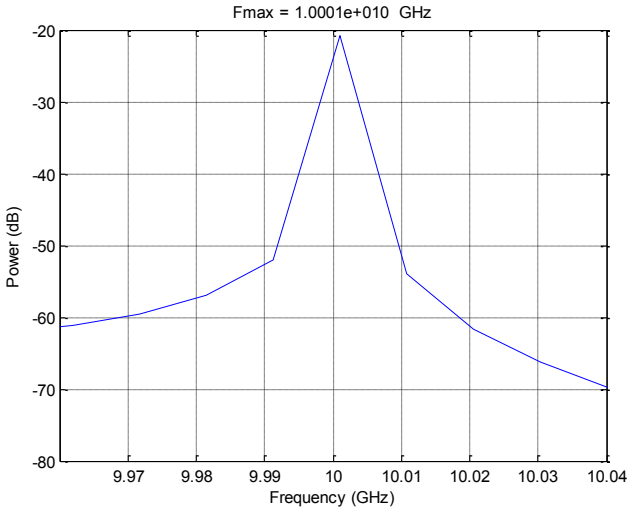

(a) $\Delta t_1 = -\Delta t_{op} = -0.25 T_L$

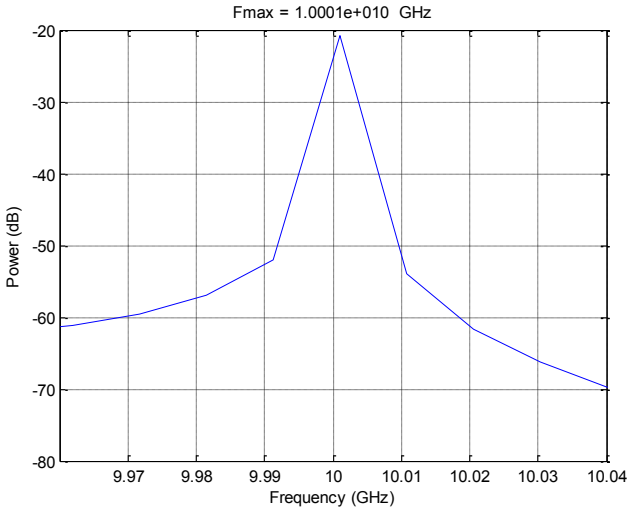

(b) $\Delta t_1 = \Delta t_{1\ (\text{best})} = -0.0512 T_L$

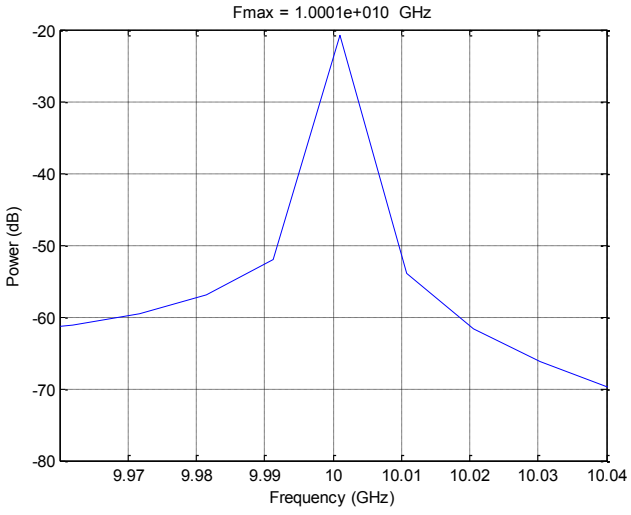

(c) $\Delta t_1 = \Delta t_{\text{op}} - (\text{n} - 1)\Delta T = 0.1476 T_L$

Figure 4-7: Electrical spectrum

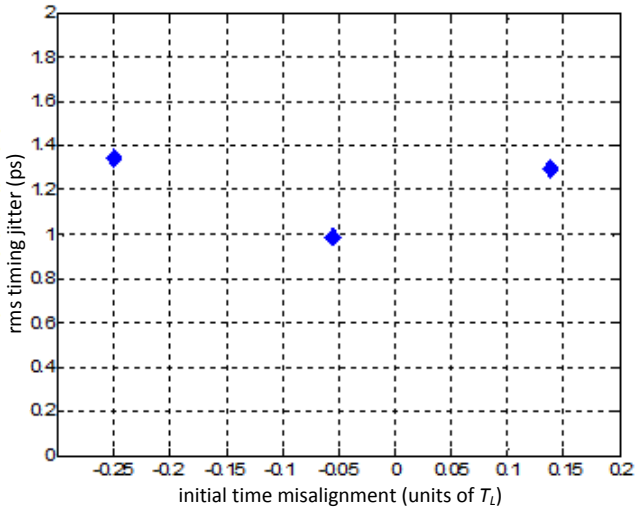

Figure 4-8: Peak-to-peak timing jitter

In Figure 4-6, it is also possible to observe the clear eye for the output retimed and synchronized RZ pulses. Once again, the eye is most clear in Figure 4-6(b) ($\Delta t_{1\ (best)}$), as for this initial time misalignment the pulses in the frame are processed in the circuit with an induced chirp that is more close to the ideal chirp, which is linear in relation to the time misalignment. In Figure 4-6(a), the bits in the beginning of the frame are processed with a chirp that is in the threshold of the operational range of the circuit, while in Figure 4-6 (c), the same happens with the bits that are in in end of the frame. Therefore, the small deviation of the chirp experimented by these bits from the ideal chirp, i.e. the deviation of the chirp from the linear condition, results in a small degradation of the eye diagram. This is shown as assymetrical "bumps" at the low level (bit 0). In (a), the "bump" appears to the left of the '1' to '0' transition, i.e. at t = 78ps and t = 178 ps, while in (c) the "bump" appear to the right of the '0' to '1' transition, i.e. at t = 32 ps and t = 372 ps. This asymmetry is due to the processing of the input pulses with Δt close to (a) $-\Delta t_{op}$ and (c) Δt_{op}, respectively. The assymmtry does not appears in Figure 4-6 (b), where the input pulses are processed in the device with Δt close to 0 (central position).

In Figure 4-7(a) (b) and (c), we can observe the clear electrical spectrum peak at the local clock frequency (f_L = 10.001 GHz), showing that the synchronization of the pulses to the local clock have performed correctly. The spectra in Figure 4-7 are sharper than those in Figure 4-4 because the number of bits processed in the optical circuit is considerably smaller here.

Finally, in Figure 4-8, we can see that the peak-to-peak timing jitter is below 1.4ps for all cases, resting below 1.0ps for the best initial time misalignment ($\Delta t_{1\,(\text{best})} = -0.0512T_L$).

We can conclude from the figures that the *FRS-unit* is correctly performing the format conversion, retiming and synchronization in all cases analyzed in the simulations. The simulation (B) above demonstrates the operation of the proposed scheme for frames up to 1024 bits and frequency offset $|\Delta f| < 1$ MHz.

Now, let us consider the maximum frequency offset modulus with larger frames.

C. $\Delta f = -1$ MHz, 4096 bits

Setup: NRZ, Pulse Carver + Time-lens

- Input signal: NRZ coding; $2^7 - 1$ PRBS; 4096 bits; bit rate f = 10 Gbps
- Local Clock signal: frequency: 10.001 GHz ($\Delta f = -1$ MHz)
- Initial time misalignments:

  (a) $\Delta t_1 = -\Delta t_{\text{op}} = -0.25T_L$

  (b) $\Delta t_1 = \Delta t_{1\,(\text{best})} = -0.2048T_L$

  (c) $\Delta t_1 = \Delta t_{\text{op}} + (\text{n} - 1)\Delta T = -0.1596T_L$

- Measurements:
    - eye diagram (Figure 4-9)
    - electrical spectrum (Figure 4-10)
    - peak-to-peak timing jitter (Figure 4-11)

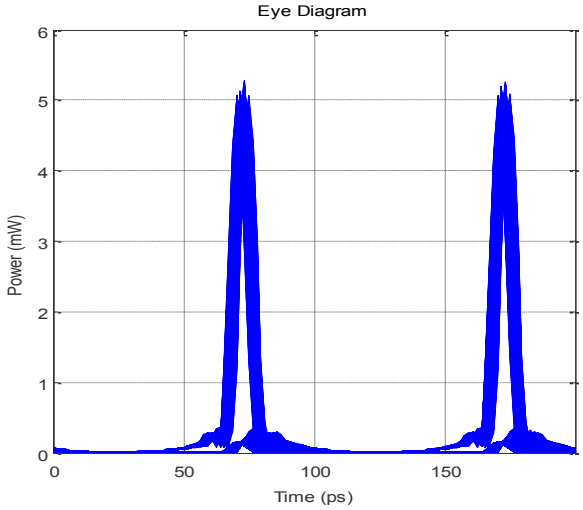

(a) $\Delta t_1 = -\Delta t_{op} = -0.25 T_L$

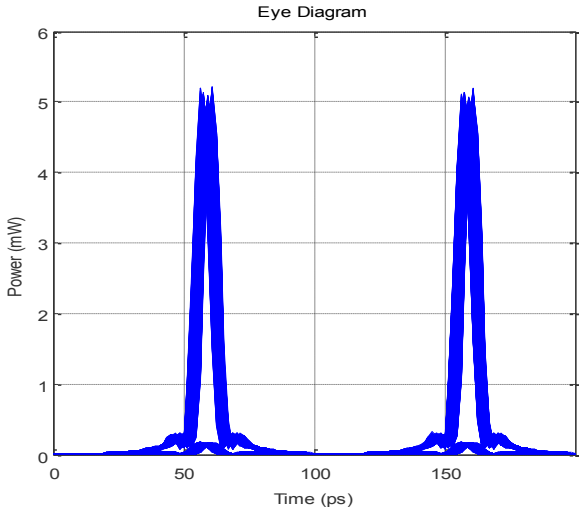

(b) $\Delta t_1 = \Delta t_{1\,(best)} = -0.2048 T_L$

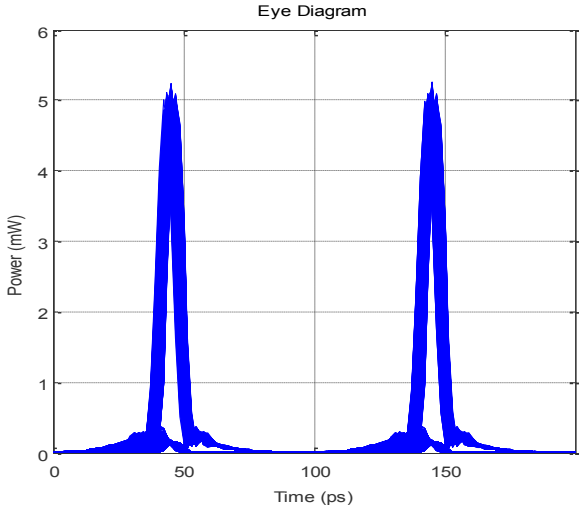

(c) $\Delta t_1 = \Delta t_{op} + (n-1)\Delta T = -0.1596 T_L$

Figure 4-9: Eye diagram (oscilloscope trigged with local clock, f_L = 10.001 GHz)

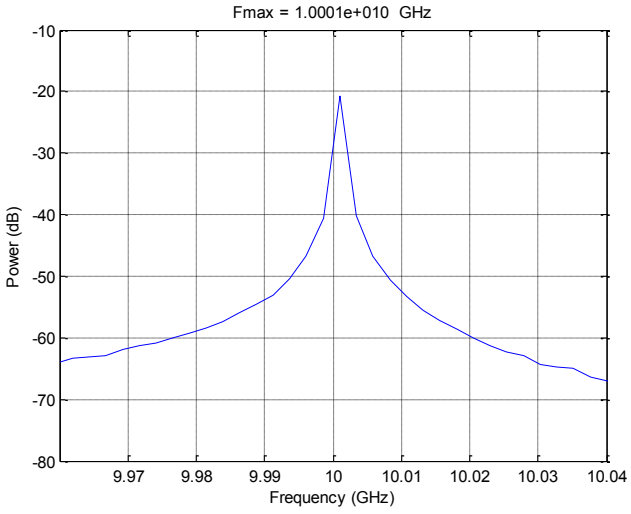

(a) $\Delta t_1 = -\Delta t_{op} = -0.25 T_L$

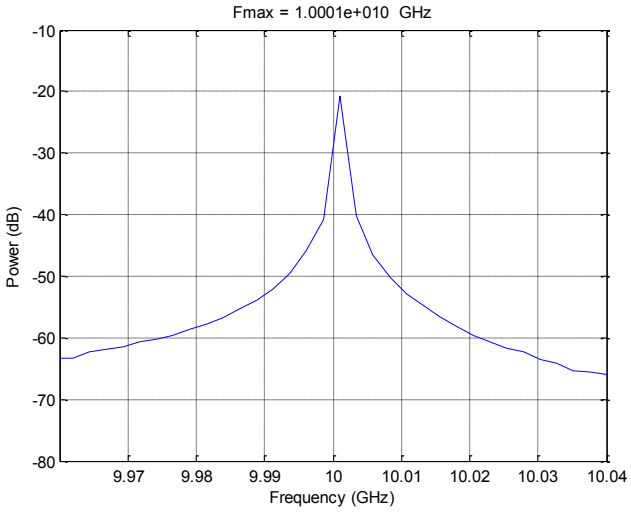

(b) $\Delta t_1 = \Delta t_{1\ (\text{best})} = -0.2048 T_L$

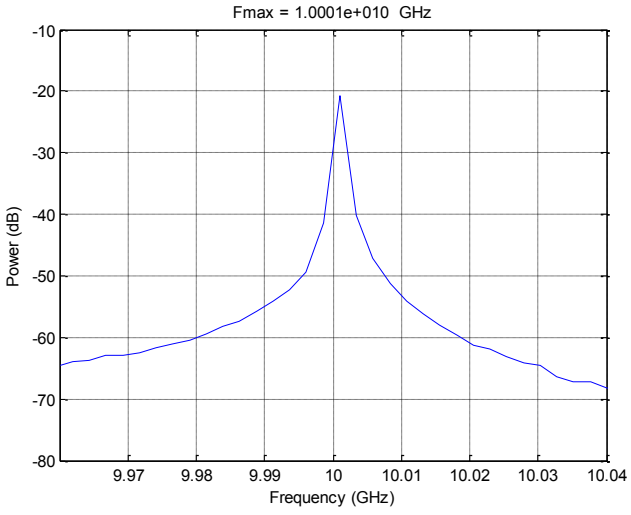

(c) $\Delta t_1 = \Delta t_{\text{op}} + (\text{n} - 1)\Delta T = -0.1596 T_L$

Figure 4-10: Electrical spectrum

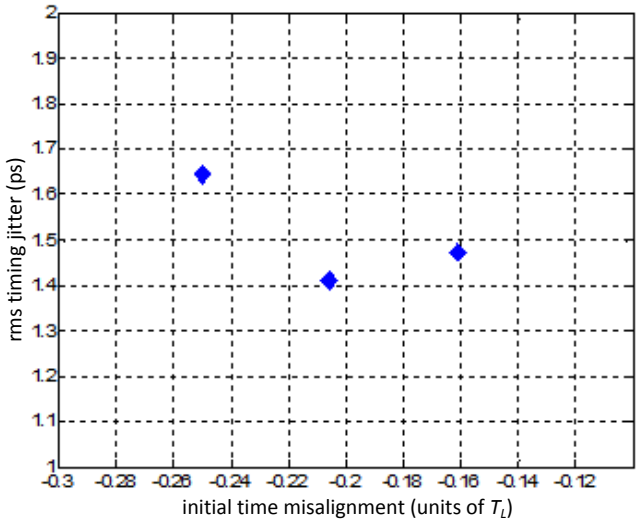

Figure 4-11: peak-to-peak timing jitter

In Figure 4-9, it is again possible to observe the clear eye for the output retimed and synchronized RZ pulses. The eye is most clear in Figure 4-9(b) ($\Delta t_{1\ (best)}$), as for this initial time misalignment the pulses in the frame are processed in the circuit with an induced chirp that is more close to the ideal chirp, which is linear in relation to the time misalignment. In Figure 4-9(a), the bits in the beginning of the frame are processed with a chirp that is in the threshold of the operational range of the circuit, while in Figure 4-9 (c), the same happens with the bits that are in in end of the frame. Therefore, the small deviation of the chirp experimented by these bits from the ideal chirp, i.e. the deviation of the chirp from the linear condition, results in a small degradation of the eye diagram. Note also that the larger frame size makes the eye-diagram line more spread than those shown in Figure 4-6. This is due to a larger number of bits being processed by the chirp unit in the range where the linear approximation is less accurate.

In Figure 4-10(a) (b) and (c), the clear electrical spectrum peak at the local clock frequency (f_L = 10.001 GHz), showing that the synchronization of the pulses to the local clock have performed correctly.

Finally, in Figure 4-11, the peak-to-peak timing jitter is below 1.7ps for all cases, resting below 1.5ps for the best initial time misalignment ($\Delta t_{1(\text{best})} = -0.2048 T_L$).

The conclusion from the figures is that the *FRS-unit* is correctly performing the format conversion, retiming and synchronization in all cases analyzed in the simulations. The simulation (C) above demonstrates the operation of the proposed scheme for frames up to 4096 bits, even when there is a maximum frequency offset, i.e. $| \Delta f | \leq 1$ MHz.

Summarazing the conclusion from these numerical simulations:

Numerical Simulation Conclusions:

- It has been demonstrated by numerical simulation that a full-sized Ethernet frame (12144 bits) can be synchronized by the FRS-unit for $|\Delta f| = 200$ kHz (i.e., 10GBASE-W conditions). In this case, rms timing jitter of output pulses is approximately 1.49ps, as shown in Figure 4-5.
- It has been numerically demonstrated that the FRS-unit is able synchronize frame with sizes of 4096 bits $|\Delta f| <$ 1 MHz (i.e., 10GBASE-R conditions). In this case, rms timing jitter of output pulses is approximately 1.41 ps (for best initial time misalignment $\Delta t_1 = \Delta t_{1\ (\text{best})}$), as shown in Figure 4-5.

4.3 Analysis of FRS-unit: Experimental Evaluation

In this section we present the experimental evaluation of the FRS-unit, in the presence of frequency offset $\Delta f \neq 0$. The results shown in this

sections have been presented in some recent papers published during the development of this thesis [27, 28, 29, 30, 31].

4.3.1 RZ input signal, Time-lens only

Experimental Setup

We performed a laboratory experiment [27] to validate the applicability of the time-lens as a synchronization unit for RZ input pulses, in presence of –1 MHz frequency offset. Frames have size of 1024 bits, which were generated by a 2^7–1 pseudorandom bit sequence (PRBS). RZ pulses have 2ps full width half maximum (FWHM). The experimental setup is shown in Figure 4-12.

We used f = 9.9535 GHz, instead of the nominal f = 10.3125 GHz because of the used laser being bound to this constraint. We do not expect to see any relevant difference in the number of bits which will be covered due the frequency difference.

In practice, the 1024 bits frame is carved out from a continuous pulse stream by an intensity modulator controlled by an electrical pulse generator just prior to OOK data modulation. The pulse generator is in sync with the data signal. The OOK modulation is derived from a bit pattern generator (BPG). Phase modulation is then applied to the data frame with alignment of Δt_1 by an electrical variable time delay. The now chirped data signal is amplified in an EDFA to compensate for component losses, and subsequently transmitted through a dispersive medium, in this case a length of dispersion compensating fiber (600 m).

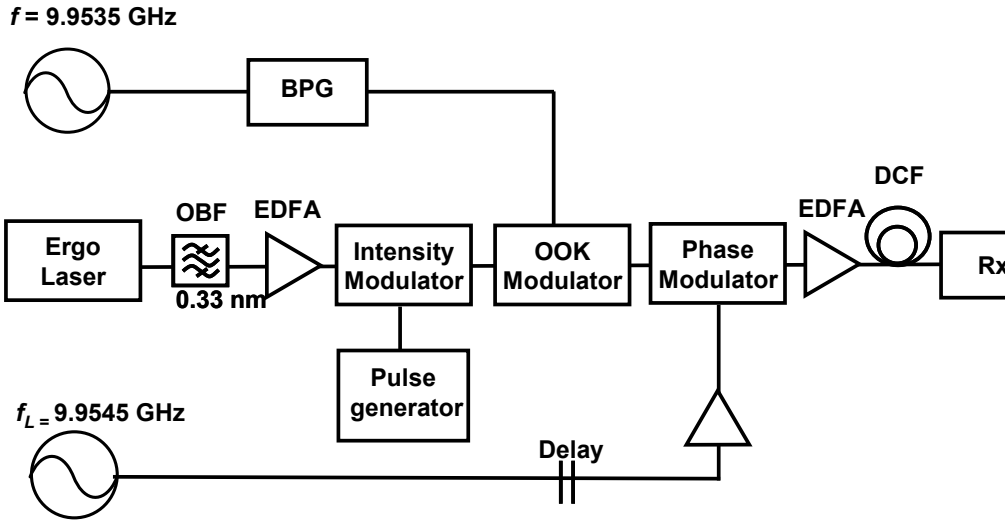

Figure 4-12: Experimental set-up to realize a FRS-unit.

Results

Figure 4-13 presents the experimental eye diagrams, without phase modulator, (a), and (b) with phase modulator. After the synchronization and retiming, a clear eye diagram (a) can be seen using the local clock as the trigger, thus clearly demonstrating that the data frame is now in sync with the local clock. (f_L). When the full time lens is employed, the data is clearly synchronized to the local clock. The leaning edge of synchronized pulses is caused by a combination of non-linear chirp and patterning effects of the EDFA.

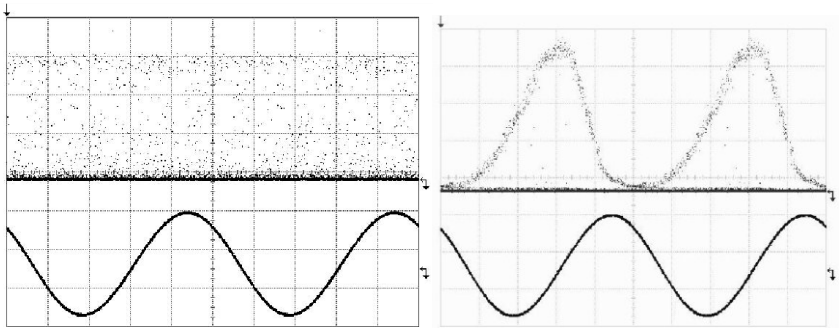

(a) without PM (b) with PM

Figure 4-13: Experimental eye diagrams: (a) without PM and (b) with PM

Figure 4-14 shows the electrical spectrum of the original (a) and synchronized (b) signals. We can observe that the maximum frequency peak of the synchronized signal has been adjusted to f_L = 9.9545 GHz.

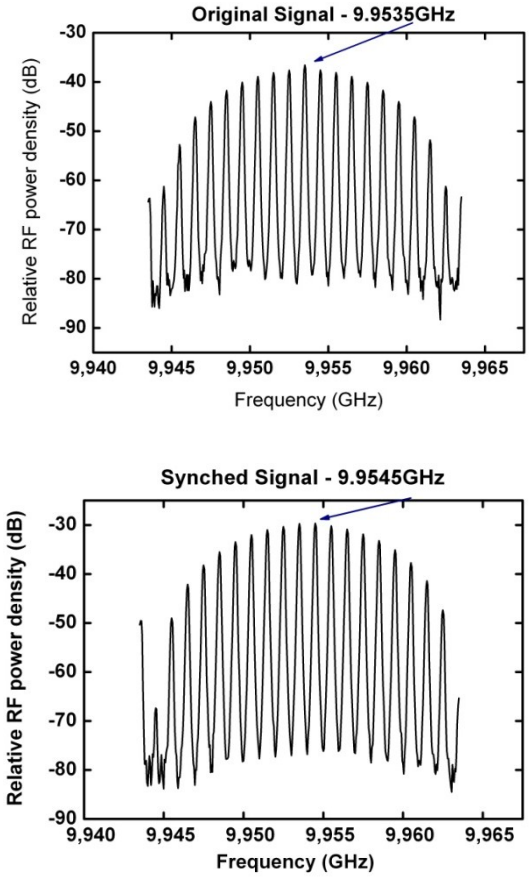

(a) (b)

Figure 4-14: Electrical spectrum: (a) original and (b) synchronized signal

Figure 4.15 shows the rms timing jitter of the synchronized pulses for various frequency offsets, considering a convenient initial time misalignment (delay) for the reception of the 1024 bits frames. In laboratory experiments, our available equipment measures rms timing jitter, instead of peak-to-peak timing jitter. The time-lens-unit allows a timing jitter bellow 1ps within the frequency offset range of $|\Delta f| < 1$ MHz.

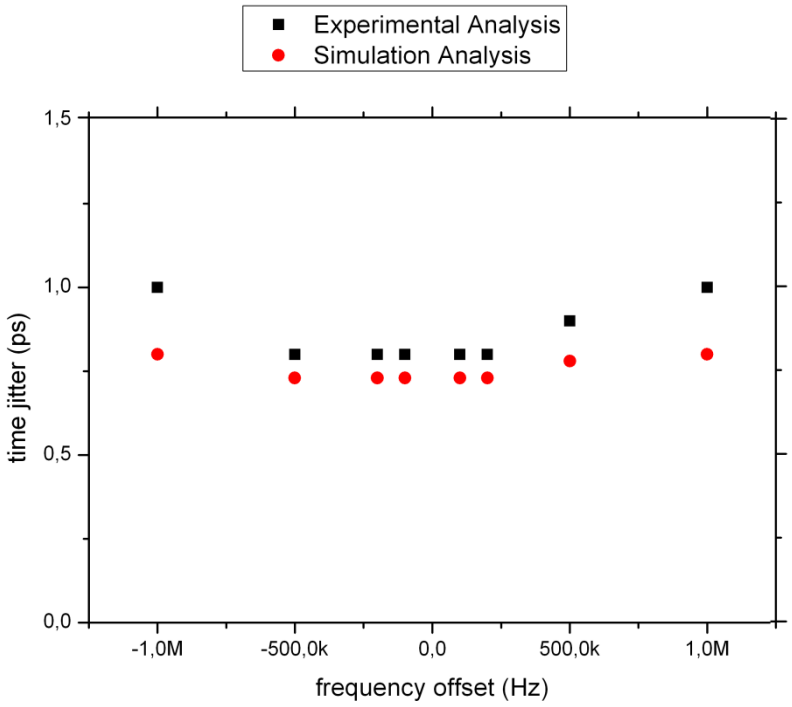

Figure 4-15: rms timing jitter vs. Δf

4.3.2 NRZ input signal, Pulse Carver + Time-lens

In this section, it is demonstrated the operation of the device in full compliance to 10GBASE-W conditions, i.e., frame sizes of 12144 bits and $|\Delta f| < 200$ kHz [31].

Experimental Setup

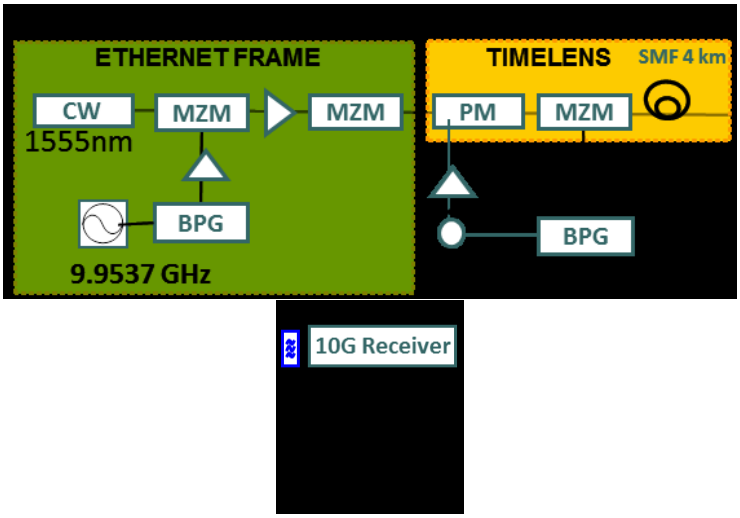

Figure 4-16: Laboratory SETUP [31]

Figure 4-16 shows the experimental setup for the time lens based 10 G Ethernet frame synchronization. It includes a 10 Gbit/s Ethernet frame generator and a time-lens based synchronizer, and a 10 Gbit/s receiver.

The external cavity laser emits continuous wave (CW) light at 1555 nm, which is encoded by on-off keying (OOK) with a 9.9537 Gbit/s PRBS (2^{31}-1) signal in a Mach-Zehnder modulator (MZM). The NRZ-OOK signal passes through another MZM driven by a square pulse from a pulse generator with duration of 2.8 µs and a repetition rate of 100 KHz, which results in a 10 Gbit/s Ethernet packet with the packet size of 28K bits, as shown in Fig. 1. In order to aggregate several 10 G Ethernet packets into a high-speed serial optical data stream, each packet has to be synchronized to a master clock. In this experiment, the Ethernet packet with the repetition rate of 9.9537 Gbit/s needs to be synchronized to the master clock of 9.9535 GHz.

In the time-lens based synchronizer, the 10 Gbit/s Ethernet packet was launched into a phase modulator and a cascaded MZM both driven by the master clock of 9.9535 GHz (200 KHz offset of input clock), and

then launched into a 4-km SMF as a dispersive element. Since the phase modulator is driven by a sinusoidal signal (modulation depth of 2π), it generates both positive and negative chirp in one period. The MZM is used to pulse carve the positively chirped part of the waveform, as described above. The length of SMF is set according to the temporal focus of the time lens (Eq. 3.14). At the same time, the positive chirp introduced by the phase modulator is also compensated by the SMF, and therefore the NRZ signal can be format converted into a RZ signal with pulse compression. Consequently, the input asynchronous NRZ Ethernet packet is converted into a synchronized RZ Ethernet packet.

In the receiver, the demultiplexed 10 G Ethernet packet is detected by a photodetector and measured by an oscilloscope and an error analyzer, which are both triggered by the master clock.

Results

Figure 4-17 shows the electrical power spectrum of the generated 10GE NRZ frame (a) and of the synchronized RZ signal (b). The peak of the spectral envelope reveals the shift of the generated frame signal from 9.9557 GHz (a) to the synchronized 9.9535 GHz (b), confirming proper operation (synchronization). The additional peaks in the spectra are separated by 100 kHz and are due to the frame repetition rate.

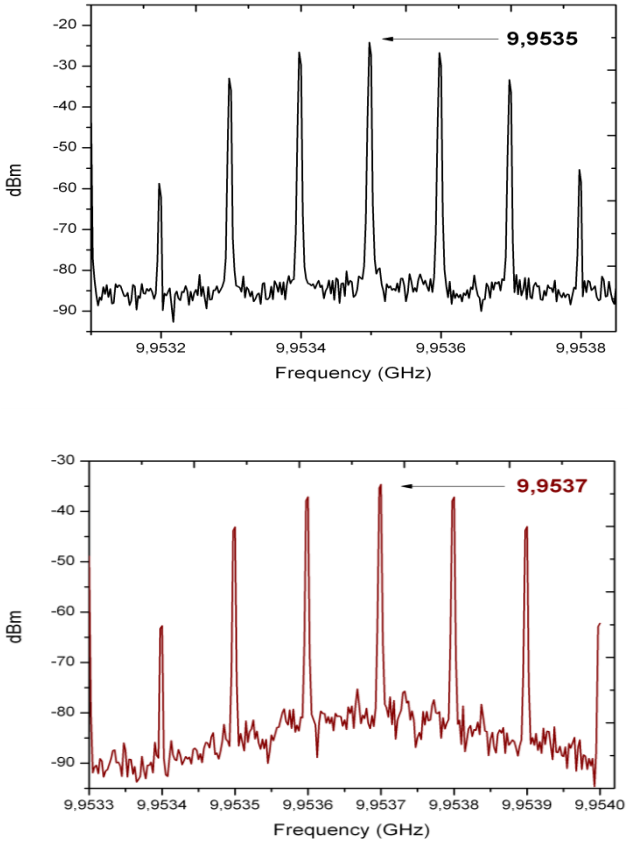

(a) input signal ($f = 9.9535\ GHz$) (b) output synchronized signal ($f_L = 9.9537\ GHz$)

Figure 4-17: input (NRZ) and output (RZ) signal power spectrum

Figure 4-18 shows the clear eye diagram for the compressed and synchronized output RZ pulses, while Figure 4-18 shows the resulting timing jitter

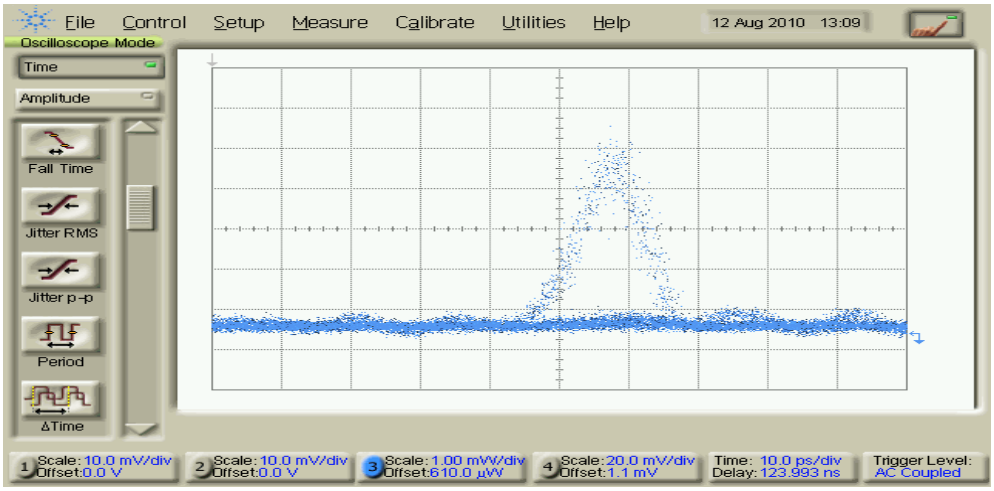

Figure 4-18: RZ synchronized output pulse (before compression stage)

Conclusions

For the 10GBASE-R standard, which transmits data using NRZ at a line rate of 10.3125 Gbit/s (T_L = 97ps) and allows for a frequency offset of up to 1MHz ($|\Delta T| \sim 9.4$fs), the FRS-unit operation (format conversion, synchronization and retiming) is demonstrated with numerical simulations for frame sizes up to 4,096 bits, provided that the initial time misalignment can be roughly adjusted [27].

For the 10GBASE-W standard, where the frequency offset is limited to $\Delta f = \pm 200$ kHz, a full-sized Ethernet frame (12.208 bits) can be correctly processed by the FRS-unit, provided that the initial time misalignment can be roughly adjusted. This was demonstrated with numerical simulation and laboratory experiments [28, 29, 31].

The experimental results show the applicability of the FRS-unit for synchronization and retiming of 10G Ethernet frames in the presence of a frequency offset, with small frame sizes. These results encourage

us to research design workarounds in order to employ the FRS-unit as a basic building block in the design of a synchronization and retiming scheme fully compliant with the requirements of all-optical 10G Ethernet frames.

5
10GB/S ETHERNET-LIKE DATA PACKETS OTDM MULTIPLEXING

Although an optical fiber is a very broadband medium for information transmission [57, 58, 59] it is currently impossible to modulate the full optical bandwidth at once. An optical signal is initially generated from an electrical data pattern and converted back into an electrical signal after transmission for the recovery of the transmitted data. As previously stated, the bandwidth limitation of most electronic and opto-electronic components (currently ~ 120GHz) consequently sets the limit on the maximum achievable optical bit-rate. Current attempts towards achieving maximal information throughput involve optical multiplexing techniques, including WDM, where the whole optical bandwidth is broken up into disjoint frequency bands, each of which is modulated separately [59] and OTDM, where higher serial transmission bit rates are obtained using a single optical wavelength by interleaving of narrow RZ pulses [9, 10, 16, 31].

The optical time-division multiplexing (OTDM) technique is a powerful tool that allows the bandwidth limitation of electronic and opto-electronic components to be overcome and can significantly increase the transmitted signal bit-rate [60, 61, 62, 63]. While WDM utilises the frequency domain to increase the overall transmitter capacity, the OTDM technique uses solely a time domain approach.

In this Chapter we describe the complete design of the conceptual OTMD multiplexer that is capable of optically multiplexing 10GE-like data frames. In our design, NRZ-RZ format-conversion, retiming and synchronization of the frame to the local master clock are performed using the time-lens based *FRS-unit* described in Chapters 3 and 4. All-optical OTDM demultiplexer is also implemented using a nonlinear optical loop mirror (NOLM) device. A complete system containing *FRS-unit* synchronizer, OTDM MUX and OTDM DEMUX is implemented and characterized in laboratory. These experiments, reported in Section 5.3, demonstrate back-to-back error free operation of the proposed scheme.

5.1 OTDM Multiplexing

The idea behind OTDM is to optically interleave several base-rate data streams in the time-domain to achieve a larger aggregate bit rate by multiplexing these signals [9, 13, 16, 31, 67, 68, 69, 70,101]. One important prerequisite for an OTDM transmitter is the use of short return-to-zero (RZ) pulses instead of conventional non-return-to-zero (NRZ) pulses to carry the binary signal information [70, 71, 72]. Since the RZ pulse energy is concentrated within a time window shorter than a bit period [73, 74], the time separation between the two consecutive data pulses can be efficiently utilised for multiplexing multiple streams of data together [9]. Hence, there is a requirement on the pulse width (i.e. full-width half-maximum). The shorter the pulse width the more data streams could be potentially multiplexed together. Very narrow (i.e. < 1 ps FWHM) RZ pulses can be obtained by optical pulse compression, e.g. using a dispersion flat highly nonlinear fiber (DF-HNLF) [based on self-phase modulation (SPM) [16, 76, 77]. The requirement is that the RZ pulse duration should be shorter than the bit period of the aggregated OTDM bit rate, as shown in Eq. 5.1.

$$RZ_{duty\ cycle} < 1 / OTDM_{\text{bit rate}} \qquad (5.1)$$

To multiplex the base-rate RZ signal into a higher-rate OTDM signal several techniques can be used [13, 16, 78, 79, 80, 81, 86, 98]. In this thesis, we are using a passive OTMD multiplexer multiplexing several 10GE-like input channels into a single OTDM serial transmission signal (Figure 1-1: OTDM system multiplexing 10GE input frames). The design is shown in Figure 5-1, which illustrates a 4x10GE multiplexer (i.e. a 40Gbit/s OTDM signal). The operation is as follows:

a) 10Gbit/s asynchronous NRZ frames arriving in each input channel are RZ converted, retimed and synchronized to the MUX master clock with a *FRS-unit*.
b) The resulting synchronous RZ-OOK pulses are further optically compressed in a HNLF, in order to obtain the required RZ pulse duration (Eq. 5.1).
c) The resulting compressed RZ pulses are temporarily interleaved with respect to each other by quarter a bit period using an adjustable delay line.
d) RZ-OOK signals are recombined using a passive optical coupler to obtain the OTDM signal.

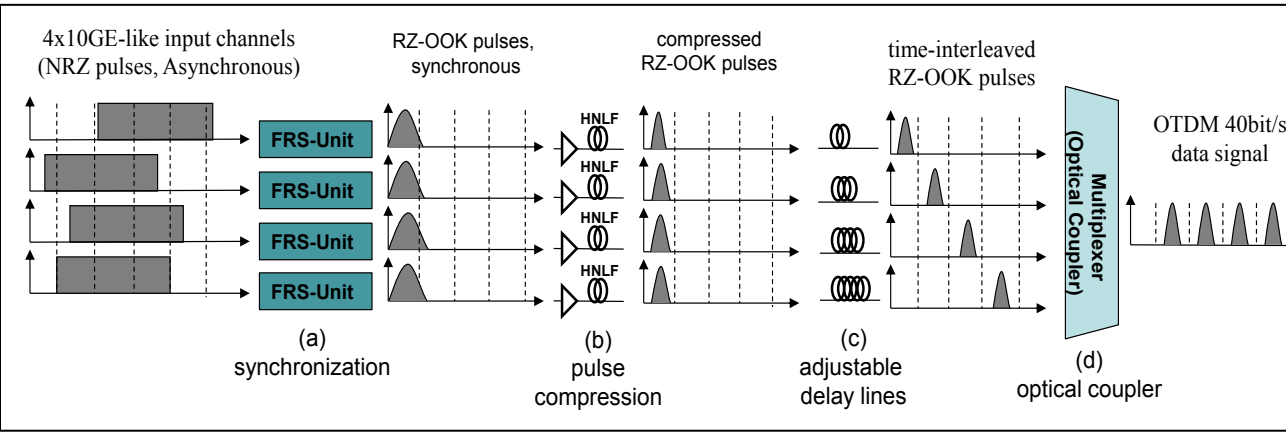

Figure 5-1: OTDM Multiplexing

In order to obtain a higher aggregated bit-rate (e.g. 320, 640Gbit/s), two approaches are possible:

- An increased number of input channels can be used. In this case, it is necessary to adjust the optical compression stage (Figure 5-1(b)) and the delay lines (Figure 5-1(c)). This is the approach used in this thesis.
- Several stages of this simple OTDM multiplexer can be cascaded. In this case, the compression stage must also be adjusted.

5.2 OTDM Demultiplexing

As shown in Figure 1-1, at the receiver, the OTDM signal is separated into the original base-rate signal by the demultiplexer. For direct detection, optical demultiplexing is implemented through cross-phase modulation (XPM) [83] obtained using a highly nonlinear fibre in conjunction with interferometric arrangements [69][87][88][89]. These include the nonlinear optical loop mirror (NOLM) [88][90][91][93][94], which was the configuration used in this thesis.

The NOLM-based demultiplexer is shown in Figure 5-2. The operation is as follows [90].

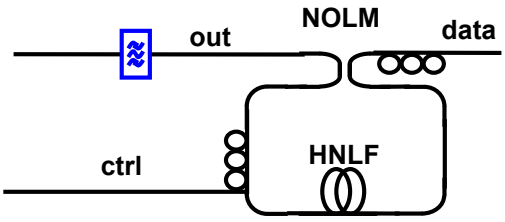

Figure 5-2: OTDM Demultiplexing

The control pulses (*ctrl* in Figure 5-2) required to demultiplex the OTDM signal (*data* in Figure 5-2) is obtained by optical clock extract-

ing directly from the *data* signal. The base-rate extracted clock signal is amplified, filtered and injected into the NOLM. Within the NOLM, the OTDM signal is split into two signals propagating clockwise (CW) and counter-clockwise (CCW) [83, 85]. The target channel of the CCW propagating OTDM signal is co-propagating with the high power control pulse and thus accumulates a nonlinear phase shift induced by XPM. After propagation through the entire loop, the two signals are recombined in the coupler. The control signal can be optimized in order to allow the target channel to experience constructive interference at the output port (*out* in Figure 5-2) of the NOLM. In this case, the NOLM acts like an optical gate and the channel is demultiplexed [90].

5.3 Laboratory Experiments

We have performed laboratory experiments to demonstrate the operation of the proposed OTDM MUX-DEMUX, described in the last Sections. Our goal is to demonstrate inline "add" (i.e. multiplexing a single 10GE-like input channel into a vacant time-slot of an OTDM signal) and "drop" (i.e. demultiplexing the same channel out of the aggregated OTDM signal). We report back-to-back bit error rate (BER) analysis (i.e. considering the digital signal generated in the binary pattern generation and the signal received and decoded in the output of the demultiplexer).

Figure 5-3 shows the experimental setup for the time-lens based 10G Ethernet frame synchronization and the multiplexing with 32 other 10 Gbit/s channels. It includes a 10 G Ethernet frame generator, a *FRS-unit* (time-lens synchronizer), a 320 Gbit/s OTDM RZ-OOK transmitter, multiplexing stages, a NOLM based OTDM demultiplexer and a 10 Gbit/s receiver. The external cavity laser emits continuous wave (CW) light at 1,555 nm, which is encoded by on-off keying (OOK)

with f Gbit/s PRBS (2^{31}-1) signal in a Mach-Zehnder modulator (MZM). The NRZ-OOK signal passes through another MZM driven by a square pulse from a pulse generator (frame generator) and repetition rate of 100 kHz. This module is used to generate the frames.

Two configurations were performed in order to demonstrate the operation of the proposed scheme:

- Square pulse of the frame generator with duration of 2.8 µs (frame size of 28 kbits) and 200 kHz frequency offset (i.e. f = 9.9537 Gbit/s).
- Square pulse of the frame generator with duration of 4 µs (frame size of 40 kbits) and 100 kHz frequency offset (i.e. f = 9.9536 Gbit/s)

The generated signal is illustrated in Figure 5-4, where Figure 5-4(a) shows the NRZ-OOK pulses and Figure 5-4(b) shows the complete frame (28 kbits per frame and 100 kHz repetition rate). In order to aggregate several 10 Gbit/s Ethernet packets into a high-speed serial optical data stream, each packet has to be synchronized to a master clock. In this experiment, the Ethernet packet with the repetition rate of 9.9537 Gbit/s needs to be synchronized to the master clock of 9.9535 GHz, which results in a frequency offset of 200 kHz (i.e. extreme offset tolerated in 10GBASE-W standard [17, 91, 92].

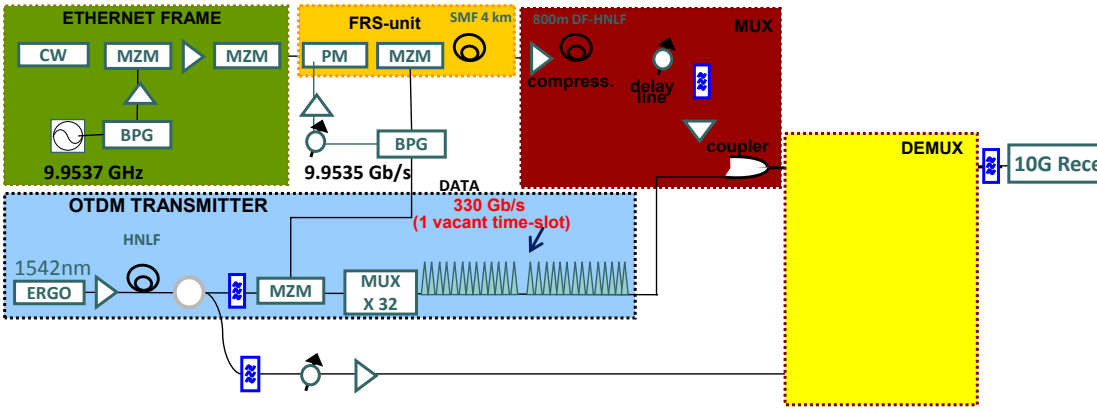

Figure 5-3: Laboratory experiment setup

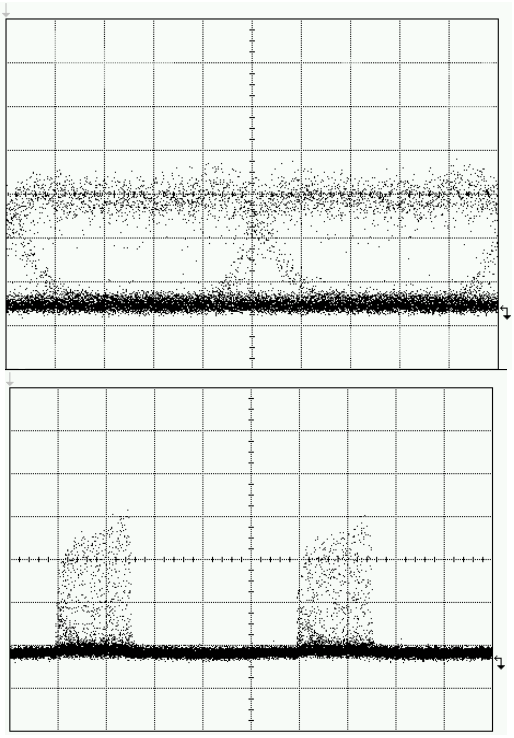

(a) NRZ-OOK pulses (b) 28 kbit frame

Figure 5-4: Input channel 10GE-like signal

In the *FRS-unit* (synchronizer), the 10 G Ethernet packet was launched into a phase modulator and a cascaded MZM both driven by the master clock of 9.9535 GHz (200 kHz offset of input clock), and then launched into a 4-km SMF as a dispersive element. Since the phase modulator is driven by a sinusoidal signal (modulation depth of 2π), it generates both positive and negative chirp in one period. The MZM is used to pulse carve the positively chirped part of the wave-form, as described in Chapter 3. The length of SMF is set according to the temporal focus of the time lens (Eq. 3.14). At the same time, the positive chirp introduced by the phase modulator is also compensated by the SMF, and therefore the NRZ signal can be format converted

into a RZ signal with pulse compression. Consequently, the input asynchronous NRZ Ethernet frame is converted into a synchronized RZ Ethernet frame. The converted RZ signal is amplified in a high-power EDFA and compressed to 800 fs in 800 m of a dispersion flat highly nonlinear fiber (DF-HNLF) [95] based on self-phase modulation (SPM).

The 330 Gbit/s RZ-OOK transmitter consists of a pulse source, a pulse compressor, an OOK modulator and a multiplexing stage. The pulse source is an erbium glass oscillating pulse-generating laser (ERGO-PGL), which produces pulses at 1,542 nm with a repetition rate of 9.9535 GHz. The pulses were compressed to 1 ps and wavelength converted to 1,555 nm in another 400-m DF-HNLF. The compressed pulses were encoded with an OOK signal with a 9.9535 Gbit/s PRBS (2^{31}-1) signal in a Mach-Zehnder modulator. The 10 Gbit/s signal synchronized with the master clock is multiplexed in time to 320 Gbit/s using a passive fiber-delay multiplexer (MUX ×32) with an empty time slot. Since the NRZ Ethernet packet has been synchronized to the master clock, format converted to the RZ packet, and compressed into short pulses, therefore, it can be time division multiplexed with the 320 Gbit/s OTDM signal in the MUX stage, thus aggregated into a 330 Gbit/s serial data stream.

In the receiver, which is also synchronized to the master clock, a nonlinear optical loop mirror (NOLM) is used to demultiplex the 10 G Ethernet packet from the 330 Gbit/s serial data stream. The NOLM operation is based on cross-phase modulation (XPM) in a 50m HNLF. The control pulse is at 1,535 nm and has a pulse width of 3 ps. Finally, the demultiplexed 10 G Ethernet packet is detected by a photodetector and measured by an oscilloscope and an error analyzer, which are both triggered by the master clock.

5.4 Results

Figure 5-5 shows (a) the eye-diagram of the synchronized (*FRS-unit*), compressed and time-delayed RZ-OOK pulse (right before the optical coupler in the multiplexer); (b) the eye diagrams for the 320 Gbit/s OTDM signal plus one vacant time slot and (c) the aggregated 330 Gbit/s serial OTDM signal, when the oscilloscope is triggered by the master clock (9.9535 GHz). The clear eye diagram shown in Figure 5-5(a) indicates the frame has been synchronized to the master clock. Figure 5-5(c) shows that the 10 G Ethernet frame is successfully synchronized and correctly positioned into a time slot in the 330 Gbit/s serial signal.

Figure 5-6 shows part of the electrical power spectrum of the signal of the generated frame pulses (a) and the compressed and retimed pulses (b). The peak of the spectral envelope reveals the shift of the generated frame signal from 9.9557 GHz (Figure 5-6 (a)) to the retimed 9.9535 GHz (Figure 5-6 (b)), confirming proper operation.

Figure 5-7 shows the eye diagram of the demultiplexed pulses for (a) 28 kbits sized frames (Δf = 200 kHz) and (b) 40 kbits sized frame (Δf = 100 kHz).

Finally, Figure 5-8 shows the measured error-free (BER<10^{-9}) BER curves in two configurations (28 kbit sized frame (Δf = 200 kHz) and 40 kbit sized frame (Δf = 100 kHz)). The error counter needs frames of 40 kbits size to count errors to BER of ~10^{-9}, but the synchronization and error detection for frames of 28 kbits size with 200 kHz offset is also successful, though measurements are limited to BER of ~$10^{-6,}$ due the equipments limitation .

The demultiplexed eye diagrams are clear and open in both the 28 and 40 kbits frame cases, corroborating successful sync and NRZ-RZ conversion as well as multiplexing and demultiplexing. The BER curves show less than 10^{-9} BER for the 40 Kbits frames, thus quantitatively

confirming proper operation of this proposed scheme. There is only about 0.5 dB difference between the 28 and 40 Kbits frame cases, and the BER slopes are the same. There is only ~1 dB penalty from the back-to-back to the sync-NRZ-RZ case, and an additional ~3 dB penalty for MUX/DEMUX.

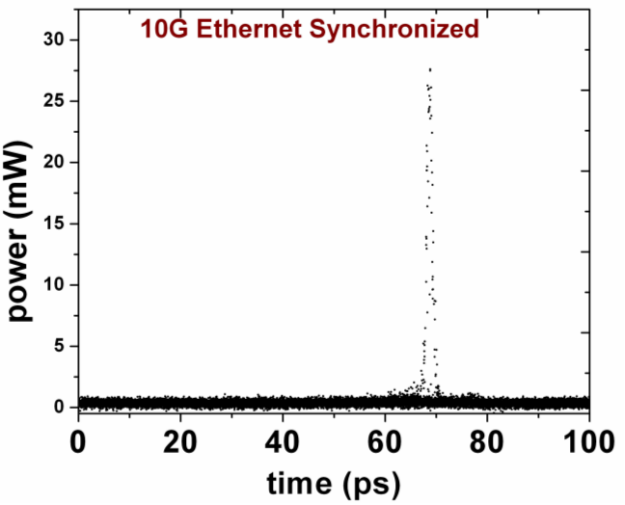

(a) NRZ to RZ converted 10 Gbit/s frame signals

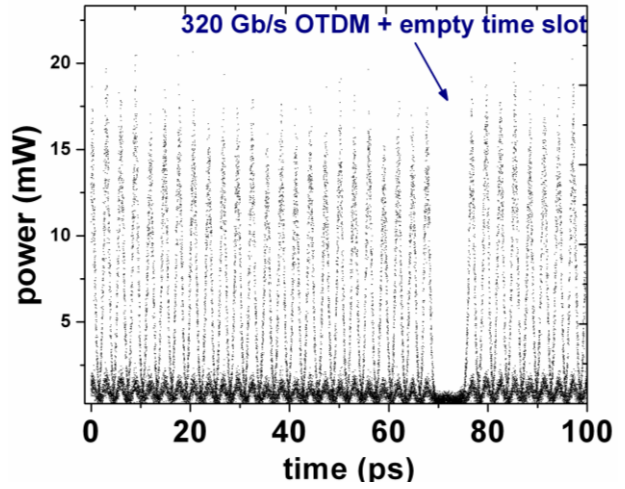

(b) 320 Gbit/s OTDM + 1 vacant time slot

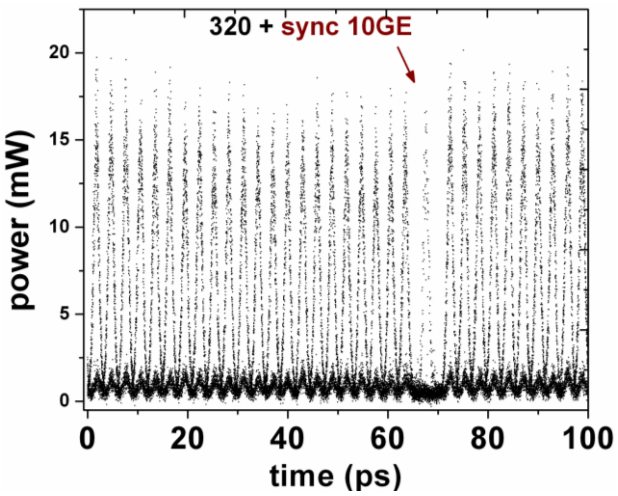

(c) 330 Gbit/s including the multiplexed 10G Ethernet channel

Figure 5-5: Eye diagrams of the experiment

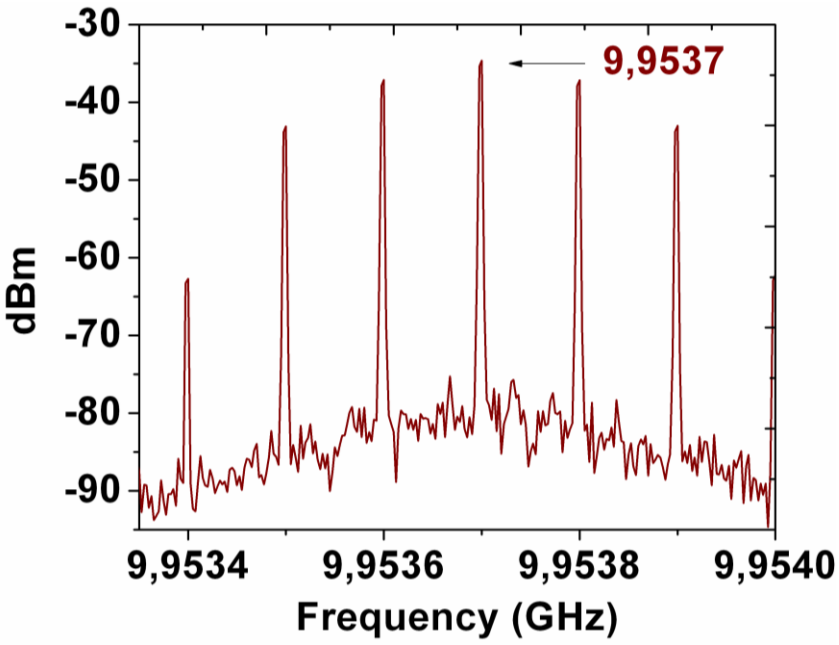

(a) generated 10GE frame pulses

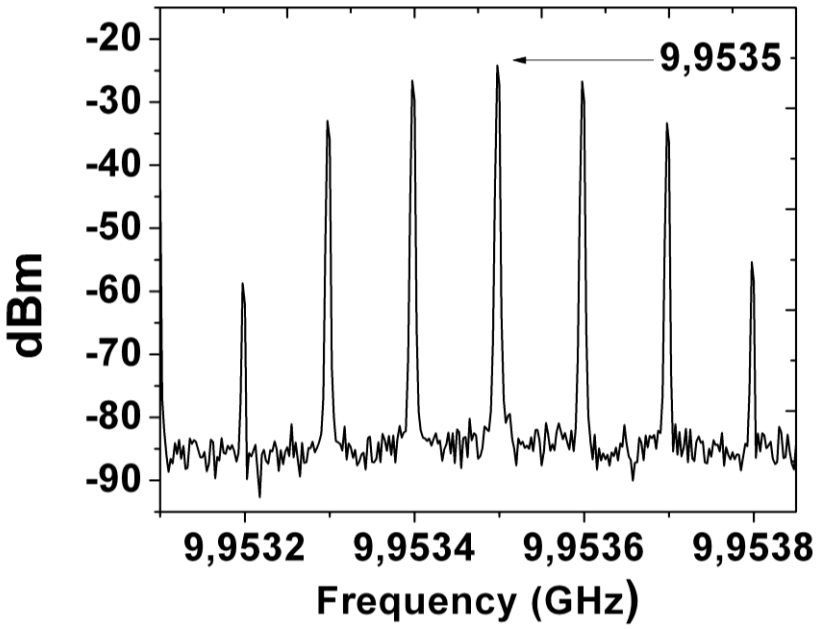

(b) synchronized and compressed 10GE frame pulses

Figure 5-6: Electrical power spectrum of generated and synchronized 10GE pulses

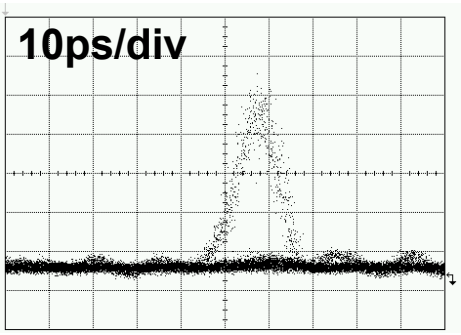

(a) 28 Kbit sized frame (Δf = 200 kHz)

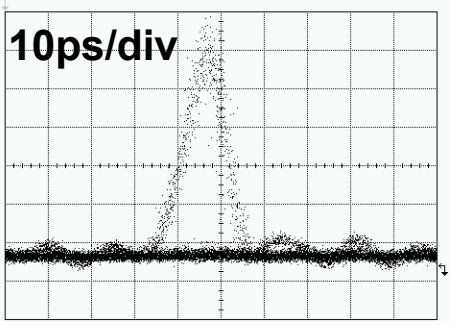

(b) 40 Kbit sized frame (Δf = 100 kHz)

Figure 5-7: Eye diagram of the demultiplexed pulses

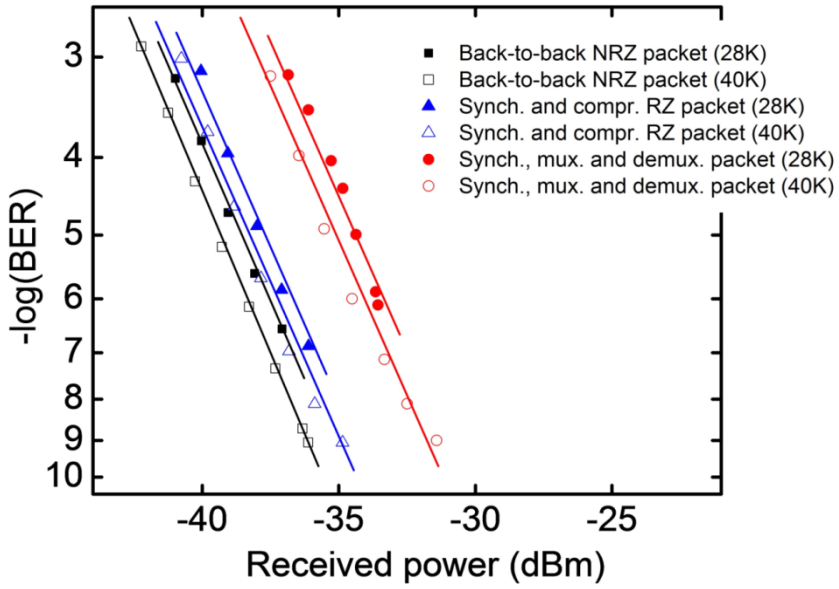

Figure 5-8: BER measurements

5.5 Conclusions

10 Gbit/s frames (10GE-like frames) containing 28 Kbits (Δf = 200 kHz) 40 Kbit sized frame (Δf = 100 kHz) were successfully synchronized to a local clock and then multiplexed into a vacant OTDM time slot of a 330 Gbit/s OTDM data signal, using a passive optical coupler (passive multiplexing/"add" operation). The multiplexed signal was demultiplexed with a NOLM demultiplexer (all optical demultiplexing/"drop" operation) and BER analysis were performed, demonstration error-free back-to-back operation.

We have successfully demonstrated the combined operations of 1) synchronizing an asynchronous Ethernet frame to a local master clock using the *FRS-unit* proposed in this thesis, 2) optical multiplexing ("add" operation) in time with an OOK single polarization and single wavelength optical TDM data signal of 330 Gbit/s.

Similar setups have recently been successfully implemented, demonstrating the applicability of the proposed schemes in obtaining even

higher rates in a serial OTDM link. Example of such experiments is [101], where an asynchronous 10 Gb/s Ethernet packet with maximum packet size of 1518 bytes is synchronized and retimed to a master clock with 200 kHz frequency offset using a time lens, then further pulse compressed to a FWHM of 400 fs and finally time-division multiplexed with a serial 1.28 Tb/s signal including a vacant time slot, thus forming a 1.29 Tb/s time-division multiplexed serial signal.

6 CONCLUSION

In this thesis we have proposed a new OTDM multiplexing scheme that is able to aggregate several 10 Gbit/s Ethernet channels into a single serial data link, using single wavelength and single polarization. The main challenge in the design process relates to the asynchronous nature of 10G Ethernet, which also requires terminal equipment to support frequency offset tolerance.

It is considered, as design requirements, the 10GBASE-R and 10GBASE-W PHY specifications, which require support for ~1 MHz and ~200 kHz frequency offset, respectively. In order to cope with the asynchronous nature of 10Gbit/s, we have designed, a time-lens based NRZ-RZ format conversion, retiming and synchronization unit (FRS-unit), which were analytically evaluated and whose operational conditions were demonstrated through both, numerical simulations and laboratory experiments. This simple device was successfully used to synchronize 10GE-like frames to the local master clock of the OTDM multiplexing system.

The operational conditions of *FRS-unit* found in this research shows that for the 10GBASE-W standard ($|\Delta f| < 200$ kHz) a full-sized Ethernet frame (i.e. 1,518 bytes) could be readily synchronized with the proposed *FRS-unit*, provided that the initial time misalignment can be roughly adjusted. In the case of the 10GBASE-R standard, we were able to synchronize up to 4kbits in the same frame, under extreme frequency offset conditions (i.e. $|\Delta f| = 1$ MHz). This result is very

encouraging, as such a simple device can be used to optically process and synchronize long 10GE-like frames.

The OTDM multiplexer is conceived as a simple all-optical device implemented by combining optical pulse compression, passive optical time delay, and a passive optical coupler. The OTDM demultiplexer was designed as a NOLM-based optical gate [97, 98]. Back-to-back error free (BER < 10^{-9}) operation was demonstrated for the complete FRS-unit synchronizer + MUX + DEMUX scheme, using a "add"/"drop" implementation for a single 10GE input channel inside a 330 Gbit/s OTDM aggregated serial link.

All the devices described in the experiments can be easily implemented using commercially available optical system components.

As the operation of multiplexing have been successfully demonstrated in higher (Tbit/s) rates it is believe that the results described in this Chapter can be readily scaled to higher OTDM data signal rates (i.e. Tbit/s rates). Therefore, the presented scheme shows great promise for future Tbit/s Ethernet solutions [99] based on Optical TDM.

6.1 Future Work

Following, we present some of the immediate extensions of the research work presented in this thesis:

- Design of a synchronizer device that is able to cope with complete 10GBASE-R conditions (i.e. synchronization of a full-sized Ethernet frame at $|\Delta f| = 1$ MHz). Preliminary evaluation and numerical simulation have shown that it is possible to use the basic *FRS-unit* described in this thesis as a building block for a 10GE Synchronizer, fully compliant with 10GBASE-R conditions.
- Design and experimentation of the proposed OTDM MUX/DEMUX using higher rates (i.e. Tbit/s). This is

viewed as a direct extension of the current results presented in this thesis as this type of multiplexer have been successfully implemented and demonstrated for OTDM rates that surpass 2Tbit/s, without the synchronization stages (i.e. for already-synchronous input channels).

- Design of all-optical switch that is able to implement aggregation of traffic originated from different 10GE links into higher capacity channels (OTDM channels), while also being able to optically commute frames into different source-destination paths. The proposed scheme could be used as a basic design for such all-optical switch, to which additional optical signaling (i.e. network path ID and addressing) and optical switching capabilities should be added, together with layer-2 (e.g. MPLS functionality).

ACRONYMS

BER: Bit Error Ratio

CD: Chromatic Dispersion

CSMA/CD: Carrier Sense Multiple Access with Collision Detection

CW: Continuous Wave

DCF: Dispersion Compensating Fiber

DF-HNLF: Dispersion Flattened Highly Nonlinear Fiber

DGD: Differential Group Delay

DWDM: Dense Wavelength Division Multiplexing

EDFA: Erbium Doped Fiber Amplifier

FRS-Unit: Format-conversion, Retiming, and Synchronization unit

FWHM: Full Width at Half Maximum

FWM: Four Wave Mixing

GBd: Giga Baud

GVD: Group Velocity Dispersion

HNLF: Highly Nonlinear Fiber

IM: Intensity Modulator

ISI: Inter Symbol Interference

LO: Local Oscillator

NRZ: Non Return to Zero

OBPF: Optical Bandpass Filter

OFT: Optical Fourier Transform

OMUX: Optical Multiplexer

OOK: On-Off Keying

OSNR: Optical Signal to Noise Ratio

OTDM: Optical Time Division Multiplexing

PM: Phase Modulator

PMD: Polarization Mode Dispersion

PolMUX: Polarization Multiplexing

RZ: Return to Zero

SMF: Single Mode Fiber

SPM: Self-Phase Modulation

TBd: Tera Baud

TDM: Time Division Multiplexing

WAN: Wide Area Network

WDM: Wavelength Division Multiplexing

REFERENCES

[1] IEEE 802.3ae-2002 Standard for Information Technology-Telecommunications and Information Exchange Between Systems- Local and Metropolitan Area Networks- Specific Requirements Part 3: Carrier Sense Multiple Access With Collision Detection (CSMA/CD) Access Method and Physical Layer Specifications Amendment: Media Access Control (MAC) Parameters, Physical Layers, and Management Parameters for 10 Gb/S Operation 2002

[2] IEEE 802.3an-2006 Standard for Information Technology - Telecommunications and Information Exchange Between Systems - Local and Metropolitan Area Networks - Specific Requirements Part 3: Carrier Sense Multiple Access with Collision Detection (CSMA/CD) Access Method and Physical Layer Specifications- Corrigendum 2: IEEE Std 802.3an-2006 10GBASE-T Correction 2007, 1-2

[3] IEEE 802.3ba-2010 IEEE Standard for Information technology-Telecommunications and information exchange between systems-Local and metropolitan area networks-Specific requirements Part 3: Carrier Sense Multiple Access with Collision Detection (CSMA/CD) Access Method and Physical Layer Specifications Amendment 4: Media Access Control Parameters, Physical Layers and Management Parameters for 40 Gb/s and 100 Gb/s Operation 2010, 1-457

[4] Hendler, James and Golbeck, Jennifer. ”Metcalfe's law, Web 2.0, and the Semantic Web” Journal of Web Semantics:

Science, Services and Agents on the World Wide Web. Vol. 6, 14-20, 2008, Elsevier.

[5] Gustav Veith, Eugen Lach, Karsten Schuh, “100 Gigabit-per-second: Ultra-high transmission bitrate for next generation optical transport networks”, Comptes Rendus Physique 9(9-10) pp. 1002-1011, November-December 2008.

[6] Desai, B. N.; Frigo, N. J.; Smiljanic, A.; Reichmann, K. C.; Iannone, P. P. & Roman, R. S. An optical implementation of a packet-based (Ethernet) MAC in a WDM passive optical network overlay Proc. Optical Fiber Communication Conf. and Exhibit OFC 2001, 2001, 3

[7] Rindos, A.; Woolet, S.; Nicholson, L. & Vouk, M. A performance evaluation of emerging Ethernet technologies: switched/high-speed/full-duplex Ethernet and Ethernet LAN emulation over ATM Proc. IEEE Southeastcon '96. 'Bringing Together Education, Science and Technology', 1996, 401-404

[8] Thatcher, J. Tutorial: how optical Ethernet is disrupting the network marketplace: understanding the causes, trends, and implications Proc. Optical Fiber Communication Conf. and Exhibit OFC 2002, 2002

[9] L. K. Oxenløwe, M. Galili, H. C. Hansen Mulvad, A. T. Clausen, and P. Jeppesen. “Terabit/s serial optical communications”. Annual Meeting of the IEEE Photonics Society 2009, Belek-Antalya, Turkey, October 2009.

[10] Oxenløwe, Leif Katsuo ; Galili, Michael ; Mulvad, Hans Christian Hansen ; Hu, Hao ; Xu, Jing ; Palushani, Evarist ; Laguardia Areal, Janaina ; Clausen, Anders ; Jeppesen, Palle. ”Ultra-high-speed optical signal processing of Tbaud data signals” European Conference and Exhibition on Optical Communication, pages: Mo.1.A.1, 2010,

[11] Gombiner, J. 2011. ”Carbon Footprinting the Internet”. Consilience-The Journal of Sustainable Development., (2011).

[12] Winzer, P. J.; Essiambre, R.-J.; , "Advanced Modulation Formats for High-Capacity Optical Transport Networks,"

Lightwave Technology, Journal of , vol.24, no.12, pp.4711-4728, Dec. 2006 doi: 10.1109/JLT.2006.885260

[13] M. Nakazawa et al, ”1.28 Tbit/s-70 km OTDM transmission using thirdand fourth-order simultaneous dispersion compensation with a phase modulator”, Electron. Lett., 36 (24), (2000), pp 2027-2029, 2000.

[14] B. Metcalfe, “Toward Terabit Ethernet”, OFC 2008, San Diego (USA), plenary talk.

[15] Emmanuel B. Desurvire, “Capacity Demand and Technology Challenges for Lightwave Systems in the Next Two Decades”, J. Lightwave Technol., Vol. 24, No. 12, December 2006.

[16] H.C. Hansen Mulvad, L.K. Oxenløwe, M. Galili, A.T. Clausen, L. Gru¨ner-Nielsen and P. Jeppesen, “1.28 Tbit/s single-polarisation serial OOK optical data generation and demultiplexing,” Electronic Letters, 45(5) pp. 280-281, Feb. 2009.

[17] IEEE 802.3-2008 Part 3: Carrier Sense Multiple Access with Collision Detection (CSMA/CD) access method and Physical Layer specifications, Section 4 (10G Ethernet). IEEE standards. 2008.

[18] B. H. Kolner and M. Nazarathy, “Temporal imaging with a time lens,” Optical Letters 14, pp. 630-632, 1989

[19] J. van Howe and C. Xu, “Ultrafast Optical Signal Processing Based Upon Space–Time Dualities,” IEEE Journal of Light-wave Technology 24(7), pp. 2649-2662, July 2006.

[20] Kolner, B.H.; , "Space-time duality and the theory of temporal imaging," Quantum Electronics, IEEE Journal of , vol.30, no.8, pp.1951-1963, Aug 1994 doi: 10.1109/3.301659

[21] Bennett, C.V.; Kolner, B.H.; , "Principles of parametric temporal imaging. I. System configurations," Quantum Electronics, IEEE Journal of , vol.36, no.4, pp.430-437, April 2000 doi: 10.1109/3.831018

[22] Bennett, C.V.; Kolner, B.H.; , "Principles of parametric temporal imaging. II. System performance," Quantum

Electronics, IEEE Journal of , vol.36, no.6, pp.649-655, June 2000 doi: 10.1109/3.845718

[23] Chattopadhyay, T. & Das, S. An efficient time lens for optical pulse compression Proc. Int. Conf. Numerical Simulation of Semiconductor Optoelectronic Devices NUSOD '06, 2006, 141-142

[24] T. Hirooka and M. Nakazawa, "Optical Adaptive Equalization of High-Speed Signals Using Time-Domain Optical Fourier Transformation," IEEE Journal of Lightwave Technology 24(7), pp. 2530-2540, July 2006.

[25] C. W. Chow, A. D. Ellis, and F. Parmigiani, "Time-division-multiplexing using pulse position locking for 100 Gb/s applications," Optics Express 17(8), pp. 6562-6567, April 2009.

[26] Thomas Dræborg Clausen, Ph.D. thesis. "Experimental and theoretical investigation of systems with potential for terabit capacity", August 2010. DTU Fotonik, Kgs. Lyngby, Den-mark.

[27] Laguardia Areal, Janaina; Hu, Hao; Peucheret, Christophe; Palushani, Evarist; Puttini, Ricardo; Clausen, Anders; Berger, Michael Stübert; Osadchiy, Alexey; Oxenløwe, Leif Katsuo. "Analysis of a time-lens based optical frame synchronizer and retimer for 10G Ethernet aiming at a Tb/s optical router/switch design." In Proc. of 14th Conference on Optical Network Design and Modeling (ONDM 2010), Kyoto, Japan, Jan. 2010.

[28] Laguardia Areal, Janaina; Hu, Hao; Palushani, Evarist; Clausen, Anders; Berger, Michael Stübert; Oxenløwe, Leif. "Time-lens based optical packet pulse compression and retiming". In Proc. of SPIE Photonics Europe (SPIE 2010), Brussels, Apr. 2010.

[29] Laguardia Areal, Janaina; Hu, Hao; Palushani, Evarist; Oxenløwe, Leif; Clausen, Anders; Berger, Michael Stübert; Jeppesen, Palle. "Time-lens based synchronizer and retimer for 10 Gb/s Ethernet packets with up to ±1MHz frequency offset."

In Proc. of 2010 Conference on Lasers and Electro-Optics (CLEO 2010), 2010.

[30] Laguardia Areal, Janaina; Hu, Hao; Palushani, Evarist; Ji, Hua; Clausen, Anders; Berger, Michael Stübert; Jeppesen, Palle; Oxenløwe, Leif. "Conversion of asynchronous 10 Gbit/s Ethernet NRZ frame into a synchronous RZ frame and multiplexing to 170 Gbit/s." In Proc. of Annual Meeting of the IEEE Photonics Society 2010, Denver, Colorado, USA, 2010.

[31] Laguardia Areal, Janaina; Hu, hu; Palushani, Evarist; Mulvad, Hans Christian; Clausen, Anders; Berger, Michael; Oxenløwe, Leif; Jeppesen, Palle. "Synchronization and NRZ-to-RZ conversion of 10 Gbit/s Ethernet-like data packets and subsequent optical TDM multiplexing to 330 Gbit/s." In Proc. of 2011 Optical Fiber Communication Conference and Exposition (OFC 2011), Los Angeles, USA, Mar. 2011.

[32] Shoch, J. F.; Dalal, Y. K.; Redell, D. D. & Crane, R. C. Evolution of the Ethernet Local Computer Network Computer, 1982, 15, 10-27

[33] John F. Shoch; Yogen K. Dalal; David D. Redell; Ronald C. Crane, "Evolution of the Ethernet Local Computer Network", IEEE Computer 15 (8): 14–26. doi:10.1109/MC.1982.1654107, August 1982.

[34] D'Ambrosia, J. Ethernet Evolution: The Path to 100 Gigabit Ethernet Proc. Digest of the IEEE/LEOS Summer Topical Meetings, 2007, 5-6

[35] V Sanchez, R.; Raptis, L.; Vaxevanakis, K.; , "Ethernet as a carrier grade technology: developments and innovations", Communications Magazine, IEE, vol.46, no.9, pp.88-94, September 2008.

[36] LAN MAN Standards Committee of the IEEE Computer Society, IEEE 802.3x-1997 and IEEE 802.3y-1997. IEEE Standards, pp. 28–31, 1997.

[37] Choi, S. IEEE 802.11e MAC-level FEC performance evaluation and enhancement Proc. IEEE Global

Telecommunications Conf. GLOBECOM '02, 2002, 1, 773-777

[38] Davik, F.; Yilmaz, M.; Gjessing, S.; Uzun, N.; , "IEEE 802.17 resilient packet ring tutorial," Communications Magazine, IEEE , vol.42, no.3, pp. 112- 118, Mar 2004 doi: 10.1109/MCOM.2004.1273782

[39] R.C. Walker; R. Dugan, "64b/66b low-overhead coding proposal for serial links" IEEE 802.3 High Speed Study Group. pp. 11-13, 2000.

[40] Barton, M. Punctured convolutional codes for supporting PCS access to ATM networks Proc. IEEE Int. Conf. Communications ICC '99, 1999, 3, 1880-1884

[41] Duelk, M. Next-generation 100 G Ethernet Proc. 31st European Conf. Optical Communication ECOC 2005, 2005, 5, 15-18

[42] Standard - Dual Simplex STP Physical Medium Dependent (PMD) Sublayer, Medium Dependent Interface (MDI), and Link Specifications 1995

[43] Duelk, M. & Zirngibl, M. 100 Gigabit Ethernet - Applications, Features, Challenges Proc. 25th IEEE Int. Conf. Computer Communications INFOCOM 2006, 2006, 1-5

[44] J. Adalid, "Modulation Format Conversion in Future Optical Networks", Master Thesis, DTU, Denmark, March 2008.

[45] Kauffman, M. T.; Godil, A. A.; Auld, B. A.; Banyai, W. C. & Bloom, D. M. Applications of time lens optical systems Electronics Letters, 1993, 29, 268-269

[46] Verdurmen, E. J. M.; Zhao, Y.; Tangdiongga, E.; Turkiewicz, J. P.; Khoe, G. D. & de Waardt, H. Error-free all-optical add-drop multiplexing using HNLF in a NOLM at 160 Gbit/s Electronics Letters, 2005, 41, 349-350

[47] Siahlo, A. I.; Clausen, A. T.; Oxenlowe, L. K.; Seoane, J. & Jeppesen, P. 640 Gb/s OTDM transmission and demultiplexing using a NOLM with commercially available highly non-linear

fiber Proc. (CLEO) Lasers and Electro-Optics Conf, 2005, 2, 883-885

[48] MJ Connelly ”Semiconductor optical amplifiers” - 2002 - Springer

[49] Ibrahim, T. A.; Van, V.; Ritter, K.; Absil, P. P.; Johnson, F. G.; Grover, R.; Goldhar, J. & Ho, P.-T. Fast nonlinear all-optical switching in a compact semiconductor microring resonator Proc. 14th Annual Meeting of the IEEE Lasers and Electro-Optics Society LEOS 2001, 2001, 2, 519-520

[50] Romisch, S.; Kitching, J.; Ferre-Pikal, E.; Hollberg, L. & Walls, R. L. Performance evaluation of optoelectronic oscillators Proc. Joint Meeting of the European Frequency and Time Forum and the IEEE Int. Frequency Control Symp., 1999, 2, 561-564

[51] Chow, C. W.; Ellis, A. D. & Parmigiani, F. (2009). Trans-multiplexer using pulse position locking for 100 Gb/s applications. Opt. Express, Vol. 17, (2009) pp. 6562-6567

[52] Agrawal, G. P. Carrier-induced group-velocity dispersion and pulse compression in semiconductor laser amplifiers Electronics Letters, 1991, 27, 620-621

[53] Bennett, C. V.; Scott, R. P. & Kolner, B. H. Temporal magnification and reversal of 100 Gb/s optical data with an up-conversion time microscope Appl Phys Lett, 1994, 65, 2513-2515

[54] Transmission Maker and VPI Component Maker: Photonic modules reference manual - VPIsystems - 2008

[55] Wuth, T.; Chbat, M. W. & Kamalov, V. F. Multi-rate (100G/40G/10G) Transport Over Deployed Optical Networks Proc. Conf. Optical Fiber communication/National Fiber Optic Engineers Conf. OFC/NFOEC 2008, 2008, 1-9

[56] Loeser, J. & Haertig, H. Using Switched Ethernet for Hard Real-Time Communication Proc. Int. Conf. Parallel Computing in Electrical Engineering PARELEC 2004, 2004, 349-353

[57] Keiser, G. 2003. Optical Fiber Communications. Encyclopedia of Telecommunications

[58] G Agrawal – 1989. Nonlinear Fiber Optics

[59] G Agrawal – 2002. Fiber-optic communication systems 3rd ed.

[60] O'Mahony, M. J. Optical multiplexing in fiber networks: progress in WDM and OTDM #IEEE_M_COM#, 1995, 33, 82-88

[61] Jepson, K. S.; Middelsen, B.; Clausen, A. T.; Poulsen, H. N.; Stubkjaer, K. E. & Vaa, M. High-speed OTDM switching Technical Digest. Summaries of papers presented at the Conf. Lasers and Electro-Optics CLEO 98, 1998

[62] Nakazawa, M. Tb/s OTDM technology Proc. 27th European Conf. Optical Communication ECOC '01, 2001, 5, 184-187

[63] Morita, I. & Edagawa, N. Study on optimum OTDM signals for long-distance 40 Gbit/s transmission Proc. Optical Fiber Communication Conf. and Exhibit OFC 2002, 2002, 5-6

[64] Nuyts, R. J. & Park, Y. K. Dispersion management of a 10 Gb/s repeatered transmission system using dispersion compensating fibers Proc. 22nd European Conf. Optical Communication ECOC '96, 1996, 2, 185-188

[65] Farbert, A.; Scheerer, C.; Elbers, J.-P.; Glingener, C. & Fischer, G. Optimised dispersion management scheme for long-haul optical communication systems Electronics Letters, 1999, 35, 1865-1866

[66] Atai, J. & Malomed, B. A. A fully stabilized scheme for dispersion management Proc. Conf. Lasers and Electro-Optics (CLEO 2000), 2000, 336-337

[67] Tucker, R.S.; Eisenstein, G.; Korotky, S.K.; , "Optical time-division multiplexing for very high bit-rate transmission," Lightwave Technology, Journal of , vol.6, no.11, pp.1737-1749, Nov 1988 doi: 10.1109/50.9991

[68] Galili, M.; Mulvad, H.; Oxenlowe, L. K.; Hu, H.; Palushani, E.; Clausen, A. T. & Jeppesen, P. Generation and detection of

2.56 Tbit/s OTDM data using DPSK and polarisation multiplexing Proc. Conf Optical Fiber Communication (OFC), collocated National Fiber Optic Engineers Conf. (OFC/NFOEC), 2010, 1-3

[69] Hao Hu; Areal, J.L.; Palushani, E.; Oxenlowe, L.K.; Clausen, A.; Berger, M.S.; Jeppesen, P.; , "Optical Synchronization of a 10-G Ethernet Packet and Time-Division Multiplexing to a 50-Gb/s Signal Using an Optical Time Lens," Photonics Technology Letters, IEEE , vol.22, no.21, pp.1583-1585, Nov.1, 2010 doi: 10.1109/LPT.2010.2073460

[70] Hamilton, S.A.; Robinson, B.S.; Murphy, T.E.; Savage, S.J.; Ippen, E.P.; , "100 Gb/s optical time-division multiplexed networks," Lightwave Technology, Journal of , vol.20, no.12, pp. 2086- 2100, Dec 2002 doi: 10.1109/JLT.2002.806781

[71] B. Pierpaolo , P. Davide, M. Diego, M. Mario. All-optical free-space processing for optical communication signals. Optics Communications Volume 181, Issues 1–3, 1 July 2000, Pages 79–88

[72] Nieznanski, J. New concept for pulse frequency synthesis Proc. IEEE Int Industrial Electronics ISIE '97. Symp, 1997, 1112-1115

[73] F. Forghieri, P. R. Prucnal, R. W. Tkach, and A. R. Chraplyvy, "RZ versus NRZ in nonlinear WDM systems", IEEE Photon. Technol. Lett., vol. 9, pp.1035 -1037 1997

[74] Lei Xu; Wang, B.C.; Baby, V.; Glesk, I.; Prucnal, P.R.; , "All-optical data format conversion between RZ and NRZ based on a Mach-Zehnder interferometric wavelength converter," Photonics Technology Letters, IEEE , vol.15, no.2, pp.308-310, Feb. 2003 doi: 10.1109/LPT.2002.806105

[75] Hu, H.; Mulvad, H. C. H.; Galili, M.; Palushani, E.; Clausen, A. T.; Oxenlowe, L. K. & Jeppesen, P. Polarisation-insensitive 640 Gbit/s demultiplexing using a polarisation-maintaining highly non-linear fibre Proc. Int. Conf. Photonics in Switching PS '09, 2009, 1-2

[76] Gholami, F.; Myslivets, E.; Zlatanovic, S.; Alic, N.; Radic, S.; , "Dispersion Characterization of Highly Nonlinear Fiber Over a 700-nm Band," Photonics Technology Letters, IEEE , vol.24, no.12, pp.1021-1023, June15, 2012 doi: 10.1109/LPT.2012.2193612

[77] Jianjun Yu; Jeppesen, P.; , "Simultaneous all-optical demultiplexing and regeneration based on self-phase and cross-phase modulation in a dispersion shifted fiber," Lightwave Technology, Journal of , vol.19, no.7, pp.941-949, Jul 2001 doi: 10.1109/50.933288

[78] Oxenlowe, L. K.; Agis, F. G.; Ware, C.; Kurimura, S.; Mulvad, H. C. H.; Galili, M.; Kitamura, K.; Nakajima, H.; Ichikawa, J.; Erasme, D.; Clausen, A. T. & Jeppesen, P. 640 Gbit/s clock recovery using periodically poled lithium niobate Electronics Letters, 2008, 44, 370-371

[79] Spirit, D.M.; Ellis, A.D.; Barnsley, P.E.; , "Optical time division multiplexing: systems and networks," Communications Magazine, IEEE , vol.32, no.12, pp.56-62, Dec. 1994 doi: 10.1109/35.336012

[80] Nakazawa, M.; Kasai, K.; Yoshida, M. & Hirooka, T. Novel RZ-CW conversion scheme for ultra multi-level, high-speed coherent OTDM transmission Proc. 37th European Conf Optical Communication (ECOC) and Exhibition, 2011, 1-3

[81] Zarris, G.; Hugues-Salas, E.; Gonzalez, N.A.; Weerasuriya, R.; Parmigiani, F.; Hillerkuss, D.; Vorreau, P.; Spyropoulou, M.; Ibrahim, S.K.; Ellis, A.D.; Morais, R.; Monteiro, P.; Petropoulos, P.; Richardson, D.J.; Tomkos, I.; Leuthold, J.; Simeonidou, D.; , "Field Experiments With a Grooming Switch for OTDM Meshed Networking," Lightwave Technology, Journal of , vol.28, no.4, pp.316-327, Feb.15, 2010 doi: 10.1109/JLT.2009.2034121

[82] Calabretta, N.; Wang, W.; Ditewig, T.; Luo, J. & Dorren, H. Data format agnostic optical label processing techniques for intelligent forwarding of packets in all-optical packet switched

networks Proc. 13th Int Transparent Optical Networks (ICTON) Conf, 2011, 1-4

[83] H. Hu, M. Pu, H. Ji, M. Galili, H. Mulvad, K. Yvind, J. Hvam, P. Jeppesen, and L. Oxenlowe, "160 Gb/s Silicon All-Optical Data Modulator based on Cross Phase Modulation," in Optical Fiber Communication Conference, OSA Technical Digest (Optical Society of America, 2012), paper OM2E.2.

[84] Reconfigurable all-optical two-channel demultiplexer based on modified dispersion asymmetric nonlinear optical loop mirror Electronics Letters, 2010, 46, 1613-1614

[85] Du, J.; Dai, Y.; Lei, G. K. P. & Shu, C. Dispersion asymmetric NOLM for reconfigurable all-optical two-channel demultiplexing using single baseband control pulse Proc. 36th European Conf Optical Communication (ECOC) and Exhibition, 2010, 1-3

[86] Schubert C. et al., "Comparison of interferometric all-optical switches for demultiplexing applications in high-speed OTDM systems," IEEE Journal of Lightwave Technology, vol. 20, no. 4, pp. 618-624, 2002.

[87] Mortimore D. B., "Fiber loop reflectors," IEEE Journal of Lightwave Technology, vol. 6, no. 7, pp. 1217-1224, 1988.

[88] Verdurmen E.J.M. et al., "OTDM demultiplexing using HNLF in a NOLM at 160 Gb/s," Proceedings of Lasers and Electro-Optics Society Conference, 2004.

[89] Schubert C. et al., "160-Gb/s all-optical demultiplexing using a gain-transparent ultrafast-nonlinear interferometer (GT-UNI)," IEEE Photonics Technology Letters, vol. 13, no. 5, pp. 475-477, 2001.

[90] A. T. Clausen, A. I. Siahlo, J. Seoane, L. K. Oxenlowe, and P. Jeppesen. 320 to 10 Gb/s demultiplexing using a NOLM based on commercially available components. Electronic Letters, 41(5):265–266, 2005.

[91] Hibino, Y. Applications for 100 ethernet and beyond Proc. Int. Nano-Optoelectronics Workshop i-NOW 2008, 2008

[92] Ishida, O. 40/100GbE technologies and related activities of IEEE standardization Proc. Conf. Optical Fiber Communication - incudes post deadline papers OFC 2009, 2009, 1-29

[93] Kolleck, C.; Hempelmann, U.; , "All-optical wavelength conversion of NRZ and RZ signals using a nonlinear optical loop mirror," Lightwave Technology, Journal of , vol.15, no.10, pp.1906-1913, Oct 1997 doi: 10.1109/50.633589

[94] Ding Wang; Golovchenko, E.A.; Pilipetskii, A.N.; Menyuk, C.R.; Arend, M.F.; , "Nonlinear optical loop mirror based on standard communication fiber ," Lightwave Technology, Journal of , vol.15, no.4, pp.642-646, Apr 1997 doi: 10.1109/50.566685

[95] Uchiyama, K.; Morioka, T.; Kawanishi, S.; Takara, H.; Saruwatari, M.; , "Signal-to-noise ratio analysis of 100 Gb/s demultiplexing using nonlinear optical loop mirror," Lightwave Technology, Journal of , vol.15, no.2, pp.194-201, Feb 1997 doi: 10.1109/50.554322

[96] S. Taccheo and P. Vavassori, Dispersion-Flattened fiber for e cient supercontinuum generation," in Optical Fiber Communication Conference, OFC 2002, Anaheim, California, USA, Mar. 2002, paper ThY5.

[97] Oxenlowe, L.K.; Slavik, R.; Galili, M.; Mulvad, H.C.H.; Clausen, A.T.; Yongwoo Park; Azana, J.; Jeppesen, P.; , "640 Gb/s Timing Jitter-Tolerant Data Processing Using a Long-Period Fiber-Grating-Based Flat-Top Pulse Shaper," Selected Topics in Quantum Electronics, IEEE Journal of , vol.14, no.3, pp.566-572, May-june 2008 doi: 10.1109/JSTQE.2007.915395

[98] Oxenlowe, L. K. Tutorial: Terabit/second OTDM systems Proc. IEEE Photonics Conf. (PHO), 2011, 650-651

[99] Blumenthal, D. J. Terabit optical ethernet and enabling integration technologies Proc. and the National Fiber Optic Engineers Conf. Optical Fiber Communication Conf. and Exposition (OFC/NFOEC), 2011, 1-3

[100] Malhotra, Y. & Shreya, S. 192 Gb/s Transmission over 30 Km G.652 Standard Fiber Using 192-to-12 Gb/s Demultiplexer Proc. Int Computational Intelligence and Communication Networks (CICN) Conf, 2011, 1-5

[101] Hu, Hao; Laguardia Areal, Janaina; Hans Christian Hansen Mulvad, Michael Galili, Kjeld Dalgaard, Evarist Palushani, Anders Clausen, Michael S. Berger, Palle Jeppesen, and Leif Katsuo Oxenløwe, "Synchronization, retiming and time-division multiplexing of an asynchronous 10 Gigabit NRZ Ethernet packet to terabit Ethernet," Opt. Express 19, B931-B937 (2011)